IMMUNOGENICITY AND ECOTOXICITY OF ENGINEERED NANOPARTICLES

A DISSERTATION
SUBMITTED TO THE FACULTY OF THE GRADUATE SCHOOL
OF THE UNIVERSITY OF MINNESOTA
BY

Melissa Ann Maurer-Jones

IN PARTIAL FULFILLMENT OF THE REQUIREMENTS
FOR THE DEGREE OF
DOCTOR OF PHILOSOPHY

Christy Lynn Haynes, Adviser

December 2012

Acknowledgements

It is very clear to me that I would not have made it to this point of finishing my Ph.D. without the support of a whole village of people. First, and foremost, I need to thank my advisor, Christy Haynes. I believe it was very serendipitous to have landed in her group, and I am incredibly grateful that it happened. Christy's enthusiasm, purposefulness, and drive for her work is evident from the first time you meet her, and I hope to emulate these traits going forward in my career. I particularly value the range of experiences she has afforded me throughout my time in her group, and through it all, she has challenged me to be a better scientist and communicator. Christy lives life with authenticity and I could not have asked for a better mentor (and urban racing partner).

I joined the Haynes group in Christy's third year at Minnesota, so I have had the opportunity to work with all of her graduate students to date. This community of people has defined my experiences in graduate school and they are an amazing group of people. I thank the graduate students that graduated before me, Bryce Marquis, Shencheng Ge, Sara Love, Kyle Bantz, and Yu-Shen Lin, for taking me under their wings, pushing me, and collaborating with me. Their work set the precedent for the group and they are responsible for creating the supportive and collaborative environment of the Haynes group. I also need to thank the current set of Haynes groupers, Secil Koseoglu, Audrey Meyer, Ben Manning, Donghyuk Kim, Katie Hurley, Solaire Finkenstaedt-Quinn, Ian Gunsolus, Xiaojie Wu, Ben Meyer, Sarah Gruba, and Sam Egger. I am grateful for all of the discussions, support, and laughs. Most of all, I thank all the Haynes group members, old and current, for their friendships.

I acknowledge the handful of undergraduate students who had to "put up" with me as their graduate student mentor. Thank you to Sarah Connolly and Jenna Christenson for developing the ROS assays, Greg Gibson for helping get the bacteria work started, and Cole Christenson for optimizing many bacteria assays.

Beyond the Haynes group, graduate school has also allowed me to meet some amazing individuals both in collaborations and friendships. First, I want to acknowledge Maral Mousavi and Li Chen from the Buhlmann group with whom I have had the opportunity to collaborate in the last year and with whom are co-authors on Chapter Five. I also need to acknowledge the friends who I am happy to have shared the triumphs and trials of graduate school. Most specifically, I would like to Lindsay Hinkle and Sarah Page. These women have been incredible supports, confidants, and cheer leaders throughout all of the hurdles of graduate school.

Of course, none of this would be possible without the love and support from my family. First, I need to acknowledge my wonderful husband, Jonathan. His commitment to making Minnesota a better place for our family is truly inspiring and I hope to bring this level of commitment to making things better with my science. I thank him so much for his patience as I finish my degree, and I am excited to continue on this journey with such an amazing person. I also need to acknowledge my parents for their love and support and their ability to keep me grounded when things have been crazy. Lastly, I need to thank my beautiful daughter, Ellen, who is my shining light that makes me smile and remember the joys of life daily.

In Chapter 2, we gratefully acknowledge Russell Anderson in the Research Analytical Laboratory Department of Soil, Water, and Climate at the University of Minnesota for obtaining ICP-AES measurements. We acknowledge Katherine L. Braun for her help with the biological TEM sample preparation. The TEM and SiO_2 XRD measurements were carried out in the Institute of Technology Characterization Facility, University of Minnesota, which receives partial support from NSF through the National Nanotechnology Infrastructure Network. The TiO_2 XRD measurements were performed with the help of Dr. Jason Myers in the Penn Research group in the Department of Chemistry at the University of Minnesota. This research was financially supported by a grant from the National Science Foundation (CHE-0645041), a Taiwan Merit Scholarship (NSC-095-SAF-I-564-052-TMS) from the National Science Council awarded to Y.-S. L, and a National Science Foundation Graduate Research Fellowship awarded to M.A.M.-J.

For Chapter 3, we acknowledge Sarah Connolly, a summer research undergraduate at the University of Minnesota, for her work on developing ROS assay protocols and Diana Freeman for her help in isolating the MPMCs. This research was financially supported by a grant from the National Science Foundation (CHE-0645041) and a National Science Foundation Graduate Research Fellowship awarded to M.A.M.-J.

In Chapter 4, we acknowledge Jeff Gralnick of the University of Minnesota for his generous gift of *S. oneidensis* MR-1 and his help answering our questions. Additionally, we thank Gregory Gibson, an undergraduate researcher at the University of Minnesota, for his work developing the bacteria protocols. This research was financially supported by a grant from the National Science Foundation, an American Chemical Society Division of Analytical Chemistry and University of Minnesota Doctoral Dissertation Fellowship awarded to M.A.M-.J., NIH Biotechnology Training Grant awarded to I.L.G. and an University of Minnesota Undergraduate Research Opportunity Program fellowship awarded to C.J.C. Parts of this work were carried out in the Characterization Facility, University of Minnesota, which receives partial support from NSF through the MRSEC program.

In Chapter 5, we acknowledge Rick Knurr of the Earth Sciences Department at the University of Minnesota for his work on the ICP-MS data collection. This research was financially supported by a grant from the National Science Foundation, the Center for Analysis of Biomolecular Signaling at the University of Minnesota, and an University of Minnesota Doctoral Dissertation Fellowship awarded to M.A.M-.J. Parts of this work were carried out in the Characterization Facility, University of Minnesota, which receives partial support from NSF through the MRSEC program.

Preparation of Chapter 6 was supported in part by National Institutes of Health (NIH), National Human Genome Research Institute (NHGRI) American Recovery & Reinvestment Act (ARRA) Challenge grant #1-RC1-HG005338-01 on "Nanodiagnostics and Nanotherapeutics: Building Research Ethics and Oversight" (S.M. Wolf, PI; J. McCullough, R. Hall, J.P. Kahn, Co-Is). This work was also supported by the National Science Foundation (CHE-0645041) and a University of Minnesota Doctoral Dissertation Fellowship awarded to M.A.M-.J. The views expressed are those of the authors and do not necessarily reflect the views of the NIH, NHGRI, or NSF.

For Chapter 7, we gratefully acknowledge Amanda Gavin and the students at East Ridge High School in Woodbury, MN for helping improve this laboratory experiment and Audrey F. Meyer for help in implementing the lab. This work was supported by the

National Science Foundation and a University of Minnesota Doctoral Dissertation Fellowship awarded to M.A.M-.J. Parts of this work were carried out in the Characterization Facility, University of Minnesota, which receives partial support from NSF through the MRSEC program.

Dedication

This work is dedicated to my wonderful partner, Jonathan, and my parents, Meg and Dave, all who are relentlessly supportive and encouraging.

Abstract

The growing use of nanoscale materials in commercially available products and therapeutics has created an urgent need to determine the toxicity of these materials so that they may be designed and employed safely. As nanoparticles have unique physical and chemical properties, the challenges in determining their physiological and environmental impact have been numerous. It is, therefore, the goal of my thesis work to employ sensitive analytical tools to fundamentally understand the how nanoparticles interact with immunologically and ecologically relevant models. My project approaches nanotoxicity studies starting with a relevant model system exposed to well-characterized nanoparticles to (1) determine if cells/organisms survive exposure using traditional toxicological assays and, if the majority survives exposure, (2) use sensitive analytical tools to determine if there are changes to critical cell/organism function. If perturbation of function is detected, (3) the mechanism or cause of changes in cell function should be determined, including assessment of nanoparticle uptake and localization. Once a mechanism of interaction is determined, this process could begin again with a modified particle that may address the toxic response.

Chapter Two describes the impact of metal oxide (TiO_2 and SiO_2) nanoparticles on mast cells, critical immune system cells, and utilizes the sensitive technique of carbon-fiber microelectrode amperometry (CFMA) to monitor changes in the important mast cell function of exocytosis. Chapter Three expands upon Chapter Two and examines in more detail the mechanism by which TiO_2 nanoparticles impact exocytotic cell function, completing the process nanotoxicity described above. From these studies, it was determined that, while nanoparticles do not decrease the viability of mast cells, there are significant changes to exocytosis upon nanoparticle exposure, and in the case of TiO_2, these changes in exocytosis are correlated to nanoparticle-induced oxidative stress. The generalizability of the mechanism of TiO_2 toxicity, as detailed in Chapter Two and Three, is explored in Chapter Four in a bacteria model, *Shewanella oneidensis*, studying the functions of biofilm formation using a quartz crystal microbalance (QCM) and flavin secretion using high performance liquid chromatography (HPLC). This study revealed that the proximity of the TiO_2 nanoparticles to *S. oneidensis* caused changes in gene expression resulting in an observed delay in biofilm growth and increase in riboflavin secretion. Chapter Five works to develop an *in situ* Ag nanoparticle characterization tool using fluorous-phase ion selective electrodes to measure dissolved Ag^+, with preliminary investigation into the toxicity of Ag nanoparticles and Ag^+ ions to *S. oneidensis*, resulting in one of the first *in situ* characterization tools for nanoparticles during toxicity assessments.

Moving beyond laboratory work, Chapter Six examines bench scientists' perspective on the regulation of nanotherapies moving from pre-clinical to first-in-human trials and the ethical considerations for the implementation of nanotechnology. Finally, Chapter Seven details the development of a 3-day nanotoxicity laboratory for introductory chemistry classes to introduce students to interdisciplinary science and the cutting edge research field of nanotoxicology.

In total, my project has considered the scientific, ethical, and educational implications for nanotoxicology and has ultimately contributed to a better understanding of the nanoparticle-cell interaction.

Table of Contents

Chapter Two

Chapter Three

List of Tables

List of Figures

Chapter One

Chapter Two

Chapter Three

Chapter Four

Chapter Five

Chapter Six

Chapter Seven

List of Symbols and Abbreviations

3t3	Swiss albino fibroblasts
AES	Auger electron spectroscopy
AFM	atomic force microscopy
Ag	silver
Al_2O_3	aluminum oxide
APF	aminophenyl fluorescein
As-syn	as-synthesized
Au	gold
BALF	bronchoalveolar lavage fluid
BET	Brunauer, Emmett, and Teller – nitrogen adsorption/desorption isotherm
BSA	bovine serum albumin
CFMA	carbon-fiber microelectrode amperometry
CTAB	cetyltrimethylammonium bromide
CuO	copper oxide
DCFDA	2',7'-dichlorodihydrofluorescein
DLS	dynamic light scattering
ED	electron diffraction
EELS	electron energy loss spectroscopy
EPS	extracellular polymeric substance
FDA	Food and Drug Administration
FMN	flavin mononucleotide
HEPES	4-(2-hydroxyethyl)-1-piperazineetanesulfonic acid
HPLC	high performance liquid chromatography
ICP-AES	inductively coupled plasma atomic emission spectroscopy
ICP-MS	inductively coupled plasma mass spectrometry
ISE	ion-selective electrode
LB	Luria-Bertani
LD_{50}	lethal dose to 50% of the population
MPMC	murine peritoneal mast cell
MTT	(3-(4,5-dimethylthiazol-2-yl)-2,5-diphenyltetrazolium bromide
MWCNT	multi-walled carbon nanotube
NAC	N-acetylcysteine
NIST	National Institute of Standards and Technology
NOM	natural organic matter
NSES	National Science Education Standards
NMR	nuclear magnetic resonance
NTA	nanoparticle-tracking analysis
P25	Evonik Aeroxide® Degussa P25
PBS	phosphate buffered saline
PEC	predicted environmental concentration
QCM	quartz crystal microbalance
qRT-PCR	quantitative reverse transcription polymerase chain reaction
RBC	red blood cell
RBL-2H3	rat basophilic leukemia cells

ROS	reactive oxygen species
SiO_2	silica
SWCNT	single-walled carbon nanotube
T-Eco	Eusolex® T-Eco
tHODE	hydroperoxy octadecadienoate
TEM	transmission electron microscopy
TEOS	tetraethyl orthosilicate
TiO_2	titanium dioxide
UV	ultra violet
UV-vis	UV-visible spectroscopy
WWTP	waste water treatment plant
XPS	x-ray photoelectron spectroscopy
XRD	x-ray diffraction
ZnO	zinc oxide

Chapter One

Introduction to Nanotoxicology

This chapter was adapted from:

M.A. Maurer-Jones, K.C. Bantz, S.A. Love, B.J. Marquis, C.L. Haynes. Toxicity of Therapeutic Nanoparticles. *Nanomedicine*. **2009**, 4, 219-241.

1.1 General Overview

Nanotechnology has provided a basis for innovation in a wide range of products, from pharmaceuticals to athletic gear, and has resulted in an exponential increase in both the deployment of nanotechnologies in products along with the development of novel materials.[1] The global production of nanoparticle-enabled products has greatly increased in the last decade, with estimated nanoparticle production to be thousands of tons in 2004[2] and projected to grow to over half a million tons by 2020;[3, 4] therefore, it is certain that humans have interacted or will interact with engineered nanoparticles and that these nanoparticles will be released into the environment. Subsequently, there is a need to understand the biological and ecological implications, both intended and unintended (i.e. toxicity), of engineered nanoparticle exposure, out of which the field of nanotoxicology has emerged.

Early studies of biological toxicity, or toxicity as relating to human health, evolved out of the aerosols field where emphasis was on the impact of ultrafine particulate pollution on human health.[5] Ecological toxicity, or toxicity as related to environmental or ecosystem health, has arisen out of the colloids community, where studies have focused on the fate and transformation of naturally occurring colloids, including their role in transport of micropollutants such as heavy metals[6] and in atmospheric chemistry.[7] Engineered nanoparticles, however, are composed of a much wider variety of materials and occur in monodisperse sizes and shapes with a suite of synthetic surface molecules distinct from naturally-occurring materials; these novel nanoparticles have prompted the aerosols and colloids communities to consider more strongly the impact of engineered nanoscale particles to human and ecosystem health in

the interdisciplinary field of nanotoxicology. In general, the field of nanotoxicology, a term coined circa 2004,[8] is defined as the study of the bio-nano interactions that occur through nanoparticle exposure, and it is aimed at elucidating mechanisms of interaction with the ultimate goal to yield nanoparticle design rules that will allow rational prediction and control of toxicity throughout the life cycle of a nanoparticle product.

While biological and ecological toxicity assessments have many different considerations, the challenges that face the nanotoxicity community transcend either area and require interdisciplinary efforts to overcome these challenges. It has become apparent within the field of nanotoxicology that there is a critical need for new or different techniques that enable the understanding of toxicity on a mechanistic level, which analytical chemistry has the expertise to address. Herein, I review important considerations for biological and ecological nanotoxicity, including nanoparticle characterization and transformation, model systems, and common toxicity assessments in addition to examining the overlapping challenges that face both areas of the nanotoxicity community. The areas of overlap yield insight into gaps in the literature that the expertise of analytical chemists can address, which ultimately may lead the nanotoxicity field to generalizable trends in toxicity and safe, sustainable design and use of nanoparticles.

1.2 Considerations of Exposure

Prior to nanotoxicological assessments, it is important to consider routes of nanoparticle exposure, the prevalence of particular nanoparticles, and the characteristics of the nanoparticles that could influence toxicity.

1.2.1 Engineered Nanoparticles in the Body

Human exposure to nanoparticles, either intentional or unintentional, can occur through a number of exposure pathways (as detailed in Figure 1.1), and it is clear that nanoparticles can translocate within the body after exposure.[9] The range of materials to which humans could be exposed is broad, particularly with the ever expanding list of nanotherapeutics, where nanoparticles are used as drug delivery vehicles, contrast agents, photothermal/photodynamic therapies, and/or some or all of these functions.[10] More specifically, materials used for intentional, nanotherapeutic purposes range from liposomes to iron oxide to gold.[11] Nanoparticles that are commonly utilized in commercially available products make up the majority of nanoparticles in unintentional human exposure.

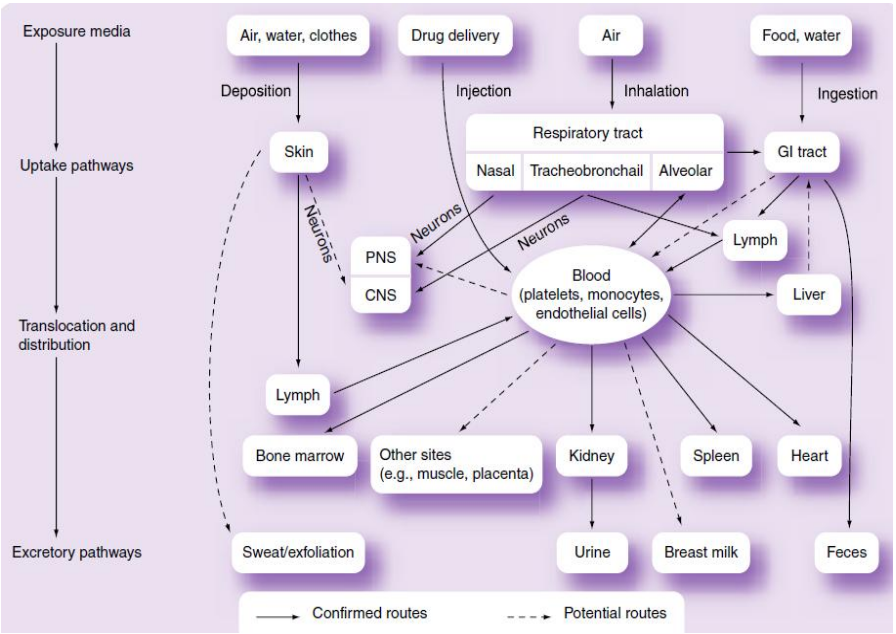

Figure 1.1 Schematic of human exposure pathways to nanoparticles and confirmed (solid line) or potential (dashed lines) routes of translocation throughout the body. Reprinted with permission from reference 1.

Due to the range of materials, uses, and pathways of exposure, it is difficult to predict relevant nanoparticle exposure levels. Intentional exposure to nanotherapeutics or UV-light filtering nanoparticles (titanium dioxide (TiO_2) or zinc oxide (ZnO)), for example, depend on the necessary dose to achieve therapeutic potential or prevent sunburn, respectively. These doses can range from 6 mg/g for gold (Au) nanoparticle therapies[12] to 2 mg/cm^2 for application of ZnO-containing sunscreen.[13] For unintentional nanoparticle exposure, efforts have been made to sample aerosolized nanoparticles from work spaces where engineered nanomaterials were handled,[14] measuring a wide range of concentrations (0-50 µg/m^3) during various tasks from a variety of nanoparticles (e.g. TiO_2, silica (SiO_2), aluminum oxide (Al_2O_3)).[15, 16] One thing to note from these examples of doses is that not only does a wide range of exposure levels exist, which is important for clearly understanding the toxicological impacts of nanoparticles, there are also many different dose metrics utilized within the literature. The importance of dose metrics becomes particularly relevant when results from *in vitro* experiments (i.e. experiments on single cell-lines or tissue) are extrapolated to *in vivo*, or whole organism, exposures. Equivalent dosing is difficult to achieve because the nanoparticle experiences a vastly more complicated delivery route and environment when administered *in vivo*.[10] Accordingly, *in vitro* toxicity response tends to overestimate the *in vivo* impact. By using a good dose metric, or measure of the dose, *in vivo* versus *in vitro* doses can be justified, and an accurate determination of the therapeutic effect or toxicity can be achieved. Donaldson *et al.* and Duffin *et al.* were recently successful in this endeavor by representing the dose in terms of nanoparticle surface area, and both groups showed correlated toxicity between *in vivo* and *in vitro* experiments.[17, 18] Due to the

complex nature of nanomaterial dosing and the relatively recent emergence of nanotoxicology as a discipline, few exposure standards for toxicity evaluation exist and are an area of much needed research.

1.2.2 Engineered Nanoparticles in the Environment

Though the number of commercial and manufactured products containing nanoparticles is growing and novel nanoparticles are continually developed, there are only a few materials that are currently in a large number of products or used in high volume, and therefore, are currently being released or will likely be released to the environment in the coming decades. These include silver (Ag), TiO_2, ZnO, SiO_2 and carbon-based nanomaterials (single-walled carbon nanotubes (SWCNTs), multi-walled carbon nanotubes (MWCNTs), and fullerenes);[19] accordingly, these are largely the main focus of nanoparticles studied within the current econanotoxicology literature.

There are various pathways into the environment, including direct application to an environmental compartment, wastewater treatment plant (WWTP) effluent, WWTP sludge, and product degradation;[20, 21] yet, it is difficult to estimate the relevant concentrations of nanoparticles that will be released at any given time. Some of the difficulty in predicting relevant concentrations of nanoparticle release is the result of limited data on nanoparticle prevalence in and use of commercial products and likely use in the future.[22, 23] Additionally, transformations of nanomaterials, such as dissolution, sedimentation, or release of surface moieties, could greatly affect the pathway and extent of environmental release. A number of risk assessment efforts have been made to model and calculate predicted environmental concentrations (PECs) of nanoparticles with the

current understanding of nanoparticle transformations and fate[20, 21, 24-29] along with a few experimental approaches to examine nanoparticle fate under natural conditions.[29, 30] A summary of the PECs is found in Table 1.1, with ranges including the lowest and highest PECs reported in the literature, and it should be noted that these values are sometimes calculated considering all species of the material (e.g. Ag_2S, Ag^+, and Ag nanoparticles) and other times considering simply the expected predominant form.

Table 1.1 Predicted environmental concentrations (PECs) of highly produced and used nanoparticles in three major pathways in the environment.

Nanoparticle	PEC – pathway into environment	Reference
Ag	0.088-10000 ng/L – surface water	20, 23, 24, 26
	0.0164-17 µg/L – WWTP effluent	24, 26
	1.29-39 mg/kg – WWTP sludge	24, 26
TiO_2	21-10000 ng/L – surface water	20, 23, 24, 25, 27, 28
	1-100 µg/L – WWTP effluent	24, 29, 30
	100-2000 mg/kg – WWTP sludge	24, 28, 29
ZnO	1-10000 ng/L – surface water	23, 24
	0.22-1.42 µg/L – WWTP effluent	24
	13.6-64.7 mg/Kg – WWTP sludge	24
Carbon-based	0.001-0.8 ng/L – surface water	20
	3.69-32.66 ng/L – WWTP effluent	24
	0.0093-0.147 mg/kg – WWTP effluent	24

1.2.3 Engineered Nanoparticle Characterization and Transformation

While molecular toxicology has provided a basis for much of the nanotoxicity assessments, one distinguishing feature of nanoparticle toxicants from molecules is the importance of their physical characteristics, including size, crystallinity, surface charge,

and surface chemistry, to their toxicity. Table 1.2 summarizes the important characteristics and the tools commonly used to characterize these features.

Table 1.2 Important nanoparticle properties and common methods for characterization. Adapted with permission from reference 31.

Physiochemical Property	Common Characterization Methods*
Size (distribution)	TEM, AFM, DLS, NTA
Shape	TEM, AFM, UV-vis (for plasmonic nanoparticles)
Agglomeration/aggregation state	DLS, UV-vis (for plasmonic nanoparticles)
Crystal structure	XRD, ED
Surface chemistry/charge/area	AES, EELS, XPS, solid state NMR, ζ-potential, BET
Stability over time/dissolution	DLS, UV-vis, ICP-AES, ICP-MS, colorimetric assays

*Abbreviations: TEM – transmission electron microscopy, AFM – atomic force microscopy, DLS – dynamic light scattering, NTA – nanoparticle-tracking analysis, UV-vis – UV visible spectroscopy, XRD – x-ray diffraction, ED – electron diffraction, AES – Auger electron spectroscopy, EELS – electron energy loss spectroscopy, XPS – x-ray photoelectron spectroscopy, NMR – nuclear magnetic resonance, BET – nitrogen adsorption/desorption isotherm, ICP-AES – inductively coupled plasma atomic emission spectroscopy, ICP-MS – inductively coupled plasma mass spectrometry

From the body of literature, it is clear that nanoparticles are transformed from their original, synthesized state no matter the type, amount, or pathway of human exposure/environmental nanoparticle release, which follows from their high reactivity. Transformations are the result of a myriad of reactions or processes, including aggregation/agglomeration, redox reactions, dissolution, and reactions with natural occurring macromolecules. These dynamic transformations in turn affect the transport, fate, and toxicity of nanoparticles in the body or environment, and therefore, it is critical to understand and characterize these transformations. Trends in nanoparticle aggregation, surface molecule transformations, and speciation/dissolution under relevant conditions are examined herein. Typically, physiological or environmental conditions are simulated in the laboratory by modeling ionic strength and protein or natural organic matter (NOM)

content, respectively, two key characteristics in nanoparticle transformation in aqueous solutions.

The size of nanoparticles is an important determinant to reactivity, transport, and toxicity, and while it is common to characterize the primary particle size, often done with electron microscopy, nanoparticles tend to agglomerate so that a system interacts with the aggregate size instead. Light scattering techniques are most commonly employed to study stability of nanoparticles in solution[31] or as an aerosol.[32] Within solutions, there are some notable aggregation trends observed no matter the nanomaterial. First, increasing ionic strength increases the rate and extent of aggregation of nanomaterials,[33, 34] and the ionic species has some effect on the extent of aggregation.[34-36] Intentionally modifying the surface of nanoparticles can prevent or enhance the effect of ionic strength on aggregation as demonstrated by Badawy et al. with Ag nanoparticles that were "bare", citrate-, PVP (polyvinylpyrrolidone)- or BPEI (branched polyethyleneimine)-capped, where steric hindrance and electrostatics prevented aggregation of PVP- and BPEI-capped Ag nanoparticles.[34]

Besides ionic strength, the presence of proteins, NOM, and other biomacromolecules (e.g. polysaccharides) plays a key role in determining the aggregation state of nanoparticles. In biological systems, the "protein corona" has been the focus of many biological toxicity studies where a layer of adsorbed proteins make-up the nano-bio interface.[37, 38] NOM is a ubiquitous, and not very well-defined, component of environmental systems that readily sorbs onto the highly reactive surface of nanomaterials.[39] Typically, NOM displaces weakly bound capping agents and forms a dynamic, heterogeneous layer of molecules.[40] With respect to aggregation, the presence

of biomacromolecules has had varied effects. There is significant evidence that, in the presence of NOM, nanoparticles are stabilized and aggregation is limited at realistic NOM concentrations (1-30 mg C/L),[35, 41] but flocculation is observed at higher NOM concentrations;[42] these trends are maintained in a model protein, bovine serum albumin (BSA).[43] Other molecules, like extracellular polymeric substance, cause an increase in nanoparticle aggregation rate,[44] while still other molecules like cysteine, a component of proteins and NOM, cause an initial increase in aggregation rate but not in the long-term aggregate size.[45] Understanding aggregation is critical for characterizing transport of nanoparticles through the body and environmental compartments. In the body, greater aggregation yields larger particles that are cleared from the body by the mononuclear phagocyte system, and in the environment, less aggregation yields lower rates of sedimentation and greater mobility; therefore, understanding the interaction of nanoparticles under natural conditions (e.g. salinities, pH, and molecular species) enables a better assessment of exposure and transport.

These aggregation studies bring to light the importance of the nanoparticle surface and localized environment around that surface in the transformation of the material. As alluded to previously, proteins and NOM are of particular importance in the nanoparticle alteration because of their pervasiveness throughout the body and environment. NOM clearly plays a role in the aggregation dynamics but itself is dynamic, with an undefined molecular structure and a variety of reactive moieties, and therefore its sorption onto nanoparticle surfaces may aid transformations beyond aggregation, such as surface reduction, where NOM can reduce ionic metals at the surface to grow the nanoparticle.[46] Proteins and other biomolecules like fatty acids can act upon the nanoparticle where

binding or interacting with the surface alters the free energy of the surface[47] and/or can influence other nanoparticle transformations.[48] In addition to organic molecules (e.g. proteins, NOM, carbohydrates), heavy metal ions also have the ability to adsorb onto nanoparticle surfaces, increasing the transport and toxicity effects of heavy metal atoms but also prompting the use of nanoparticles in heavy metal pollutant remediation.[49]

Beyond sorption of extraneous molecules/atoms, the transformation of the nanomaterial itself into other species plays a role in the toxicity assessment. For example, the dissolution of Ag nanoparticles (Ag^0 to Ag^+) is responsible for the antimicrobial nature of Ag nanoparticles,[50] and therefore, understanding this speciation, studied primarily using atomic spectroscopy, is important for assessing nanotoxicity. However, the surface of Ag nanoparticles, in addition to surface adsorption of proteins, NOM and other macromolecules, is susceptible to reaction with oxygen and sulfur atoms, making it unlikely that Ag(0) is the primary form of the atoms at the nanoparticle surface.[36] Other nanoparticles (e.g. Au, ZnO, and copper oxide (CuO))[51] experience similar speciation either in the dissolution to ions or chemical reactions that, in turn, could affect other physicochemical changes in the nanoparticles and ultimately, nanoparticle translocation and toxicity.

The interplay between the different, dynamic nanoparticle transformations discussed above (Figure 1.2) and the importance of the nanoparticle state on subsequent transport and toxicity necessitates careful time-dependent characterization of nanoparticles in environmentally relevant conditions. Current analytical methods yield limited insight into a subset of these transformations; development of sensitive, *in situ*

characterization tools, a strength of the analytical chemistry community, would significantly advance this field.

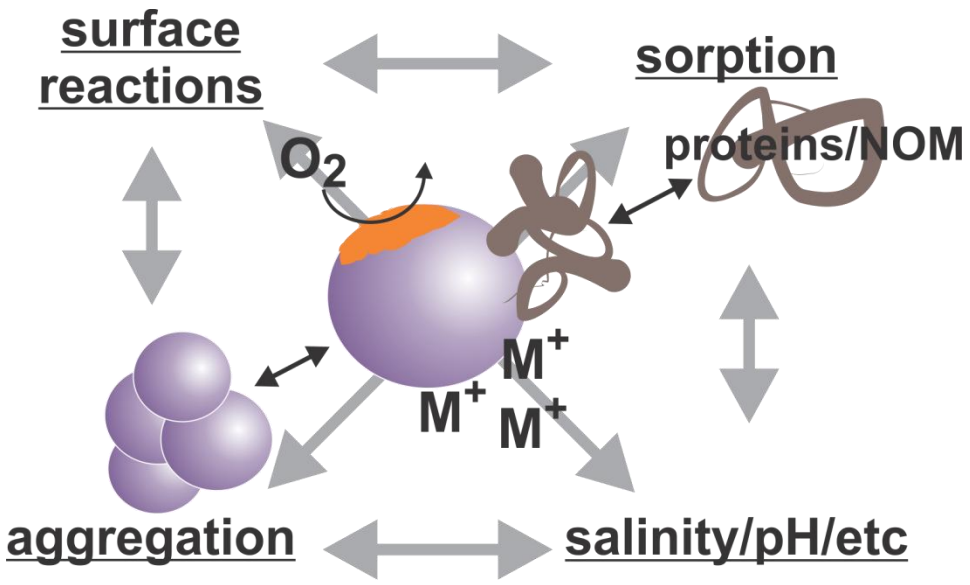

Figure 1.2 Illustration of the dynamic transformations nanoparticles may undergo in the body or the environment and the interplay between these

1.3 Considerations of Model Systems

It is important for understanding functional impacts of nanoparticles to humans and/or the environment to investigate toxicity in model systems. Common biological and ecological model systems are discussed below.

1.3.1 Biological Models

Biological toxicity studies often utilize two categories of model systems: *in vivo*, whole organism, and *in vitro*, cells or tissue. *In vivo* toxicity studies provide vital information to assess the health and safety of nanoparticles as they provide a systemic

response to nanoparticles.[52] Depending on the potential application of the nanomaterial, any number of animal models or physiological mechanisms can be studied, such as zebrafish embryo development,[53] rabbit ocular toxicity,[54] rat pulmonary toxicity,[55] and LD_{50} (lethal dose to 50% of the population)[56] or immune cell distributions in mice.[57] These types of studies have several limitations including the long experimental time required, the high cost, and the ethical concerns regarding the treatment of laboratory animals. Yet, *in vivo* studies are necessary to explore nanoparticle biodistribution and determine appropriate cell types to be used in *in vitro* studies. *In vitro* methods are relatively fast and inexpensive and minimize ethical concerns regarding animals; however, many of these methods require more extensive validation with *in vivo* studies to evaluate their toxicological predictive capability.

For *in vitro* toxicity, there is a wide range in model systems. Choices that must be made when selecting a model cell include: whether to use primary culture or immortal cell lines (i.e. cells isolated directly from an animal or a self-propagating cell line), whether to use cells of human origin or animal origin (typically rat, mouse or hamster), whether the physiological function of the model cell is relevant, and whether the model cell is found in the tissue likely exposed to the nanoparticle. Primary culture of human cells presents the ideal model for studying human toxicity, but these models are generally restricted to commercially available cells capable of continuous propagation or cell types isolated from small samples of donor blood such as mononuclear cells,[58] B lymphocytes, and T lymphocytes.[59] An alternative is to use primary culture of cells from animal models which require less regulation.[60] Primary cell culture yields heterogeneous mixtures of cells that then typically require density gradient or flow cytometry sorting to isolate the

model cell of interest. These separation techniques often damage cells in the process of isolation. Additionally, primary culture cells are often obtained in limited numbers and have a limited lifetime in culture. For these reasons, immortal cell lines are commonly used for *in vitro* toxicological testing, and a wide variety are commercially available for use as both cancer cell models and immortalized representations of normal cells. The major drawback of using immortal cell lines is that the mutations required for the immortalization of the lines may affect the way the cells respond to nanoparticles. To improve the reliability of interpretations from immortal models, studies can be compared using different cell lines that have the same physiological function. Co-culture models can be also used to yield a better representation of *in vivo* conditions,[61, 62] although the presence of two cells in culture can complicate interpretation.

1.3.2 Ecological Models

Model organisms for ecological toxicity studies vary greatly and are often chosen based on their level in the food web. Herein, I detail a selection of the organisms used at various trophic levels. Bacteria act as the base of the food chain and serve integral environmental functions; they are ubiquitous members of ecosystems with particular importance in global nutrient cycling. This ecological import along with the relative ease of culture has made bacteria a primary focus of study for econanotoxicity studies to date, including use of a wide range of model organisms and toxicity assays to assess the impacts of nanoparticles. Bacterial model choices for nanotoxicity studies vary greatly and have included common research species such as *Escherichia coli*,[63] *Bacillus subtilis*,[64] and *Pseudomonas aeruginosa*[65] along with bacteria that play key roles within

environmental compartments, such as *Nitrosomonas europaea*[66, 67] (nitrifying bacteria/ waste water treatment). The breadth of choices in these monoculture systems has led to some challenges within the field in generalizing experimental results. That is, the deepest studies utilize the common microbial species that may not be environmentally relevant, while more environmentally relevant species have been considered less thoroughly. To overcome this issue, some research groups have pursued toxicity studies on naturally-sampled bacteria.[68-70] Natural isolates increase the complexity of the model system, providing environmental relevancy; however, these community-based studies are typically limited in their ability to elucidate mechanisms of toxicity because individual species functions are not separated from the response of the whole.

Beyond single cell organisms like bacteria, plants and multi-cellular aquatic and terrestrial organisms have been utilized in nanotoxiciological studies. Plants are particularly relevant in considerations of econanotoxicity based on their interaction with air, soil, and water, all of which may contain engineered nanoparticles. In addition, plants present a significant opportunity to facilitate nanoparticle transfer among various species in the food web because they are consumed by lower organisms, animals, and people. Though there are a wide variety of plant species within the ecosystem, most nanotoxicity work to date has focused on plants for human consumption, such as maize,[71] wheat,[72, 73] soybean,[74] tobacco,[75] and many fruit or vegetable plants, such as pumpkin,[76] cucumber,[73, 77, 78] and radish.[73, 78, 79]

Animals in aquatic and terrestrial environments have many important functions within the ecosystem, including food sources. Understanding the impact of nanoparticles at this level of the food web directly relates to human health. For aquatic systems,

Japanese medaka and zebrafish are standard organisms, considered the aquatic equivalent of the famous Drosophila fruit fly. Zebrafish are hardy freshwater fish, reproduce quickly, and were one of the earliest organisms to have its genetics examined in detail.[80] Medaka are hardy, reproduce rapidly, can live in a variety of salinities, and its genome has been sequenced, which is important for understanding genetic impacts of nanoparticles in the environment.[81] The literature is the deepest regarding effects of nanomaterial exposure to zebrafish with at least 200 studies so far. Most, however, are concerned with measuring toxicity levels (i.e. LD_{50}), although some nanomaterial fate/metabolism work has begun to appear. In soil, earthworms comprise a critical component of the ecosystem[82] and are model detrivores in ecological studies.

1.4 Common Toxicological Assessment Methods

1.4.1 Biological Toxicity

The toxicity assessment methods utilized in nanoparticle toxicity experiments depend on the model system choice, *in vivo* or *in vitro*. As alluded to above, *in vivo* assessments are important for providing a systems response to nanoparticles, including long term effects, tissue localization, biodistribution, and retention/excretion. Beyond LD_{50} determinations or histological investigation of tissue damage, *in vivo* studies have examined biochemical markers of stress.[83] These studies are performed by isolation of blood[84] or a bronchoalveolar lavage fluid[85, 86] and testing for cell counts[84] and/or molecules of interest using colorimetric/fluorescent assays[86] or mass spectrometry.[85] Localization and biodistribution are most commonly investigated either by scanning the organism after nanoparticle exposure with MRI, PET, or fluorescent scans or by isolation

of organs followed by ICP-AES or ICP-MS analysis.[83] Excretion has been monitored by measuring excrements for nanoparticle matter.[87]

In vitro mammalian cell toxicity assessments are by far the most developed within the toxicity literature and will be briefly reviewed, herein (for detailed reviews see references 31, 83). The *in vitro* techniques reviewed, including viability, proliferation, apoptosis/necrosis, oxidative stress, and inflammatory response, provide examples of the techniques used thus far in assessing nanoparticle toxicity. Many of the assays herein rely on the detection of changes in probe molecules to determine the correlating toxicity biomarker concentration as a result of probe/biomarker reactions. Due to the increased reactivity of nanomaterials, it is important to determine probe/nanomaterials reactivity to eliminate false positive results arising from these reactions.

Changes in cellular viability after exposure to nanoparticles result from changes in proliferation and/or cellular death and are measured as a general assessment of cellular health. The most common method of this assessment is through the mitochondrial reduction by enzymatic cleavage of tetrazolium-based dyes such as MTT,[88] XTT,[89] or WST-1,[90] where mitochondrial activity is used as a proxy for viability. Increasingly popular is the monitoring of the reduction of the resazurin based Alamar Blue dye, which also correlates cellular reduction with viability.[91] All of these dyes generate cleavage products that can be detected colorimetrically and give a static picture of cell health. To examine the proliferation in a more dynamic fashion, changes in the numbers of live cells can be monitored over time using the same viability assays. Another approach to assessing proliferation is through the incorporation of radiolabeled [^{3}H]thymidine into DNA, where increased proliferation yields increased uptake of [^{3}H]thymidine into newly

synthesized DNA.[92] An alternative to this technique is the analysis of 5-bromo-deoxyuridine incorporation into newly synthesized DNA,[93] which is less expensive and less toxic to cells.

Cell death, both through apoptosis and necrosis, is also measured during *in vitro* toxicological assessment. Compromised membrane integrity is the most commonly used marker for cellular death, arising from both necrosis and late stage apoptosis. Trypan blue[94-96] and propidium iodide[97, 98] are charged molecules that are excluded from cells with intact membranes; their presence in cells is used to quantify cell death colorimetrically or fluorescently. Neutral red accumulates in all cells but undergoes protonation, and accordingly a color change, only in living cells; thus, stained cells allow quantitation of cell death. Additionally, a combination assay can be performed using calcein acetoxymethyl ester and ethidium homodimer where calcein acetoxymethyl ester undergoes a hydrolysis reaction within living cells producing a green fluorescent product and ethidium homodimer, a red fluorescent dye, accumulates only within dead cells.[99] The leakage of lactate dehydrogenase (LDH) into the culture medium is another marker for membrane integrity, where the LDH activity is assessed through a two-step assay based on NADH production during the conversion of lactate to pyruvate.[100] Apoptosis, or programmed cell death, is also assayed during *in vitro* toxicological assessment and is often combined with membrane integrity measurements to yield a more complete picture of cell death. Phosphatidylserine is commonly found on the outer cellular membrane during apoptosis and is assayed using a fluorescein isothiocyanate(FITC) tagged Annexin-V label.[101] The caspases are a series of proteases found in an activity cascade closely associated with apoptosis.[102] This activity is detected as a biomarker for

apoptosis using any of a number of commercially available caspase activity kits which involve the conjugation of a fluorescent or colorimetric probe molecule with a peptide cleaved specifically by an initiator caspase (caspase 2,8, 9 or 10) or an effector caspase (caspase 3, 6 or 7). Enzymatic digestion of DNA occurs during apoptosis and the resultant DNA fragments can be assayed during *in vitro* toxicity experiments using DNA laddering techniques,[103] the comet assay,[104] or the TUNEL assay.[105]

DNA fragmentation may also be the result of oxidative stress, a common toxicity mechanism that is explored during *in vitro* toxicity assessment of nanoparticles. During oxidative stress, increases in reactive oxygen species (ROS) or reactive nitrogen species (RNS) result in oxidative damage to biomolecules including nucleic acids, proteins and lipids. ROS and RNS are assayed by the oxidative production of fluorescent dyes using probes such as 2',7'-dichlorodihydrofluorescein diacetate (DCFDA)[106] or Dihydrorhodamine123.[107] Other probes, such as C11-BODIPY that localizes in the plasma membrane[108] or MitoSOX Red that localizes in the mitochondria,[109, 110] can give information regarding the location of oxidative stress. The oxidative products can also be used as markers for oxidative stress. For example, malondialdehyde is the end-product of lipid peroxidation by ROS and RNS and is assayed with thiobarbituric acid[111] and detected by either fluorescence or UV-Vis absorption. Glutathione is an important cellular anti-oxidant and can be a biomarker for oxidative stress. Due to the presence of both disulfide bridged glutathione and monomeric glutathione, total glutathione is quantified by reducing the disulfide with glutathionereductase and then assaying total glutathione with the 5,5′-dithio-bis(2-nitrobenzoic acid) probe, yielding a product that can be detected colorimetrically.[112] Superoxide dismutase (SOD) is a cellular enzyme

used to reduce the oxidative stress a cell undergoes, and its activity is used as a biomarker for oxidative stress. SOD activity is determined indirectly via the inhibition of the oxidation of an absorptive substrate, nitro blue tetrazolium, by exogenously generated superoxide. Since SOD is an inducible enzyme, the interpretation of SOD activity is complicated as increases or decreases in SOD activity can be interpreted as indirect evidence of increases in oxidative stress. For this reason, it is often preferable to use the aforementioned direct detection assays of ROS or RNS.[113]

To predict therapeutic nanoparticle effects on inflammatory response, the production of inflammatory mediators is assayed *in vitro*. Pro-inflammatory mediators are assayed using enzyme-linked immunosorbent assay (ELISA) techniques[114] and include cytokines such as IL-2, IL-8, IL-6 TNF-α, IFN-γ and EMAP-II.[115, 116] All the assays discussed above represent only a fraction of the traditional *in vitro* toxicological techniques available.

1.4.2 Ecological toxicity

Much of the early work in nanotoxicology has focused on biological consequences of nanomaterials, and only in the last few years has focus begun to move more toward developing an understanding of ecological toxicity. Therefore, the depth of ecological toxicity assays employed is shallow and few standard procedures exist. Additionally, ecological nanoparticle toxicity assessments depend on the model system, with many of same biological toxicity assessments discussed above utilized for both single cell organisms (bacteria or algae - like *in vitro*) and multicellular plants/animals (like *in vivo*).

For bacteria, much of the current understanding of nanotoxicity has been informed by analysis of bacterial viability and growth, using traditional microbiological methods such as colony forming unit assays and optical density measurements to create growth curves or calculate minimum inhibitory concentrations.[117] As in *in vitro* assays, membrane integrity assays have been used to quantify viability upon nanoparticle exposure. Most often, membrane integrity is quantified with a slight modification to the propidium iodide stain as described above where in addition to propidium iodide, a green fluorescent molecule (SYTO-9) in also used to stain non-membrane compromised (i.e. living) cells.[66] Morphological changes and reactive oxygen species generation have also been commonly observed using electron microscopy (e.g. TEM) and fluorescent probes (e.g. DCFDA), respectively, as in biological toxicity.[118, 119] Less common methods to assess the bacteria-nanoparticle interaction have included FT-IR for metabolic profiling[120] and mass spectrometry to characterize the binding of nanoparticles to bacterial surface proteins.[121]

Bacterial nanotoxicity has also moved to genetic methods such as quantitative-polymerase chain reaction (qPCR)[122] to observe targeted gene expression and terminal restriction fragment length polymorphism to assess community composition of naturally-sampled bacterial isolates.[68] More than any other model system, bacteria can be transfected easily, which has prompted studies to use genetically modified bacteria to understand the nanoparticle-bacteria interaction. In one specific example, Jiang *et al.* utilized a plasmid-based green fluorescent protein (GFP) *E. coli* bacterium to explore the impacts of TiO_2 nanoparticles. GFP fluorescence intensity was used as a measure of

viability but with a higher sensitivity to cell death than any of the previously mentioned microbiology techniques.[123]

While plants have some toxicity measures that are similar to bacteria, cells, and mammals (e.g. cell viability, oxidative stress, DNA damage, organism growth and morphology), there are also unique toxicity considerations. These unique phytonanotoxicity measures include assessment of: seed germination rates,[76, 78, 124] root elongation rates,[73, 78, 125] nitrogen fixation,[74] and soil enzyme levels.[72] All of these measures are done using traditional "by eye" assessment. In the current literature, there has been little analytical methodology innovation in studies of plant nanotoxicology.

Studies of nanoparticle toxicity to aquatic and terrestrial organisms mirror that of *in vivo* nanotoxicity studies, but unique consideration is given to embryo/larvae development[126, 127] and behavior.[128] As with plants, these assessments are typically done by manual inspection, though some species (i.e. *Caenorhabditis elegans*, *Danio rerio*, and *Daphnia magna*) are transparent for all or some of their development, making fluorescent labeling and quantification of specific biomarkers possible.

1.4.3 Uptake

Interpretation of toxicity results depends upon an understanding of how nanoparticles and the living systems interact. That is, it is important to quantify the number of nanoparticles to which cells are exposed as well as the amount of nanoparticles internalized or associated. A variety of techniques have been utilized to characterize uptake. For example, ICP-MS was used to probe the Au content of HeLa and A594 cells, cancer cell lines,[129] or zebrafish embryos exposed to Au nanoparticles.[130]

While ICP, with either MS or AES detection, allows easy sample preparation and quick results, it gives limited information about the cellular location of the nanoparticles, cannot distinguish between internalized or externally adherent nanoparticles, is applicable to only a subset of nanomaterial elements, and does not discriminate between nanoparticles and preexisting ions of the same element. Transmission electron spectroscopy (TEM) allows the location of the nanoparticles to be visualized as Dasari *et al.* showed Ag nanoparticle association with membranes of bacteria isolated from river water.[131] Monteiro-Riviere and coworkers also employed TEM to determine not only the location of quantum dots (QDs) but the behavior of the particles within the cell by examining nanoparticle aggregation as well.[132] Some of the advantages of TEM include the ability to determine internalized nanoparticle localization, concurrent characterization of nanoparticle and cell/tissue morphology, and complementary elemental analysis using spectroscopic methods. Conversely, TEM analysis of biological samples entails time-intensive preparation that may induce artifacts while providing only a static picture of a small sample population. In another technique, fluorescence microscopy has been employed to determine nanoparticle uptake. For example, Moghe and coworkers employed confocal fluorescence microscopy to evaluate the location of fluorescently-labeled micelles within individual cells.[133] Fluorescence spectroscopy offers highly sensitive measurements with time resolution, but requires confocal fluorescence techniques to determine nanoparticle localization. For nanoparticles that are not natively fluorescent, a tag or label is crucial that may alter nanoparticle characteristics and toxicity. While advancements are being made with TEM and confocal fluorescence microscopy, new techniques are also being employed to perform dynamic nanoparticle

tracking in cells.[53] As stated previously, understanding nanomaterial interaction (both amount and localization/association of nanoparticles) is essential for determining mechanisms of interaction, and the limitations of these common techniques necessitates the further development of new methods to assess nanoparticle uptake.

Whether using an *in vivo*, *in vitro*, or ecotoxicity approach, there is a wide variety of tools for assessing the impact of nanoparticles, and through these assessments, some mechanistic understanding of toxicity can be gained; however, the lack of a standard set of toxicological assessment methodology (i.e. model, dose, assay, uptake tool, controls, and data analysis) makes cohesive interpretation between results complicated and does not actively lead to understanding the nanoparticle-induced mode of toxicity.

1.5 Perspective

In the last decade, our understanding of the transformation, fate, and toxicity of engineered nanoparticles has expanded greatly, in part due to the strategic use of model systems and nanoparticles. However, there are still many scientific challenges in the study of nanoparticle toxicity. Many of these challenges center on the tension between understanding the mechanism of toxicity or the nanoparticle transformation as it relates to more complex whole organism or ecosystem models.

Increasing the complexity of a model system makes a functional assessment of fate, transformation, and toxicity difficult and presents the need for the development of toxicity methods to address this challenge. In particular, there is a large call to develop a toxicological methodology with specific *in vitro* techniques and models that are high-

throughput, reproducible (both intra and inter lab), as well as predictive of toxic response *in vivo*. In the realm of biological model systems, complex culture systems allow for more reliable results[61] and are worthy of further exploration. Although traditional toxicological assays have been found to correlate well with LD_{50} studies,[134] they have struggled to accurately predict more complex toxicological mechanisms during *in vivo* studies[61] and have yielded misleading results due to nanoparticle reactivity to the probe molecules *in vitro.*[135] While it is clear that we need new assessment tools to study nanotoxicity, the literature examples are shallow. In one example, efforts of Nel and coworkers to develop high throughput *in vitro* screening has yielded quick analysis of engineered nanoparticles that impact inflammation signaling pathways critical in toxic responses,[136] which may lead to more targeted *in vivo* screening of the nanoparticles with the most desirable response in the screening assay. In a less traditional approach, toxicity is examined without the use of a probe molecule by employing single-cell amperometry to explore biophysical characteristics of cells both with and without nanoparticle exposure.[10] Within econanotoxicity literature, few studies of cell/organism functional changes have been performed and only recently have more complex, multi-trophic level mesocosm studies been performed. For example, Ferry *et al*. followed the transportation and uptake of gold nanorods in an estuarine mesocosm where nanomaterials were introduced into the seawater, and viability and Au content was assessed for all organisms and compartments (i.e. water and sediment) using ICP-MS.[128] However, mesocosm studies rely only on viability and/or behavior as an assessment of toxicity and elucidating more nuanced views of toxicity (i.e. on a functional level) has the potential for providing a better mechanistic view of nanoparticle impacts. The gaps in assessment technology

for nanoparticles must be addressed in order to effectively address other areas of nanotoxicology, such as dosing.

Determining the dose of nanoparticles in biological toxicity assessments is complex, and inconsistency in describing dose, as is evident by the multitude of concentration units used for dose reporting, further complicates interpretation of toxicity. While a single unit of quantification will not be suitable in all cases, the nanotoxicology community would greatly benefit from a chosen preferred dosage unit relevant to the type of nanoparticle. In addition to accurate representation of nanoparticle dose, it is critical to explore nanoparticle uptake pathways, for both intentional and unintentional exposure. This exploration of uptake pathways relates directly to another challenge to create new instrumentation to measure possible exposure to nanomaterials through air and water, leading to "smart" nanosensors with the ability to detect potential exposure hazards and identify potential environmental and/or health reactions.[137] Clearly, this challenge will only be met with collaboration between scientists with expertise in instrument design and toxicologists. In addition, many more studies are needed on the topics of chronic exposure, biodistribution, clearance, and possible bioaccumulation of nanoparticles.

If nanotoxicology is ever going to achieve predictive capability, it is necessary to have a complete and accurate description of the nanoparticle within a realistic biological/ecological environment when performing toxicological assessment. The most common techniques used to characterize nanoparticles provide only a static picture of the nanoparticle (e.g. TEM, x-ray diffraction, or atomic spectroscopy) without consideration of the relevant biological environment. For example, characterization is either performed where the biological environment is ignored, in water or organic solvent alone or under

vacuum, or in oversimplified models systems, such as adding BSA to model protein coverage. New characterization methods are needed to study, for example, how protein adsorption (i.e. opsonization) on the surface of the particle or particle aggregation/agglomeration may impact the uptake/clearance mechanisms. Unfortunately, there are currently few techniques available for such analysis even though characterization of nanomaterials both before and during exposure is important for understanding mechanisms of toxicity.

The challenge of creating new nanotherapeutics and other nanoparticle-enabled products and making a realistic assessment of their toxicity will be optimally pursued with the collaboration of scientists from materials science, chemistry, biomedical engineering, medicine, ecology, and toxicology, with each scientist performing the task at which they are an expert. Provided the field can address the need for nanoparticle-specific toxicity assays, understanding and consistent expression of nanoparticle dosing, relevant controls and appropriate model systems, the full potential of nanoparticles can be safely realized.

1.6 Goals and Scope of Thesis

The goal of my thesis work is to employ sensitive analytical tools to fundamentally understand how nanoparticles interact with immunologically and ecologically relevant models. My project approaches nanotoxicity studies as detailed in Figure 1.3, starting with a relevant model system exposed to well-characterized nanoparticles to (1) determine if cells/organisms survive exposure using traditional toxicological assays and, (2) use sensitive analytical tools to determine if there are

changes to critical cell/organism function. If perturbation in function is detected, (3) the mechanism or cause of changes in cell function should be determined, including assessment of nanoparticle uptake and localization. Once a mechanism of interaction is determined, this process can begin again with a modified particle that may address the toxic response or an alternate model system to determine the generalizability of the toxic response.

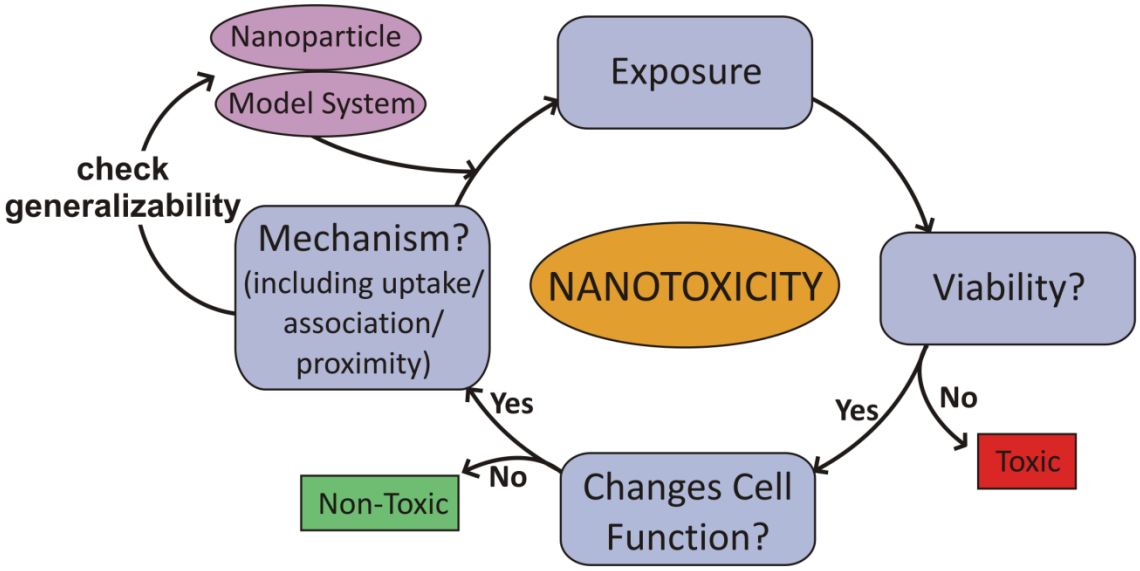

Figure 1.3 Summary of methodological approach to studying nanoparticle toxicity. Reprinted with permission from reference 138.

Chapter Two describes the impact of metal oxide (TiO_2 and SiO_2) nanoparticles on mast cells, critical immune system cells, and utilizes the sensitive technique of carbon-fiber microelectrode amperometry (CFMA) to monitor changes in the important mast cell function of exocytosis. Chapter Three expands upon Chapter Two and examines in more detail the mechanism by which TiO_2 nanoparticles impact exocytotic cell function,

completing the cyclical approach to nanotoxicity described in Figure 1.3. The generalizability of the mechanism of TiO_2 toxicity, as detailed in Chapter Two and Three, is explored in Chapter Four in a bacteria model, *Shewanella oneidensis.* Chapter Five works to develop an *in situ* Ag nanoparticle characterization tool using fluorous-phase ion selective electrodes to measure dissolved Ag^+, with preliminary investigation into the toxicity of Ag nanoparticles and Ag^+ ions to *S. oneidensis*. Moving beyond laboratory work, Chapter Six examines bench scientists' perspective on the regulation of nanotherapies moving from pre-clinical to first-in-human trials. Finally, Chapter Seven details the development of a 3-day nanotoxicity laboratory for introductory chemistry classes to introduce students to interdisciplinary science and the cutting edge research field of nanotoxicology.

Chapter Two

Functional Assessment of Metal Oxide Nanoparticle Toxicity in Immune Cells

This chapter adapted from:

M.A. Maurer-Jones, Y.-S. Lin, C.L. Haynes. Functional Assessment of Metal Oxide Nanoparticle Toxicity in Immune Cells. *ACS Nano*. **2010**, 4, 3363-3373.

2.1 Introduction

With the intense focus on nanomaterial development and the boom in the number of nanoparticle-enable commercially available products, the field of nanotoxicology has emerged in an effort to understand the interaction of nanomaterials with the environment and human physiology. Nanotoxicology faces many challenges as nanoparticles, with many novel properties, are placed into complex, dynamic biological systems.[1, 2] One challenge is the limitation in technology to characterize nanoparticles throughout their interaction with the biological system and to accurately quantify nanoparticle uptake location and concentration. Additionally, while a myriad of *in vivo* and *in vitro* nanotoxicity assessments have been performed to characterize the toxicology of engineered nanoparticles[1-3] many of the assessment methods were designed to study molecular toxicants, which likely have different cellular interactions than nanoparticles. The *in vitro* toxicity assays that are often employed for these studies do not necessarily accurately predict *in vivo* response,[4, 5] and they may fail in the presence of nanoparticles.[6-8] To overcome these limitations and gain a deeper understanding of nanoparticle-cell interactions, we have employed carbon-fiber microelectrode amperometry (CFMA) to explore fundamental questions regarding the impact of nanoparticles on the critical cell function of exocytosis.[9, 10] During exocytosis, a highly conserved cellular function across cell types and species, intracellular granules fuse with the plasma membrane and the granule contents are released, enabling communication between cells through secreted chemical messengers.[11] CFMA is a single-cell analysis technique that reveals a wealth of information regarding the biophysics of exocytosis, and

accordingly, changes in this critical cell function should nanoparticles interfere with any components of the exocytotic machinery.

One cell type well-known for exocytotic delivery of chemical messengers is the mast cell. Mast cells are found in many tissues of the body and play a critical role in immune system responses,[12, 13] making them a good model for nanotoxicity studies. To mimic an *in vivo* environment with the *in vitro* CFMA assay, we have chosen to co-culture primary murine peritoneal mast cells (MPMCs) with Swiss albino fibroblasts (3t3).[9, 10] Not only does this co-culture better simulate multi-cellular tissue, but it has also been demonstrated that the MPMC/3t3 co-culture allows the primary culture MPMCs to secrete more chemical messenger molecules and maintain their exocytotic cell function in culture for up to a month.[14]

While nanoscale particles can be fabricated with diverse elemental compositions, metal oxide nanoparticles are of particular importance based their widespread use in a variety of crystalline forms. Specifically, silica (SiO_2) and titanium dioxide (TiO_2) nanoparticles are the focus of this work because they are two of the most commonly used materials in commercially available products,[15] and both nanoparticles are the focus of much forward-looking research as well. SiO_2, while used as additives in various commercially available products, has also become a critical nanoparticle in biomedical and biotechnological fields. Particular attention has been paid to mesoporous SiO_2 composites because of their potential as a multifunctional template for diagnosis, imaging, targeting, and drug delivery.[16-18] The porosity of these particles drastically increases the total surface area, allowing for the presence of more reactive surface atoms that have the potential to contribute to cytotoxicity. Within the nanotoxicology

community, surface reactivity is of great concern as it is proposed to be a major cause of toxic response, likely through the production of reactive oxygen species.[19, 20] While it is thought that an increased surface area indicates an increase in surface reactivity because there are more surface atoms available to react with cells or the environment, there have been limited studies that directly monitor the impact that highly porous structures have on the toxicity of the nanoparticle.[21-24] Herein, we aim to understand the nanoparticle-cell interactions of the porous particles as compared to their non-porous counterparts by exposing immune system cells to Stöber and mesoporous SiO_2 of similar diameter.

The composition and crystallinity of a nanoparticle is also likely to influence impacts on cell health. To shed light on these effects, the biophysical ramifications of SiO_2 nanoparticles on exocytotic behavior were compared to those of another metal oxide, TiO_2. TiO_2 is commonly found in cosmetics,[25] including sunscreen, and has proven to be a particularly promising technology as a photocatalyst in pollutant remediation[26, 27] and photoactive material in solar cells.[28, 29] *In vitro* studies using traditional toxicological assays have shown that nanoscale TiO_2 induces oxidative stress, with anatase having larger impacts than rutile, decreasing cellular viability and causing cell death.[30-32] Herein, we will compare the impact of anatase TiO_2 nanoparticles on cellular exocytosis to the effects of the aforementioned SiO_2 material.

This work demonstrates that MPMCs differentially internalize nanoparticles with different porosities and composition and experience variation in extent of toxicity, as confirmed using traditional toxicological assays. Using CFMA on nanoparticle-exposed MPMC/3t3 co-culture, we reveal new insights regarding the biophysical impact of nanoparticles with varying porosity and material on exocytotic cell function of MPMCs,

illuminating details about how a surviving cell adapts to the presence of metal oxide nanoparticles.

2.2 Methods

2.2.1 Nanoparticle Fabrication

2.2.1.1 Stöber Non-porous SiO_2 Nanoparticles

Non-porous SiO_2 nanoparticles were synthesized using a modified Stöber method[33] as shown in related work.[34] Briefly, 0.75 mL of 28-30% ammonium hydroxide (Mallinckrodt, Phillipsburg, NJ) was added to 40 mL of 95% ethanol (Pharmco-Aaper, Brookfield, CT) held at 40 °C, followed by the addition of 0.5 mL tetraethyl orthosilicate (TEOS) (Sigma-Aldrich, Milwaukee, WI). The mixture was continuously stirred at 40 °C for 12 h to form the ultrafine SiO_2 nanoparticles. The nanoparticles were purified through centrifugation, rinsing with ethanol between centrifugation steps and finally stored in ethanol. Nanoparticles were rinsed and resuspended in calcium- and magnesium-free PBS (Sigma-Aldrich, Milwaukee, WI) for at least a week prior to exposure.

2.2.1.2 Mesoporous SiO_2 nanoparticles

Porous SiO_2 nanoparticles were prepared in highly dilute and base-catalyzed conditions as described in a paper by Lin *et al.*[35] Typically, 0.29 g of n-cetyltrimethylammonium bromide (CTAB, 99%) was dissolved in 150 mL of 0.128 M ammonium hydroxide solution at 60 °C. Then, 2.0 mL of 0.88 M ethanolic TEOS was added to the solution under vigorous stirring (600 rpm). After 1 h, the mixture solution

was aged for another 12 h. The as-synthesized colloids were transferred to 50 mL of ethanolic ammonium nitrate solution (6 g/L) and kept under stirring at 60 °C for 1 h to remove surfactants. The surfactant extraction step was repeated twice. The extracted nanoparticles were washed with ethanol twice and suspended in absolute ethanol. Nanoparticles were transferred and resuspended in PBS for a minimum of a week prior to exposure.

2.2.1.3 Non-porous TiO_2 Nanoparticles

Nanoparticles were synthesized in an acid-catalyzed sol-gel synthesis as described previously by Isley and Penn.[36] Briefly, 125 mL of isopropyl alcohol (BDH, West Chester, PA) and 12.5 mL titanium (IV) isopropoxide (Sigma-Aldrich, Milwaukee, WI) were stirred in an ice bath for 30 min after which 7.4 mL of 3.2 M nitric acid (BDH, West Chester, PA) was added drop-wise. The mixture was allowed to come to room temperature and then refluxed for 24 h. The as-synthesized nanoparticle suspension was dialyzed in regenerated cellulose tubing (nominal MWCO 3500, Fisher Scientific, Pittsburgh, PA) against Milli-Q purified water (Millipore Corporation, Burlington, MA) for 5 days, changing the water at least 10 times. Following dialysis, an aliquot of nanoparticle suspension was placed in an acid digestion bomb with water (3:5 nanoparticle suspension:Milli-Q water) and put in a 200 °C oven for 48 h.

2.2.2 Nanoparticle Characterization

TEM: Transmission electron microscope (TEM) images were taken on a JEOL 1200 EXII (JEOL, Tokyo, Japan) at 100 kV. Specimens were prepared by evaporating

one drop of ethanolic nanoparticle solution on a Formvar-coated copper grid (Ted Pella, Redding, CA).

XRD: Powder X-ray diffraction (XRD) for porous SiO_2 was performed on a Bruker-AXS D-5005 (Siemens) with Cu Kα radiation at 45 kV and 40 mA. Spectra were collected from 1.5° to 8° by step scan with a step size of 0.04° and a dwell time of 1.0 s. XRD of TiO_2 was performed on a PANalytical X'Pert Pro diffractometer (Almelo, Netherlands) with a high speed X'Celerator detector and a Co Kα radiation source at 45 kV and 40 mA. Spectra were collected from 25° to 95° by continuous scan with a step size of 0.017° and a dwell time of 250 s. TiO_2 phase compositions were determined by the Rietveld method[37] using X'Pert High Score Plus (version 2.0.1) software (PANalytical, Almelo, Netherlands) and the known crystal structures of anatase, brookite, and rutile as starting points. The parameters that were refined were the scale factor, specimen displacement, background, unit cell parameters, extinction coefficients, preferred orientation, and W, U, and V profile parameters.

Hydrodynamic diameter and ζ-potential analysis: Non-porous SiO_2, porous SiO_2, and non-porous TiO_2 were suspended in PBS (Sigma-Aldrich, Milwaukee, WI) at a concentration of 100 μg/mL. Hydrodynamic diameter was determined with dynamic light scattering (DLS - 90Plus) and ζ-potential was determined using ZetaPALS Zeta Potential Analyzer (Brookhaven Instruments Corporation, Holtsville, NY) with 5 runs, 10 cycles per run.

2.2.3 Cell Culture and Nanoparticle Exposure

3t3-Swiss albino fibroblasts, obtained from the American Type Culture Center (Manassas, MA), were grown in Dulbecco's Modified Eagle's Medium (HyClone, Logan, UT) with 4.5 g/L glucose, 110 μg/mL sodium pyruvate, and 4.00 mM L-glutamine and supplemented with 10% bovine calf serum (HyClone, Logan, UT), 100 μg/mL streptomycin, and 100 U/mL penicillin (Gibco, Carlsbad, CA). Fibroblast media was replaced every 2 days and cells were passaged every 3-4 days. Before experiments, fibroblasts were plated onto uncoated 35 mm Petri dishes and allowed to grow to confluence prior to the mast cell collection.

MPMCs were harvested from male wild type C57BL\6J mice (Jackson Labs, Bar Harbor, ME) by peritoneal lavage. Before the peritoneal lavage, mice were euthanized according to protocol #0807A40164 as approved University of Minnesota Institutional Animal Care and Use Committee. Then, 5 mL of cold growth culture media (same media and additives as described for fibroblast culture) was injected into the peritoneal cavity and the abdomen was vigorously massaged for 2 minutes to loosen the mast cells from the tissue. The media was recovered and the peritoneal cavity was rinsed twice with 2 mL of cold growth media. The collected media was centrifuged at 300g for 6 minutes to isolate the cells; the supernatant was removed, and the cells were resuspended in fresh, warmed growth media. Harvested MPMCs were then plated onto fibroblasts that had grown to confluence and allowed to set for at least 1 h without disturbance. Both the MPMC/3t3 co-culture and fibroblasts alone were kept at 37 °C with 5% carbon dioxide. The MPMC/3t3 co-culture was exposed to non-porous SiO_2, porous SiO_2, and non-porous TiO_2 passively for 24 hours through the addition of PBS-suspended nanoparticles

directly to the culture dish media so that the final nanoparticle concentration was 100 μg/mL, a median dose given in previous studies.[22, 38] Control exposures were performed by adding PBS to the cell culture in the same volume as the nanoparticle suspension to account for media dilution effects.

2.2.4 Nanoparticle Uptake: Biological TEM and ICP-AES

TEM: MPMCs were harvested, plated, and exposed to nanoparticles as detailed in the cell culture section, except that they were not co-cultured with fibroblasts. After 24 h exposure to nanoparticles, cells were removed from the plate through vigorous rinsing with media from the plate and collected by centrifugation at 555g for 5 min. Cell pellets were rinsed 3 times with 0.1 M sodium cacodylate buffer (Sigma Aldrich, St. Louis, MO), centrifuging at 89g between each rinse. Upon rinsing, cells were fixed using 2.5% glutaraldehyde (Sigma Aldrich, St. Louis, MO) in 0.1 M sodium cacodylate buffer for 1 h. Cells were post-fixed for 1 h using 1% osmium tetraoxide (Sigma Aldrich, St. Louis, MO) in 0.2 M sodium cacodylate buffer with minimal light exposure. The cells were dehydrated against a series of solutions with increasing ethanol concentration in water followed by exposure to propylene oxide (Sigma Aldrich, St. Louis, MO). Finally, samples were infiltrated with 50% propylene oxide/50% Epon resin for 2 h and subsequently 100% Epon resin for 48 h, refreshing the resin 5 times within the 48 h period. The resin was cured at 45 °C for 24 h followed by 60 °C for 48 h. Samples were sectioned using a diamond knife (Delaware Diamond Knives, Inc., Wilmington, DE) on an ultramicrotome (Reichert, Wien, Austria) into 60-nm-thick sections. The sections were collected and stained with uranyl acetate and lead citrate on Formvar-coated copper

TEM grids (Ted Pella, Redding, CA). Sections were imaged using a JEOL JEM-1200 EXII TEM (JEOL, Tokyo, Japan) with a 60 kV accelerating voltage.

ICP-AES: After harvesting and isolating the MPMCs from the peritoneal cavity, the cells were resuspended in RBC lysis buffer prepared in-house followed by at least 2 rinses with PBS. RBC lysis buffer solution of 0.15 M NH_4Cl (Sigma Aldrich, St. Louis, MO), 10 mM $KHCO_3$ (Sigma Aldrich, St. Louis, MO), and 0.1 mM EDTA (Acros Organics, Morris Plains, NJ) was made with Milli-Q water, pH adjusted to 7.3, and filtered. Finally, the cells were resuspended in warm, fresh growth media and plated at a density of 1 x 10^6 cells per well without fibroblasts in a 24-well plate. Nanoparticle exposures were performed in triplicate as described in the cell culture section at both 100 μg/mL and 200 μg/mL concentrations, after which wells were rinsed twice with PBS. Cells were removed from the well using a 0.25% trypsin solution (Gibco, Carlsbad, CA), and the sample volume was diluted to 5 mL with an aqueous acid solution (5%:1% HCl:HNO_3). Prior to injection onto the ICP-AES instrument, non-porous and porous SiO_2 samples were sonicated for 1 h. To complete the digestion of TiO_2 nanoparticles, an aliquot of cell-nanoparticle suspension was mixed in a 1:1 ratio with HF (Mallinckrodt Baker, Phillipsburg, NJ) and allowed to incubate overnight. A Perkin Elmer Optima 3000DV ICP-AES system (Waltham, MA) was used to measure Si and Ti content of the SiO_2 and TiO_2 samples, respectively, monitoring Si emission at 251.611 nm and Ti emission at 334.940 nm.

ICP-AES data, reported in mg/L, was converted to the number of nanoparticles internalized by the mast cells by first determining the mass of Si or Ti per

nanoparticle. The conversion of mg/L to nanoparticles per cell was completed according to Equation 2.1

$$(2.1)\quad \frac{nanoparticles}{cell} = \frac{ICP-AES\ result}{1000} \times volume\ of\ sample \times \frac{1}{mass\ of\ Si\ or\ Ti\ per\ particle} \times \frac{1}{cells\ per\ sample}$$

2.2.5 Hemolysis Assay

Whole, EDTA-stabilized, human blood was obtained from Memorial Blood Center (St. Paul, MN) and used within 3 hours of being drawn. First, 5 mL of blood was washed 5 times with 10 mL PBS, centrifuging at 10016g for 5 min between rinses, to isolate the RBCs, after which the RBCs were diluted to 50 mL with PBS. Then, 0.2 mL of RBC cell suspension was added to 0.8 mL of nanoparticle suspension with concentrations ranging from 12.5 to 400 μg/mL, mixed by vortexing, and incubated for 3 h at room temperature. PBS and Milli-Q water were used as negative and positive controls, respectively. After incubation, samples, all run in triplicate, were vortexed again followed by centrifugation at 10016g for 3 min. The samples' supernatants were transferred to a 96-well plate and optical density was measured at 570 nm with subtracted reference at 655 nm. The absorption at 570 nm is attributable to hemoglobin released upon rupture of the RBC. Hemolysis percentage was calculated using Equation 2.2.

$$(2.2)\quad hemolysis\ percentage = \left(\frac{sample\ abs - negative\ control\ abs}{sample\ abs - positive\ control\ abs}\right) \times 100$$

2.2.6 MTT Assay

MPMC/3t3 co-culture cells were plated on a 24-well plate and exposed to nanoparticles as described in the cell culture section. After a 24 h exposure time, cells were rinsed twice with PBS and incubated for 2 h in a 0.5 mg/mL MTT solution (Invitrogen, Eugene, OR) in growth media lacking bovine calf serum and antibiotics. The MTT solution was removed and 0.4 mL of dimethyl sulfoxide (Sigma Aldrich, St. Louis, MO) was added to dissolve the formazan crystals that form upon interaction with active mitochondria in live cells. Optical density of the samples was measured at 570 nm with a reference wavelength of 655 nm. Equation 2.3 was used to calculate the cellular viability:

(2.3) $$cell\ viability = \left(\frac{sample\ abs_{570} - sample\ abs_{655}}{control\ abs_{570} - control\ abs_{655}}\right) \times 100$$

2.6.7 Carbon-fiber Microelectrode Fabrication and CFMA

Carbon-fiber microelectrodes were fabricated as outlined by Wightman and co-workers,[39] where carbon-fibers of 7 μm diameter were aspirated into 4-inch glass capillaries (1.2/0.68 mm o.d./i.d.) and pulled with a micropipette puller (Narishige, Tokyo, Japan) to form a seal around the fiber. The fiber was secured using Epo-Tek 301 epoxy (Epoxy Technology, Billerica, MA), and electrodes were polished to a 45° angle using a diamond polishing wheel (Sutter Instruments, Novato, CA) and placed into isopropyl alcohol immediately before experiments. Electrodes were pretreated in a 0.1 M NaOH solution (Mallinckrodt Baker, Phillipsburg, NJ) by cyclically scanning from -0.4 V to 1.0 V versus Ag/AgCl (BASi, West Lafayette, IN) with a waveform frequency of 60

Hz for 15-30s. For the CFMA experiments, cell media was replaced with Tris buffer and the cell plate was maintained at 37° C by DH-35 Petri dish warmer (Warner Inst., Hamden, CT) on a Nikon Eclipse TE2000U inverted microscope (Nikon USA, Melville, NY). Tris buffer solution consisted of 12.5 mM Trizma hydrochloride (Sigma-Aldrich, Milwaukee, WI), 150 mM NaCl (Mallinckrodt Baker, Phillipsburg, NJ), 4.2 mM KCl (Mallinckrodt Baker, Phillipsburg, NJ), 5.6 mM alpha-D(+)-glucose (Acros Organics, Morris Plains, NJ), 1.5 mM $CaCl_2$ (Sigma-Aldrich, Milwaukee, WI), and 1.4 mM $MgCl_2$ (Sigma-Aldrich, Milwaukee, WI), with pH adjusted to 7.3 using NaOH. The carbon-fiber microelectrode was held at +700mV versus Ag/AgCl, which is sufficient to oxidize serotonin released from MPMCs, and placed directly on the surface of a single MPMC. To stimulate the MPMC to exocytose, a micropipette made from an empty 4-inch glass capillary pulled to a diameter of 15-20 µm and filled with 10 µM A23187 (Sigma-Aldrich, Milwaukee, WI), a calcium ionophore, was placed 20-100 µm from the cell of interest. A Picospritzer III (Parker Hannifan, Cleveland, OH) was connected to the stimulant micropipette that enabled projection of a 3 s bolus of the ionophore onto the cell. A LabView module (National Instruments, Austin, TX) and a break-out box made in-house were utilized for control of experimental parameters and data acquisition. Data were collected for 90 s, starting 3 s prior to stimulant projection. Electrodes were pretreated, as described above, after every cell and discarded after 6 cell measurements.

2.2.8 Amperometry Data Analysis

Amperometric traces were analyzed using MiniAnalysis Software (SynaptoSoft Inc, Fort Lee, NJ). A typical amperometric trace of MPMCs on fibroblasts contains ~150

current spikes where each spike reveals secretion from a single serotonin-filled mast cell granule.[14] The spike discrimination value was set at 5 times the root-mean-square of the current noise with an area threshold for each spike of 60 fC. Automated peak selection was performed followed by manual inspection of each spike to ensure accuracy of peak selection. The mean values of various spike parameters were combined for all cells within a given culture condition, excluding those cells with values 2 times the logarithmic standard deviation away from the logarithmic mean. While amperometric spike analysis reveals a myriad of information about the biophysics of exocytosis, two spike parameters of particular interest are the area under each spike (Q) and the amperometric spike half-width ($t_{1/2}$). Q can be used to determine number of molecules being released for each granule based on Faraday's law, Q=nFN, where Q is the charge, n is the number of electrons gained or lost in the oxidation or reduction reaction, F is Faraday's constant, and N is the number of moles of the secreted electroactive molecules. The $t_{1/2}$ reveals the rate at which granules expel their contents. Spike frequency indicates the efficiency with which a cell transports, initiates, and completes granule-cell membrane fusion. In all cases, amperometric traces were measured from a minimum of 16 cells in each condition and the average of the each cell's average spike parameter (Q and $t_{1/2}$ only since each cell trace yields a single frequency value) were compared using pairwise student's t-tests ($p<0.05$) (Microsoft Excel, Microsoft Corp, Seattle, WA). Significant changes in any of these parameters following nanoparticle exposure reveals not only nanoparticle-induced functional changes but also gives insight into the biophysics of these changes, creating the potential for informed nanoparticle redesign to control toxicity.

2.3 Results and Discussion

2.3.1 Nanoparticle Characterization

Non-porous SiO_2, porous SiO_2, and non-porous TiO_2 were synthesized and then characterized using transmission electron microscopy (TEM), x-ray diffraction (XRD), ζ-potential analysis, and nitrogen adsorption/desorption, with results summarized in Table 2.1.

Table 2.1 Nanoparticle characteristics.

Nanoparticle	Size (nm)	Total Surface Area (m^2/g)	Pore Volume (cm^3/g)	ζ-Potential (mV)	Crystallinity
Non-Porous SiO_2	24±3	127	-	-28.16	amorphous
Porous SiO_2	25±4	1164	0.92	-16.94	amorphous
Non-Porous TiO_2	11±5	234	-	-13.58	93.5% anatase 6.5% brookite

Based on TEM analysis (Figure 2.1), non-porous and porous SiO_2 are 24±3 (n = 220) and 25±4 nm (n = 250) in diameter, respectively, whereas the non-porous TiO_2 particles are 11±5 nm (n =306). While it would be ideal, for comparison purposes, for the non-porous SiO_2 and TiO_2 to be the same size, it is difficult to maintain the monocrystallinity of TiO_2 nanoparticles when they are larger than ~12 nm diameter.[40] The state of nanoparticle-nanoparticle association ahead of cell interaction is likely critical in determining extent of uptake. Herein, nanoparticles are considered to be agglomerated if they experience reversible adhesion whereas aggregation is considered to be the irreversible bonding of nanoparticles. Based on sonication of nanoparticle suspensions leading to a disassembly of nanoparticle groupings, it can be assumed that the studied nanoparticles are reversibly agglomerated. It is evident from Figure 1C and dynamic light scattering measurements (See Table 2.2) that the TiO_2 nanoparticles tend to agglomerate

more than either class of SiO_2 nanoparticles (Figure 2.1A & B); among the silica nanoparticles, the light scattering measurements indicate that porous SiO_2 agglomerates slightly more than non-porous SiO_2. Although it is common for these nanomaterials to be synthesized as aggregates, this study deliberately did not control this aggregation state because it reflects more relevant conditions of industrially produced material.

Table 2.2 Hydrodynamic diameter of SiO_2 and TiO_2 nanoparticles in PBS after ultrasonication.

Nanoparticle	Hydrodynamic Diameter (nm)
Non-porous SiO_2	555.19
Porous SiO_2	796.72
Non-porous TiO_2	1054.98

The XRD analysis of crystallinity showed that the non-porous and porous SiO_2 particles are amorphous but the non-porous TiO_2 particles are crystalline, with 93.5% anatase and 6.5% brookite composition as determined by the Rietveld method of refinement.[37] Using BET modeling of nitrogen adsorption/desorption isotherms to determine total nanoparticle surface area, the porous SiO_2 nanoparticles have a considerably higher surface area (1164 m^2/g) than the non-porous SiO_2 (127 m^2/g). The increased surface area can be attributed to the porous nature of the nanoparticles; however, the majority of the surface area in the porous nanoparticles is on the inside of the cylindrical pores and therefore, there is a limited contactable surface area for cell-bound molecules and proteins to interact. In fact, since the non-porous and porous SiO_2 are of similar size, it can be assumed that the non-porous SiO_2 has a greater external surface that is accessible to cells than the porous nanoparticles because the pores decrease the external surface area.[24] The calculated surface area of the non-porous TiO_2 was 234 m^2/g and presents a

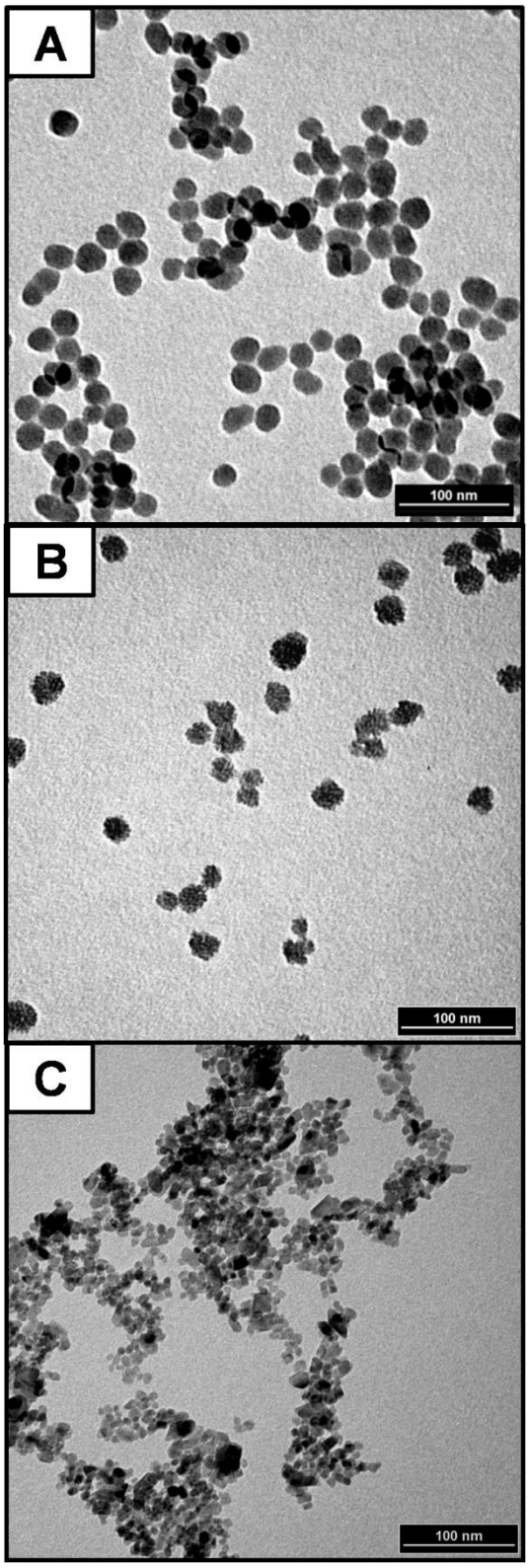

Figure 2.1 TEM images of (A) Stöber non-porous SiO_2, (B) porous SiO_2, and (C) non-porous TiO_2.

solid surface comparable to the non-porous SiO_2, facilitating comparison between the effects of SiO_2 and TiO_2 surfaces. All ζ-potentials were negative, indicating relative stability within a suspension. TiO_2 has the lowest magnitude ζ-potential, which is consistent with TiO_2 nanoparticles having the greatest extent of agglomeration, followed by porous SiO_2 and then non-porous SiO_2. Because all three classes of nanoparticles have a ζ-potential with smaller magnitude than -30 mV, they are considered to have a similar relative stability,[41] making aggregation state an unlikely determinant of cellular toxicity. While the aforementioned characteristics are the best estimate of the state of the nanoparticles as 'seen' by the cells, it is likely that the surface of the nanoparticle will change en route to and following cellular uptake.[19, 42]

2.3.2 Nanoparticle Uptake

To accurately assess nanoparticle impact on cell function, it is essential to first characterize the internalization of nanoparticles. In the literature, nanoparticle uptake has been shown to depend on nanoparticle size and surface chemistry.[43-45] Herein, TEM was employed to qualitatively characterize nanoparticle uptake while atomic emission spectroscopy (ICP-AES) was used to quantify nanoparticle uptake. Using TEM after a 24 h exposure to 100 μg/mL nanoparticles, the nanoparticles are apparent within the cell regardless of the particle type, and generally seen localized within the secretory granules of the MPMCs (Figure 2.2). Based on the TEM images, neither non-porous nor porous SiO_2 nanoparticles tend to agglomerate outside the cell during uptake; however, the TiO_2 nanoparticles are seen both inside and outside the plasma membrane in agglomerates of tens of nanoparticles. Qualitatively, the TEM images of non-porous TiO_2 uptake indicate

that about half of the nanoparticles are taken up by the MPMCs. Because sectioned TEM images are not appropriate for quantitation, the complementary technique of ensemble-averaged atomic spectroscopy has also been employed herein.

ICP-AES allows for quantification of cellular nanoparticle uptake by detection of titanium or silicon atomic emission, which can be converted to the number of nanoparticles internalized by each cell as described in the experimental section and supporting information. From the results shown in Table 2.3, where cells were exposed to nanoparticles in varying concentrations (100 and 200 μg/mL) for 24 h, we observed that cells take up significantly ($p<0.05$) more nanoparticles when exposed to higher concentrations. It follows that decreasing the exposure concentration would likely yield a decrease in the number of nanoparticles internalized by the cells. This supports many literature examples where an increase in nanoparticle dose has a greater influence on cell function and viability.[21, 22, 46] The ICP-AES data also reveal that nanoparticles are internalized differently based on the type of nanoparticle. It is readily apparent that mesoporous SiO_2 is more efficiently incorporated into cells than its non-porous counterpart of the same size, potentially due to a higher degree of agglomeration. This result is similar to a recently published paper where the authors showed that mesoporous SiO_2 nanoparticles exhibited higher cellular labeling efficacy than non-porous SiO_2 nanoparticles.[47] In addition, it appears that the smaller diameter and higher degree of agglomeration of the TiO_2 nanoparticles facilitate more extensive interaction with the cells than either of the SiO_2 nanoparticle classes; however, because ICP-AES data does not reveal nanoparticle localization within a cell, much of this could be due to

extracellular adhesion rather than internalization. Even if, as indicated by TEM, half of the TiO_2 nanoparticles are outside the cell, TiO_2 uptake is still more efficient than either of the SiO_2 nanoparticle classes considered at both 100 and 200 µg/mL concentrations ($p<0.05$).

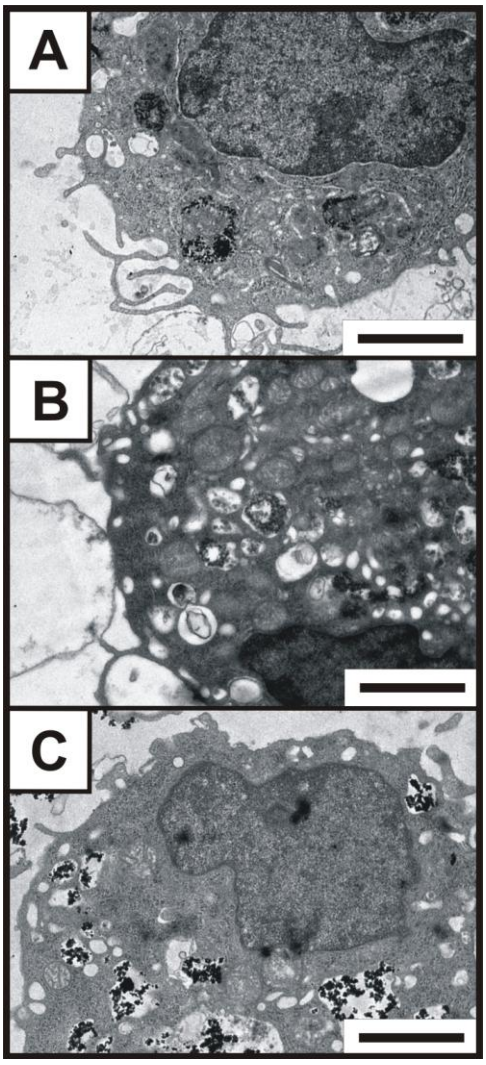

Figure 2.2 TEM images of MPMCs used in experiments showing nanoparticle uptake after 24h exposure to 100 µg/mL of (A) non-porous SiO_2, (B) porous SiO_2, and (C) non-porous TiO_2 nanoparticles. Nanoparticles appear to localize within the granules. Each scale bar = 2µm.

Table 2.3 ICP-AES uptake data in MPMCs after 24h exposure to 100 μg/mL and 200 μg/mL non-porous SiO_2, porous SiO_2, and non-porous TiO_2. All nanoparticle types are internalized significantly different than the others ($p<0.05$), and MPMCs internalize nanoparticles at 100 μg/mL significantly less than when cells are exposed to 200 μg/mL ($p<0.05$).

Nanoparticle	100 μg/mL Dose (nanoparticles/cell)	200 μg/mL Dose (nanoparticles/cell)
Non-Porous SiO_2	4.5×10^4	1.1×10^7
Porous SiO_2	2.0×10^5	3.5×10^7
Non-Porous TiO_2	7.2×10^7	1.5×10^8

The combined picture of TEM-based localization information and ICP-AES nanoparticle count reveals important trends about cellular uptake of nanoparticles in and of itself. More important to this work, however, is the ability to correlate nanoparticle uptake with both cell viability and cell function.

2.3.3 Effects of Porosity and Surface Area

Studies have shown that mesoporous SiO_2 induces varying degrees of toxicity. That is, *in vitro* viability assays have shown decreased cell viability upon exposure to mesoporous SiO_2.[21-23] It has also been demonstrated that mesoporous SiO_2 inhibits cellular and mitochondrial respiration[48] and causes oxidative stress within the exposed cells.[49] To our knowledge, however, these studies have not isolated the variable of porosity on the effects of toxicity and therefore are missing important information on a nanoparticle class with growing use.

To examine the impact of nanoparticle porosity on cellular toxicity, the mast cells were exposed to one of two types of SiO_2 nanoparticles, where the only significant difference between the types was the porosity. Overall viability was measured by monitoring hemolysis of isolated human red blood cells (RBCs) as well as mitochondrial

activity in mast cells. The hemolysis behavior (Figure 2.3) is significantly different, with the non-porous SiO_2 particles damaging RBCs at much lower concentrations than their porous counterparts. In fact, 50% hemolysis requires 270 µg/mL porous SiO_2 but only 20 µg/mL non-porous SiO_2. Similarly, the MTT (3-(4,5-dimethylthiazol-2-yl)-2,5-diphenyltetrazolium bromide) viability assay reveals that porous SiO_2 nanoparticles do not influence mast cell viability (compared to control cells) but that cell viability drops significantly to 72% in the presence of non-porous SiO_2 of the same dose (100 µg/mL) (Figure 2.4). In both cases, it is clear that at least a portion of the mast cells survive nanoparticle exposure for functional assessment.

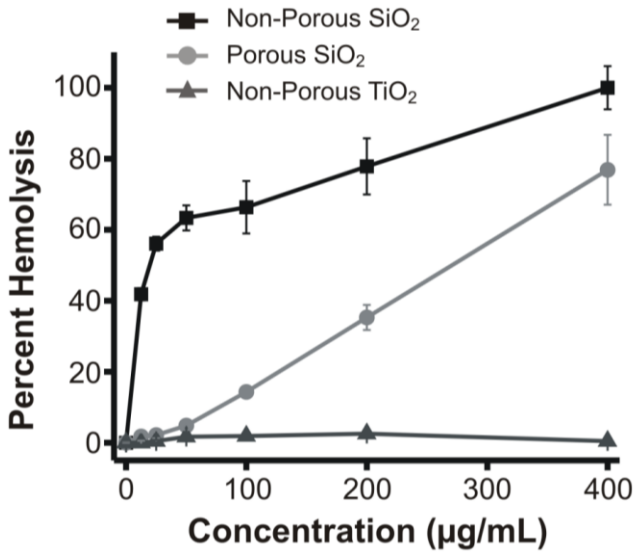

Figure 2.3 Hemolysis after 3 h exposure to varying concentrations of non-porous SiO_2, porous SiO_2, and non-porous TiO_2 nanoparticles. Both non-porous and porous SiO_2 nanoparticles cause a concentration-dependent lysis of RBCs. Non-porous TiO_2 induces minimal to no hemolysis in RBCs (n = 3).

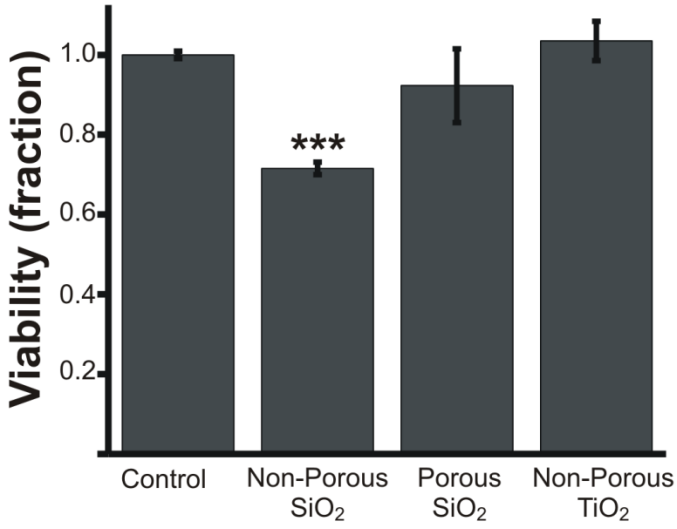

Figure 2.4 MPMC/3t3 cell viability, as measured with the MTT assay, following exposure to different conditions: control, 100 µg/mL non-porous SiO_2 nanoparticles, 100 µg/mL porous SiO_2 nanoparticles, and 100 µg/mL non-porous TiO_2 nanoparticles for 24 h. *** indicates $p<0.005$ ($n = 4$) compared to the control ($n=4$).

To reveal potential functional changes in surviving nanoparticle-exposed mast cells, real-time measurement of exocytotic function was performed following cell exposure to either porous or non-porous SiO_2 nanoparticles. Representative amperometric traces from the MPMC/3t3 co-culture can be seen in Figure 2.5. Analyzing the spike parameters, it is clear that both non-porous and porous SiO_2 cause a decrease in amperometric spike area (Figure 2.6A). That is, there is a 23% and 22% decrease in the number of molecules released from an average granule during MPMC exocytosis when exposed to non-porous and porous SiO_2 nanoparticles, respectively. This difference corresponds to a drop from an average of 1.09×10^7 serotonin molecules per granule to 8.40×10^6 and 8.42×10^6 serotonin molecules per granule, respectively. Interestingly, the porous and non-porous SiO_2 nanoparticle-exposed cells are not distinguishable from one another ($p>0.05$) in regard to the number

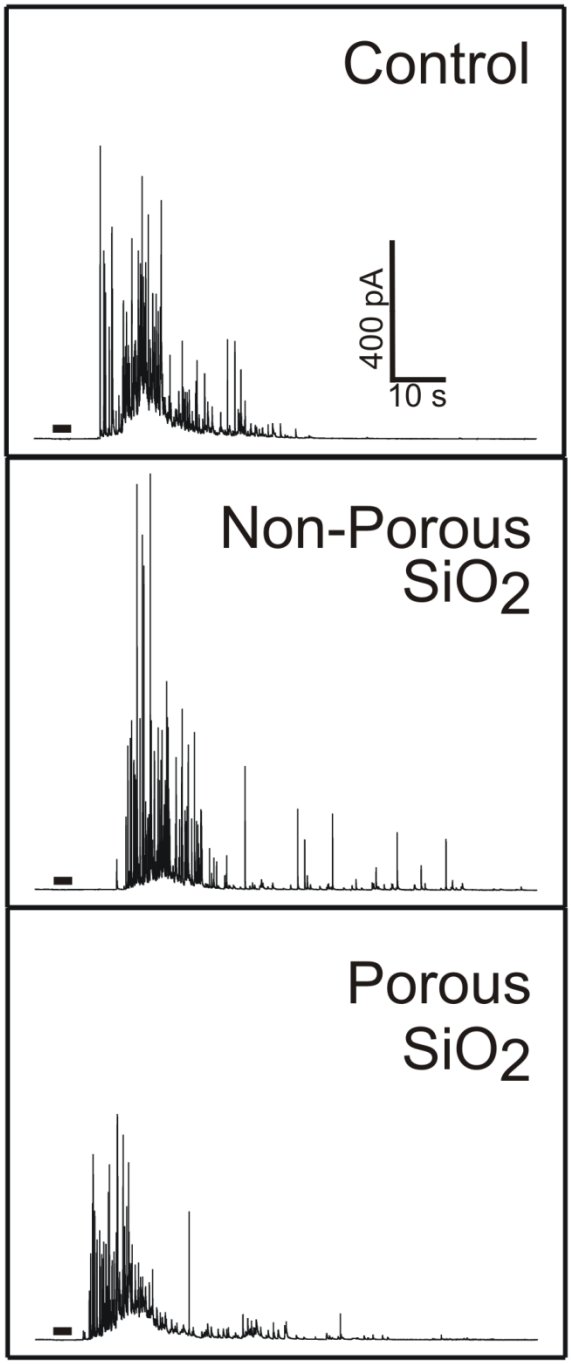

Figure 2.5 Representative amperometric traces from MPMCs co-cultured with 3t3 fibroblast following exposure to different conditions: control, 100 µg/mL non-porous SiO_2 nanoparticles, and 100 µg/mL porous SiO_2 nanoparticles for 24 h. The bold line on each trace indicates the three second bolus of stimulant delivered to the cell. Traces were chosen that best represented averages per condition.

of chemical messenger molecules released, suggesting that it is the nanoparticle itself, not the porosity, that induces a change in chemical messenger storage/delivery. While neither non-porous nor porous SiO_2 nanoparticles significantly alters the kinetics of individual granule fusion or molecule secretion (i.e. no significant change in the $t_{1/2}$) (Figure 2.6B), the non-porous particles do cause a significant alteration to the frequency of granule release (decrease of 18%) as compared to the control (Figure 6C), indicating some disruption of granule trafficking, docking, or lipid membrane fusion that is avoided when mesoporous nanoparticles are used instead. While this characteristic of depressed molecular secretion is similar to that measured in previous work with Au nanoparticle-exposed mast cells,[10] the lack of a correlated change in kinetics suggests that the presence of SiO_2 nanoparticles influence the serotonin content of the granule rather than the heparin proteoglycan sulfate matrix' ability to unfold and release the serotonin. In addition, the alteration of secretion frequency suggests that non-porous SiO_2 nanoparticles interfere with the cytoskeletal machinery, fusion machinery, or membrane characteristics; this interference is unprecedented in measurements made using Au nanoparticles. Therefore, it is clear that non-porous SiO_2 particles have an overall greater impact on the cell function of MPMCs than either their porous counterpart or non-porous Au nanoparticles of similar size. These data suggest that both surface chemistry and surface area influence nanoparticle toxicity. Surface area is generally considered to be one of the greatest contributors to nanoparticle toxicity with an oft made simple assumption that larger surface area leads to more toxicity;[50, 51] however, the results presented herein indicate that porous particles, with large internal surface areas, defy this trend. The more relevant measure is cell-contactable surface area, or the area with which

cell membrane, cell-bound proteins, and cell-associated molecules can interact. While small, liberated proteins and molecules may adsorb within the nanoparticle, only cell-bound species are of interest in this case because they are involved directly in the exocytosis function. For these cell-bound species to adsorb into the pores of the mesoporous SiO_2, the nanoparticle and cell would have to align perfectly and even then, the contactable surface by these species is minimal. Therefore, it appears that the greater external, cell contactable surface area of the non-porous SiO_2 yields a greater impact on cellular function. A comparison of the hemolytic activity between non-porous and porous SiO_2 nanoparticles of varying size also concludes that nanoparticle toxicity correlates to the cell-contactable surface area as opposed to total surface area.[35]

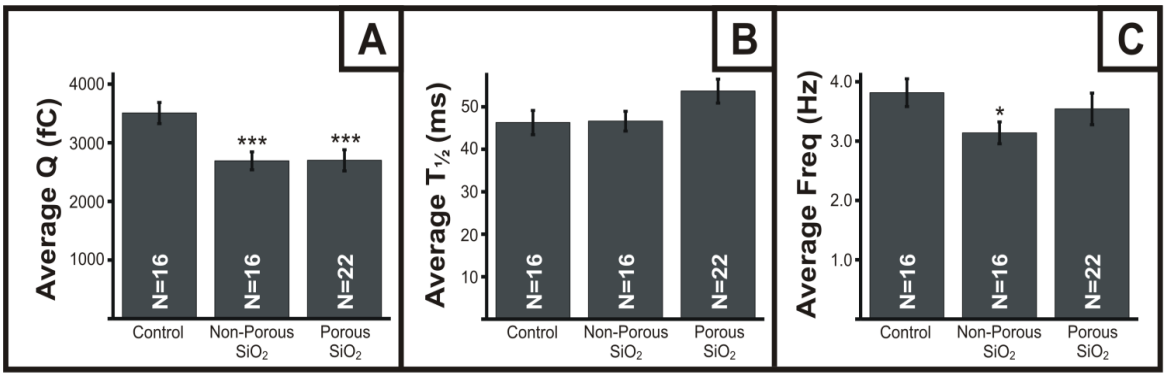

Figure 2.6 Average amperometry spike parameters from MPMCs in a co-culture with 3t3 fibroblast after 24 h exposure to control conditions, 100µg/mL non-porous SiO_2 nanoparticles, and 100µg/mL porous SiO_2 nanoparticles. A) Exposure to both non-porous and porous SiO_2 nanoparticles cause a decrease in average spike area (Q) as compared to control conditions, but B) do not affect the average half-width ($t_{1/2}$) of the amperometric spikes. C) Non-porous SiO_2 causes a decrease in frequency of spike release as compared to the control. Error bars represent SEM and * indicates $p<0.05$ and *** indicates $p<0.005$.

2.3.4 Material Effects

Based on the apparent differences between the Au nanoparticles explored in previous work[9, 10] and the SiO_2 nanoparticles included herein, a similar set of analyses were also employed to further explore the impact of nanoparticle composition on cell function with crystalline TiO_2 nanoparticles. It can be seen from the hemolysis assay (Figure 2.3) that non-porous SiO_2 nanoparticles cause the greatest percentage of RBC lysis and non-porous TiO_2 particles demonstrate almost no impact on RBCs. The difference in hemolytic activity between non-porous SiO_2 and non-porous TiO_2 is an early indicator the material in contact with the cell plays a critical role in toxicity. The MTT assay was performed on the MPMC/3t3 co-culture following TiO_2 exposure (Figure 4), and the results reveal that non-porous TiO_2 nanoparticles do not affect the viability of the cells, despite the significantly enhanced cellular uptake of the smaller TiO_2 nanoparticles compared to the larger SiO_2 nanoparticles. However, in a comparison between non-porous amorphous SiO_2 and non-porous crystalline TiO_2, we see different effects on the biophysics of exocytosis in a MPMC/3t3 co-culture after 24 h exposures at the same mass concentration. Figure 2.7A shows that SiO_2 causes a significant decrease in Q, or the number of molecules released, but Q is maintained after exposure to TiO_2 as compared to the control. Conversely, TiO_2 causes a 17% slowing in the kinetics of chemical messenger release (i.e. larger $t_{1/2}$) as can be seen in Figure 2.7B, whereas SiO_2 does not alter this biophysical property. This change in kinetics of secretion may be due to the fact that TiO_2 has a higher affinity for protein adsorption than SiO_2,[52] and since MPMC granules contain many proteinaceous mediators,[53] internalized TiO_2 delays

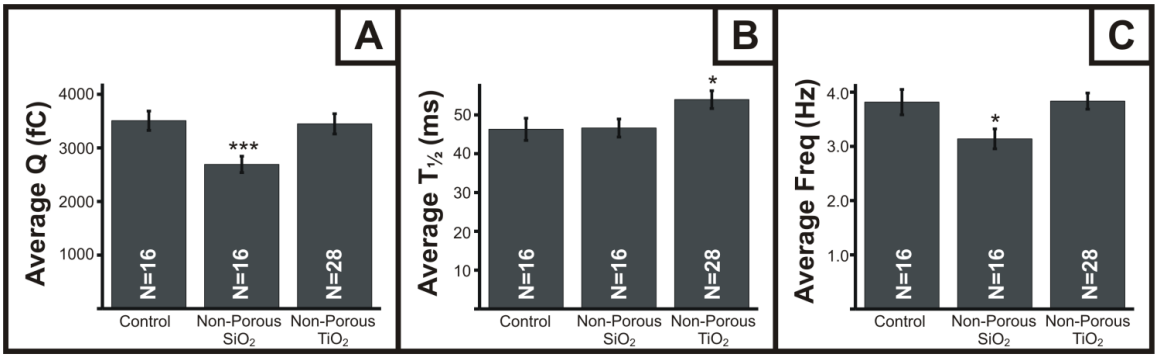

Figure 2.7 Average amperometry spike parameters for MPMC/3t3 co-culture after exposure to control conditions, 100µg/mL non-porous SiO_2 nanoparticles, and 100µg/mL non-porous TiO_2 nanoparticles. A) Non-porous SiO_2 nanoparticles cause a decrease in the spike area (Q) as compared to the control, whereas non-porous TiO_2 does affect the number of molecules released. B) Non-porous TiO_2 significantly increases the average half-width ($t_{1/2}$) of spikes but non-porous SiO_2 does not as compared to the control. C) Non-porous SiO_2 significantly decreases the average spike frequency as compared to the control. Error bars represent SEM and * indicates $p<0.05$ and *** indicates $p<0.005$.

content release from the granules. It also appears, based on the unchanging granular secretion frequency (Figure 2.7C), that the TiO_2 nanoparticles do not alter the cellular machinery that controls granule transport, docking, or fusion unlike their non-porous SiO_2 counterparts. Based on the varying biophysical response from MPMC/3t3 co-culture, it can be concluded that the mechanism of interaction between nanoparticles and cells is dependent on the material, which has been implicated in other studies.[54, 55] This difference likely arises from the difference in surface chemistry between particles of different composition, due in part to the surface species (hydroxyl/water groups for TiO_2[56, 57] and silanol for SiO_2),[58] the surface atoms (Ti or Si), and the structure in which they are present on the surface of nanoparticles (highly ordered for anatase crystals and amorphous in the case of SiO_2). More work is being pursued on a variety of other materials with systematically varied properties in order to arrive at more generalizable conclusions about the toxicity of nanomaterials. Towards this goal, work will be aimed

at understanding the mechanism of impact the nanoparticle have on cell function such as determining the concentration of reactive oxygen species present upon nanomaterial exposure.

2.4 Conclusions

Safe implementation of nanotechnology requires an intimate understanding of biological-materials interactions. A significant portion of nanotoxicology effort has focused only on *in vitro* cell survival following nanomaterial exposure. The work presented herein goes one major step further, examining cell function in cells that have survived the internalization of metal oxide nanoparticles. With an *in vitro* MPMC/3t3 co-culture, we have demonstrated that non-porous SiO_2, porous SiO_2, and non-porous TiO_2 are internalized by the cells and interfere with cell function. From CFMA results, non-porous SiO_2 causes the greatest impact on exocytotic cell function through a decrease in molecules released per exocytotic granule and a decrease in the frequency of release as compared to porous SiO_2. Common viability assays support this trend as both MTT and hemolysis assays show non-porous SiO_2 having a greater impact on cells. Our results indicate that, while other properties may have toxic impacts, a major feature in predicting nanoparticle toxicity is the external surface area of the nanoparticle, and that while porous SiO_2 are more readily taken up by cells, there is less cell-contactable reactive surface area to perturb cell function.

Not only is the area of reactive surface available important for understanding nanoparticle toxicity, our results suggest that the surface chemistry is also critical in determining the nanoparticle-cell interaction. That is, SiO_2 causes significant impact on cell viability and hemolysis as well as disturbing the exocytotic cell

function. Interestingly, however, while TiO_2 does not appear to affect the toxicity as predicted with the traditional ensemble assays, it is internalized by cells and causes changes in the exocytotic cell function. In addition to supporting the role of surface chemistry in determining the nanoparticle-cell interaction, these data support the need for alternative methods of assessing cellular impact of nanoparticles as the bulk assays did not reveal the altered cell function. Along with developing CFMA as a toxicological tool, continued work is needed to understand the causes of change in exocytotic cell function so that we may better control nanoparticle toxicity.

Chapter Three

TiO_2 Nanoparticle-Induced ROS Correlates with Modulated Immune Cell Function

This chapter adapted from:

M.A. Maurer-Jones, J.R. Christenson, C.L. Haynes. TiO_2 Nanoparticle-Induced ROS Correlates with Modulated Immune Cell Function. *J. Nanopart. Res*. **2012**, (in press).

3.1 Introduction

With ever increasing human exposure to nanoparticles in commercially available products, the need to understand the interaction of nanoparticles with biological systems continues to increase in urgency. Toxic response to nanoparticles will best be avoided if there is a fundamental understanding about which nanoparticle characteristics elicit such responses, and this includes not only examining cell viability after exposure but also changes in function of those cells that survive and determining the mechanisms of function perturbation.[1] It is likely that some common mechanistic disruptions will emerge, facilitating the possibility of toxicity prediction for nanoparticle classes and thus potential design rules for safe nanomaterials.

The cellular function under consideration in this work is regulated exocytosis, the process where, upon stimulation, cells secrete chemical messenger molecules to the extracellular space. Due to its conservation among many cell types and species, exocytosis function is a good candidate for drawing systematic conclusions. Additionally, exocytosis is a critical cell function for cells within the body to communicate with other cells, and studies of exocytosis have implications for whole organism health. Examples where changes in exocytosis resulted in disease include diabetes with decreased levels of exocytosed insulin[2, 3] and Crohn's disease, where an increased number of the exocytotic enterochromaffin cells contributes to the autoimmune inflammatory response.[4] Exocytosis is also critically important in the cascade of signaling molecules used in the immune system (e.g. during inflammation); if the signaling events are perturbed, there is the potential for dysfunction in the body's ability to respond to a substance and this could cause harm. Within the immune system

response, mast cells play a particularly important role. They are most commonly known for their role in allergies and inflammation and are often tasked with pathogen recognition and response,[5] which they achieve via the secretion of proteins, lipids, and other small messenger molecules during exocytosis.[6] In addition to their contribution in the immune system's first line of defense, mast cells are found throughout the body, and nanoparticles would likely encounter these cells in all exposure pathways (i.e. inhalation, injection, ingestion, and transdermal). Understanding the impact of nanoparticles on mast cells yields an understanding of the immunogenicity of the nanoparticles, which is critical for assessing the impact nanoparticles have on human health.

The secretion of molecules from mast cells can be measured in real time using carbon-fiber microelectrode amperometry (CFMA); this method has many advantages that address some of the aforementioned *in vitro* assay limitations. In CFMA, a carbon-fiber microelectrode is placed on the surface of a single cell, and electroactive mediators released from the cell are oxidized at the electrode surface, causing current transients. This technique enables a fast (i.e. submillisecond resolution), dynamic, and extremely sensitive (i.e. limit of detection of ~ 5000 molecules) measurement from single cells within a heterogeneous cell population.[7] Not only does CFMA give rich information regarding the biophysics of exocytosis in cells that survive nanoparticle exposure, but it is also unaffected by the presence of nanoparticles as demonstrated by previous work in our group.[8-11] The work presented herein utilizes CFMA to explore the toxicity and exocytotic impact of a commonly used nanomaterial, TiO_2.

TiO_2 nanoparticles are among the most produced nanomaterials, incorporated into a variety of everyday and nanotechnology-enabled products and

applications.[12] Applications for TiO_2 nanoparticles range from colorant additives in food and cosmetics[13] to more innovative applications as heterogeneous catalysts.[14] TiO_2 nanoparticles are also good photocatalysts, where under ultra-violet (UV) illumination, the nanoparticle becomes a strong oxidizing agent with the ability to oxidize many organic and biological molecules through the production of free radical species or reactive oxygen species (ROS).[15, 16,17] Evidence suggests that TiO_2 nanoparticles,[18] as well as their products after UV exposure, amplify damage to cells via a ROS-mediated mechanism.[19] Functional toxicity studies on various nanoparticle types have implicated ROS as one cause of decreased cell function and viability,[20-22] including studies of TiO_2 nanoparticles' impact on dendritic cell function in a simulated immune system[23] and fibroblast stiffness.[24] The extent of oxidative stress can be determined directly through measurement of ROS molecules and/or indirectly through measurement of oxidative stress markers such as glutathione and superoxide dismutase activity and compared to viability results from other bulk cell assays.[25, 26] However, no studies to date have correlated the effect of nanoparticle-induced ROS to dynamic cell function perturbation. The work presented in this study aims to accomplish this by correlating the presence of intracellular ROS to the dynamically measured cellular function of exocytosis, thereby addressing the mechanism component of the aforementioned fundamental studies for nanotoxicity, making use of uptake and localization studies done in previous work.[8]

Elevated levels of ROS caused by internalized nanoparticles are known to influence cell viability, as measured with traditional toxicological assays;[25-27] we, therefore, hypothesize that TiO_2 nanoparticle-induced ROS will impact the biophysics of exocytosis where increased ROS causes greater changes to exocytotic parameters.

Herein, we report the oxidative stress impact of TiO_2 nanoparticles on primary culture mast cells using assays that measure ROS, and we correlate these data with exocytotic functional assessment. Since TiO_2 is commonly known to generate ROS upon UV light illumination, we also utilized UV light to induce greater ROS within cells exposed to nanoparticles to further explore TiO_2 nanoparticle-induced oxidative stress impacts on exocytosis. Results implicate ROS as a likely cause of toxicity and functional impairment to immune system cells induced by exposure to nanomaterials.

3.2 Methods

3.2.1 Nanoparticle Synthesis and Characterization

TiO_2 nanoparticles were synthesized and characterized as previously described in Section 2.2 using an acid-catalyzed sol-gel method.[8] Briefly, the TiO_2 nanoparticles were 11 nm in diameter and monocrystalline, a characteristic of TiO_2 nanoparticles shown to influence toxicity.[28] The crystallinity was 93.5% anatase and 6.5% brookite.[8] Aggregation, agglomeration, or flocculation was not controlled during the experiment because this characteristic would likely not be controlled in unintentional TiO_2 exposure, though aggregation/agglomeration is influenced by many environmental factors, including salts, proteins, and temperature,[29, 30] which in turn may affect cellular upake.[31] Though not controlled, the aggregation/agglomeration was studied over 24 h, the time of the experiments, by taking periodic dynamic light scattering (DLS) measurements of 100 µg/mL samples in H_2O, PBS, and cell culture medium.

3.2.2 Cell Culture and Nanoparticle Exposure

MPMC/3t3 cell culture and nanoparticle exposure were performed as described in section 2.2.3. Briefly, 3t3 Swiss albino fibroblasts (3t3) were plated on 35 mm Petri dishes at least 3 days prior to experiments to ensure cells had grown to confluence before introduction of MPMCs. MPMCs were obtained through a lavage of the peritoneal cavity of male, wild-type C57BL\6J mice (Jackson Laboratories, Bar Harbor, ME) immediately after euthanasia according to protocol #0807A40164, as approved by the University of Minnesota Institutional Animal Care and Use Committee. Cells were plated on a confluent layer of 3t3s, and the co-culture was maintained in a 37 °C incubator in a 5% carbon dioxide environment.

24 h prior to experimentation, the MPMC/3t3 co-cultured cells were passively exposed to 100 µg/mL TiO_2 nanoparticles from a suspension of nanoparticles in PBS that were sonicated prior to exposure. Control cells were exposed to PBS in the same volume as the added TiO_2 nanoparticle suspension. This 100 µg/mL dose, while high for an acute exposure, enables a functional assessment of nanoparticle-cell interaction and is in agreement with doses used in previous studies. In addition, it could potentially model the effects of multiple exposures and/or bioaccumulation.[32] After 23.5 h of exposure, the cells were rinsed twice with PBS (Sigma-Aldrich, Milwaukee, WI) followed, in some cases, by 20 min exposure to 365 nm UV light (Spectronics Corp, Westbury, NY) placed approximately 10 cm above the culture dish (irradiance of 14.5 J/m^2 determined experimentally). UV light exposure was performed at the end of the 24 h nanoparticle incubation to ensure nanoparticle uptake, and a 20 min exposure time was chosen based on CFMA experimental constraints, as described in the section 2.2.7. Control conditions

entailed adding PBS to the growth media in the same volume as the nanoparticle suspension to account for media dilution effects. Additionally, some cells cultured in control conditions were also exposed to 20 min UV light as described above. For experiments using N-acetylcysteine (NAC), cells were exposed to 1 mM N-acetylcysteine amide (Sigma Aldrich, St. Louis, MO) at the same time as cells were exposed to TiO_2 nanoparticles.

3.2.3 MTT Assay

Mast cell viability after nanoparticle exposure was assessed using the ensemble viability MTT assay. Prior to MTT experiments, it was confirmed that TiO_2 nanoparticles did not cause false positives by incubating nanoparticles with a 0.5 mg/mL MTT solution, and no interference was observed (data not shown). The MPMC/3t3 co-culture was plated within a 24-well plate, and exposures to nanoparticles or control conditions and UV light were performed as described above, with half of the plate exposed to UV light. All exposures were done in quadruplicate. After exposures, the MTT assay was performed as described in section 2.2.6 and viability was calculated by equation 2.3.

3.2.4 Trypan Blue Assay

MPMC viability was also assessed using the Trypan Blue cell staining (Sigma Aldrich, St. Louis, MO) where cells with permeable membranes (i.e. dead cells) are stained blue. The MPMC/3t3 co-culture was plated in a 24-well plate and exposures to nanoparticles and controls were performed as described in the cell culture section. Cells

were incubated with a 0.25% Trypsin solution for 5 min to remove the cells from the wells, and the contents of each well was placed in an individual microcentrifuge tube, with half of the samples being exposed to 20 minutes of UV light. Cells were dyed by mixing 200 µL cell suspension with 200 µL of the as-purchased Trypan Blue solution. Upon mixing, 20 µL of the stained cells were plated onto each side of a hemocytometer and cells were counted under an inverted light microscope (Eclipse E200, Nikon USA, Melville, NY). Cell viability was determined by equation 3.1.

(3.1) $$Percent\ Viable\ Cells = \frac{total\ number\ cells - blue\ cells}{total\ number\ cells} \times 100$$

3.2.5 ROS Assays

Intracellular ROS were monitored using fluorescence assays. MPMC/3t3 co-culture was plated on a 96-well plate and, prior to nanoparticle exposure as described above, cells were incubated for 1.5 h in 10 µM 2',7'-dichlorodihydrofluorescein diaceate (DCFDA) or 2 h in 5 µM aminophenyl fluorescein (APF, Invitrogen, Eugene, OR) made in growth media. DCFDA or APF solution was removed, and cells were rinsed twice with PBS followed by exposure to varying concentrations (12.5-400 µg/mL) of TiO_2 nanoparticles and, in some cases with the DCFDA assay, 1 mM NAC. The range of nanoparticle doses was chosen to include both realistic nanoparticle doses along with doses that are extremely high (200 and 400 µg/mL) to amplify any oxidative stress response. After 23.5 h, cells were rinsed with PBS twice and half the plate was illuminated for 20 min with UV light, as described above. As DCFDA or APF enters a cell and reacts with various ROS species, the probe molecule is converted into a

fluorescent product. Fluorescence intensity was measured (BioTek Instruments, Inc, Winooski, VT) immediately following UV light exposure (λ_{ex}=485/20 nm λ_{em}=528/20 nm). The fluorescent probe molecule is assumed to be intracellular because multiple wash steps were performed; however, it is possible that fluorescence may be from probe molecules associated with or adherent to the cell membrane.

To test the antioxidative power of serotonin, 67 mM sodium hypochlorite (household bleach) and serotonin hydrochloride (Alfa Aesar, Ward Hill, MA) of varying concentrations (5 µM to 5 mM) were added to wells of a 96-well plate, adjusting to equal volumes with water, and allowed to react for 1 h. Following reaction time, 10 µM DCFDA was added each well, incubated for 10 min, and fluorescence intensity, caused by the reaction of hypochlorite with the DCFDA molecule, was measured at λ_{ex}=485/20 nm λ_{em}=528/20 nm. Each serotonin concentration was measured in triplicate.

3.2.6 CFMA and Data Analysis

CFMA was performed as described in previous work and in detail in section 2.2.7.[8, 10, 11] Briefly, a carbon-fiber microelectrode, fabricated in-house, was placed on the surface of a single MPMC and held at a constant +700 mV (vs Ag/AgCl), a potential sufficient to oxidize serotonin, an electroactive molecule stored in the MPMC granules. No changes in cell morphology were observed due to the culture condition, though the electrode pressed to the cell surface deformed the cell slightly because of the pressure. A stimulating pipette loaded with a chemical secretagogue (A23187, SigmaAldrich, St. Louis, MO) delivered a 3 s bolus onto the cell to stimulate exocytosis, and current from the oxidized serotonin was recorded. CFMA was performed on cells following exposure

to 100 µg/mL TiO_2 nanoparticles as described above, including selected cell plates being exposed to 20 min UV light.

Data analysis is described in detail in section 2.2.8. To be included in the peak analysis, the amplitude of the exocytotic spike was required to exceed 5 times the root-mean-square of the current noise, and the area had to surpass 60 fC. Average area and full-width at half maximum ($t_{1/2}$) of the amperometric spikes were determined for each cell along with the frequency of release, and these values were pooled together with cells of the same culture condition. Cells that had an average spike area that was more or less than 2 times the logarithmic standard deviation from the logarithmic mean were excluded from further data analysis.

As explained in Chapter 2, amperometry affords much insight into the biophysics of exocytosis; spike area, $t_{1/2}$, and spike frequency are of particular interest. The area under individual spikes is equivalent to charge (or Q), a quantity that can be converted into the number of molecules released using Faraday's law ($Q=nFN$). The $t_{1/2}$ is a measure of the rate of release of molecules from individual granules, and the overall spike frequency reveals the efficiency of granule trafficking, docking, and fusion to the plasma membrane. In each condition, data from at least 14 cells was pooled and the average of each cell's average spike parameter was compared using pairwise student's t-testing ($p<0.05$) (Microsoft Excel, Microsoft Corp, Seattle, WA). Significant changes in these spike parameters between culture conditions gives insight into the interaction of nanoparticles with cells by elucidating the impact they have on the critical cell function of exocytosis.

3.3 Results and Discussion

3.3.1 Nanoparticle Synthesis and Characterization

TiO_2 nanoparticles were synthesized and characterized as previously described,[8] and a summary of the nanoparticle characteristics can be found in Table 3.1. Nanoparticles were suspended in PBS and introduced to the cell culture immediately after sonication. Stability of the nanoparticles over the time course of the experiment in water, PBS, and cell culture medium is demonstrated in Figure 3.1. In monitoring the aggregate/agglomerate stability using dynamic light scattering (DLS), it is evident that TiO_2 nanoparticles agglomerate quickly, which will impact the sedimentation rate and therefore the localized dose.

Table 3.1 TiO_2 nanoparticle characteristics.

Characteristic	Nanoparticle Environment	Value
Size (TEM) – primary particle	dry	11 ± 5 nm
Size (DLS) – hydrodynamic radius	H_2O	806 ± 121 nm
	PBS	1576 ± 782 nm
	culture media	1204 ± 75 nm
ζ-potential	H_2O	-34.4 ± 0.4 mV
	PBS	-13.6 ± 4.1 mV
	culture media	-16.0 ± 3.0 mV
Crystallinity	dry	93.5% anatase; 6.5% brookite
Surface area	dry	234 m^2/g

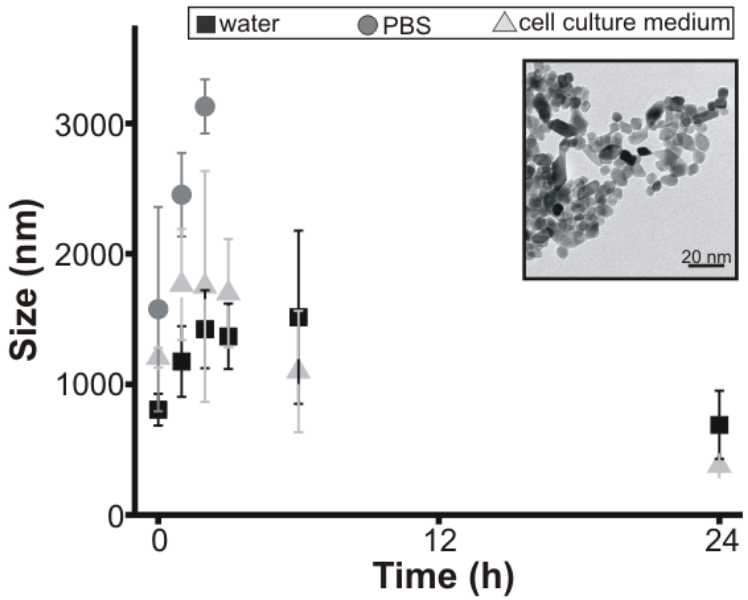

Figure 3.1 DLS measurement of the size of TiO_2 nanoparticles and their aggregates/agglomerates in varying solvents over 24 h, with nanoparticles pictured in the inset. All solutions quickly agglomerated (i.e. within 2 h) and after 2 h in PBS, the agglomerate sizes are larger then the capabilities of the instrument. In the case of water and cell culture medium, the measured agglomerate size gets smaller after 2 h because the larger agglomerates drop out of solution.

3.3.2 Cellular Viability

Previous studies have shown that murine peritoneal mast cells (MPMCs) take up nanoparticles and localize them within the secretory granules.[8, 10] Additionally, increasing the concentration of TiO_2 nanoparticles increases the number of nanoparticles internalized by the cell.[8] It is important to note that the description of concentration as related to uptake is difficult because it is affected by the degree of nanoparticle agglomeration, which in turn affects sedimentation rate and localized dose,[33] but the qualitative correlation of increased concentration introduced to the cell culture yielding increased uptake is still maintained.

With this understanding of nanoparticle uptake behavior already in hand for the exact model system (MPMCs co-cultured with Swiss-albino fibroblast line (3t3)), we first

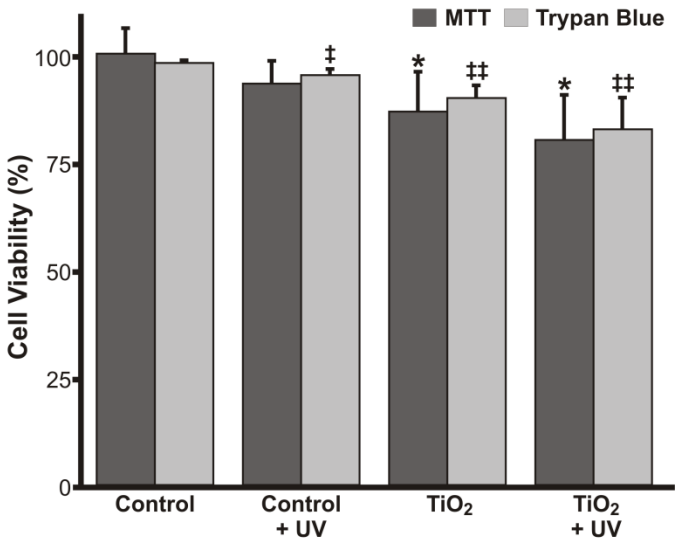

Figure 3.2 Cellular viability of MPMC/3t3 co-culture, as measured with the MTT and Trypan Blue assay, after exposure to 100 µg/mL TiO_2 nanoparticles for 24 h. Half of the control and nanoparticle-exposed cells were illuminated with UV light for 20 min at the end of the 24 h exposure period. Percent cell viability was calculated for each assay as described in the text and varies between the two assays. * indicates $p<0.05$ (n=4) as compared to the control in the MTT assay (n=4). ‡ indicates $p<0.05$ and ‡‡ indicates $p<0.005$ (n=4) as compared to the control in the Trypan Blue assay (n=4)

examined the overall cellular toxicity of TiO_2 nanoparticles on MPMCs using the MTT and Trypan Blue viability assays. The co-culture model system was chosen to make an *in vitro* technique maximally relevant towards understanding *in vivo* response as mast cells were cultured with a supporting cell-type with which they are found *in vivo*.[10, 34] 24 h prior to experimentation, the MPMC/3t3 co-cultured cells were passively exposed to a suspension of 100 µg/mL TiO_2 nanoparticles in PBS (sonicated prior to exposure). As mentioned previously, this dose enables a functional assessment of nanoparticle-cell interaction and has been used in previous work within the group. Some cells were exposed to 20 min UV light (λ=365 nm), after cells were rinsed with PBS, to intentionally increase ROS generation. As shown in Figure 3.2, MPMC exposure to TiO_2 nanoparticles causes a significant decrease in the cellular viability, as does exposure to

nanoparticles followed by 20 min UV light exposure (each compared to the control cells). Although there is a significant decrease in viability as measured with both MTT and Trypan Blue, the majority of the cells, approximately 80%, are still viable, consistent with other studies where TiO_2 nanoparticles cause minimal effect on cell survival.[8, 35]

3.3.3 Intracellular ROS Content

It is possible that intracellular ROS increases without killing the cells. Since ROS has been implicated in cytotoxicity after exposure to nanoparticles,[36, 37] cellular ROS content was measured using the DCFDA assay. DCFDA, a fluorescein-based probe, reacts with most ROS species and therefore, gives an overall measure of ROS content. As the nanoparticles introduced into the MPMC culture increase in concentration (12.5 – 400 µg/mL), and thus yield increased cellular uptake, more ROS is generated within the cell (Figure 3.3).

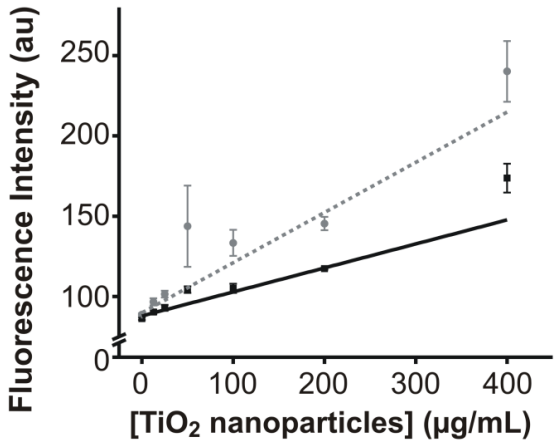

Figure 3.3 DCFDA assay after 24 hour cell exposure to varying concentrations of TiO_2 nanoparticles, with half of the cells being exposed to 20 min of UV light at the end of the 24 h (n=4 for each condition). Regression analysis indicates a significant trend for both non-UV (black solid line; $p<0.0001$) and UV (gray dotted line; $p<0.0001$) illuminated cells, and the two regression lines are significantly different from one another ($p<0.001$).

As predicted, an even higher amount of total ROS is present in the cells exposed to both nanoparticles and UV light (20 min of λ=365 nm light), with greater nanoparticle exposure concentrations exhibiting greater ROS content. Keeping in mind that previous work indicates that MPMCs internalize more nanoparticles as the exposure concentration increases,[8] it follows that the increasing concentration leads to more oxidative stress within the cell. This dose response was also observed with the second common ROS probe, APF (Figure 3.4A). While this trend holds true for TiO_2-exposed cells without subsequent UV light exposure, there is an even greater rate of ROS production in the UV-exposed cells ($p<0.001$). Again, the UV light exposure here is not meant to model organism sun exposure but instead acts as a positive control yielding increased ROS production. Performing the same DCFDA experiment with an immortal mast cell-like cell line, rat basophilic leukemia cells (RBL-2H3, ATCC, Manassas, VA) yielded a similar dose-dependent increase in ROS along with the increased rate of ROS production in the UV-exposed cell (Figure 3.4B). To verify that the increased fluorescence intensity was not the result of the UV light transforming the probe molecule itself, solutions of 10 μM DCFDA in PBS were plated in 96-well plates and half of the wells were exposed to UV light as in the cell experiments. No difference was observed in the fluorescence intensity for the wells in the dark versus those that were light exposed (Figure 3.4C). In total, these results indicate that, while UV light exposure alone does cause oxidative stress within the control cells (shown as the 0 μg/mL data point), the dramatic increase in ROS with nanoparticles present indicates their synergistic role in generating oxidative stress within the cell.

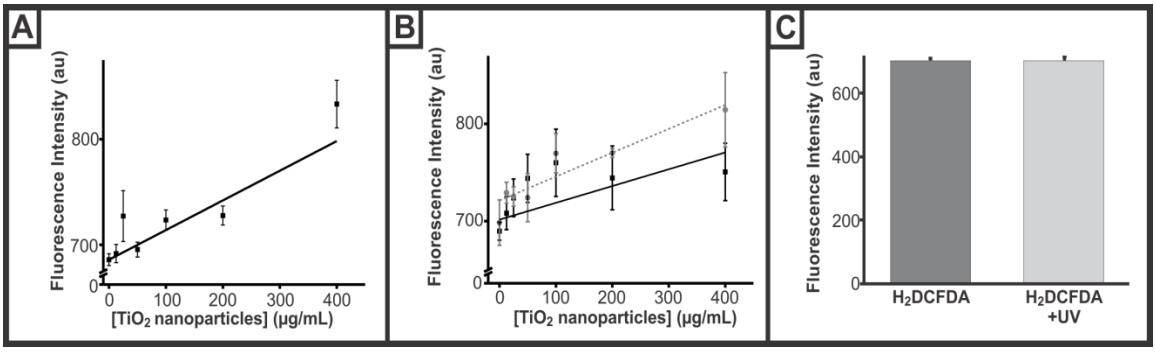

Figure 3.4 ROS assays with varied fluorescent probes, varied cell types, or varied light exposure. (A) APF assay in MPMCs after 24 h exposure to varying concentrations of TiO_2 nanoparticles. Regression analysis indicates a significant trend ($p<0.0001$). UV light exposure data was not shown for the APF assay as it is unclear if the UV light exposure would itself cause APF to decompose. (B) DCFDA assay in RBL-2H3 cells after 24 h exposure to varying concentrations of TiO_2 nanoparticles with half of the cells being exposed to 20 minutes of UV light at the end of 24 h. Regression analysis indicates a significant trend for both non-UV (black solid line; $p<0.005$) and UV (gray dotted line; $p<0.0001$) illuminated cells and the two lines are significantly different from one another ($p<0.05$). (C) Fluorescence intensity of DCFDA solution (10 µM in PBS) before (n=10) and after (n=10) UV light exposure.

3.3.4 Effects on Exocytosis

Real-time measurements using CFMA were employed to reveal the fundamental effect TiO_2 nanoparticles and UV light exposure have on exocytosis in an effort to correlate results to cellular oxidative stress. Representative amperometry traces from the four culture conditions (control, control+UV, TiO_2 nanoparticles, TiO_2 nanoparticles+UV) tested are shown in Figure 3.5. After spike-by-spike analysis of amperometry data, and in comparison to the control, MPMCs exposed to UV light, 100 µg/mL TiO_2, and 100 µg/mL TiO_2 and UV light each showed a significant decrease in the average area per amperometric spike, decreasing by 23%, 37%, and 45%, respectively (Figure 3.6A). Using Faraday's Law to convert spike area, or charge (Q), into molecules,

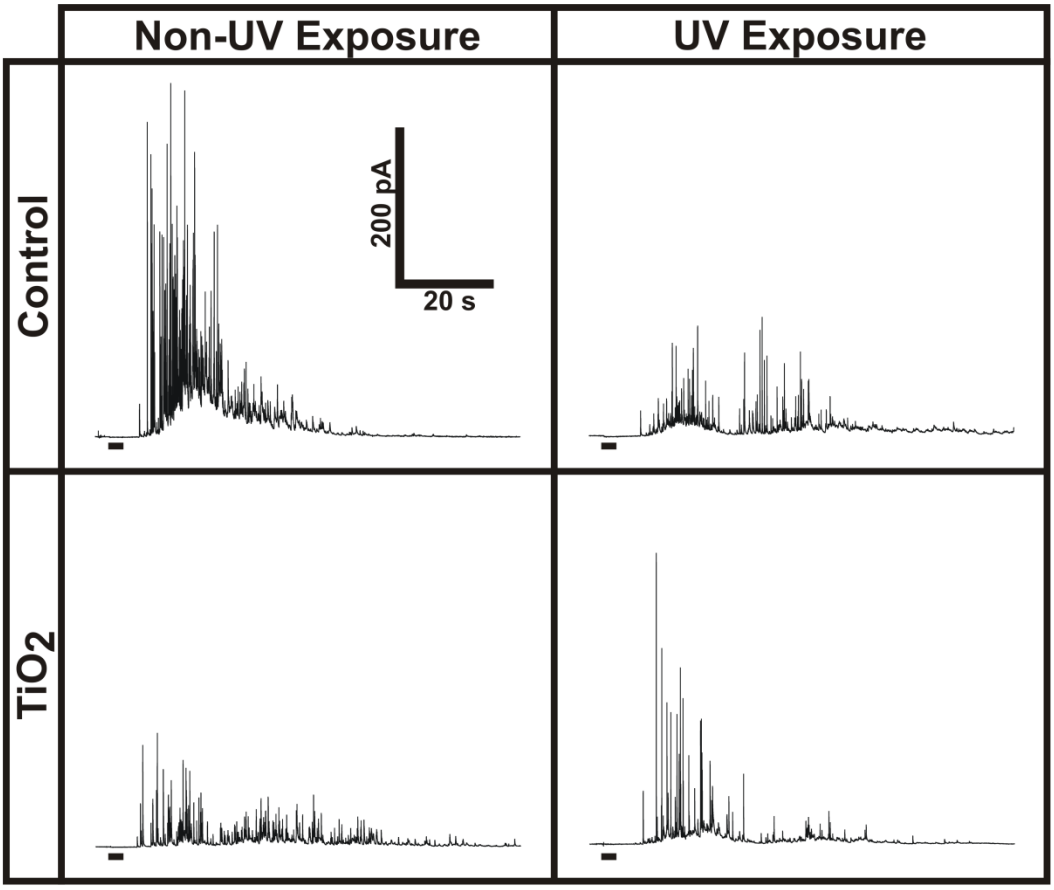

Figure 3.5 Representative amperometric traces from MPMCs co-cultured with 3t3s for 24 h with the following exposure conditions: control, control + 20 min UV light illumination, 100 µg/mL TiO_2 nanoparticles, and 100 µg/mL TiO_2 + 20 min UV light illumination. Bold lines below traces indicate 3 s bolus of stimulant delivered to cell.

these decreases in spike area are equivalent to a decrease to 4.6×10^6, 3.7×10^6, and 3.3×10^6 molecules, respectively, per granule compared to the control condition (6.0×10^6 molecules). The decrease in average area per spike follows the trend in ROS presence in that more ROS present within a cell correlates to a greater decrease in the number of serotonin molecules being released. This is the same exocytotic function trend measured when cells are exposed to other nanoparticles (where ROS was not monitored).[8, 10, 11] In

addition, comparison of the average Q measured for UV-exposed control and UV/TiO_2-exposed cells reveals a significant difference, indicating that the presence of nanoparticles contributes to the cellular dysfunction. As seen in Figure 3.6B, there is a significant increase ($p<0.05$) in the average half-width ($t_{1/2}$) measured from cells exposed to TiO_2 and UV light as compared to the control. An increase in the $t_{1/2}$ indicates that the kinetics of chemical messenger secretion are hindered; these data support previous work, where, in the presence of nanoparticles, cell delivery of chemical messenger molecules is impaired. [8, 10, 11] The frequency of release is also affected under experimental conditions (Figure 3.6C); there is a significant decrease in the exocytotic frequency from cells exposed to both nanoparticles and UV light as compared to the control, suggesting that the combination of nanoparticles and ROS interferes with granule trafficking within the cytoplasm and/or docking machinery at the cell membrane. This is the first evidence that this change in chemical messenger release correlates to increased ROS, in which ROS may be the cause of this exocytotic impairment.

Correlating the presence of ROS within cells to the perturbation in exocytotic cell function, we see a greater impairment to exocytosis when more ROS is present. The relationship between average Q and intracellular ROS content (Figure 3.6D) exhibits an exponential decay where increasing amounts of ROS correlate to less change in the number of serotonin molecules being released. Furthermore, while the $t_{1/2}$ and frequency are perturbed when the highest measured levels of ROS occur, Q appears to be more sensitive to alterations when ROS is generated, as all experimental culture conditions have Q values that are significantly different than the control (Figure 3.6A). This

suggests that the serotonin content is more readily affected by nanoparticles, which also cause oxidative stress, than the kinetics of release or granule trafficking.

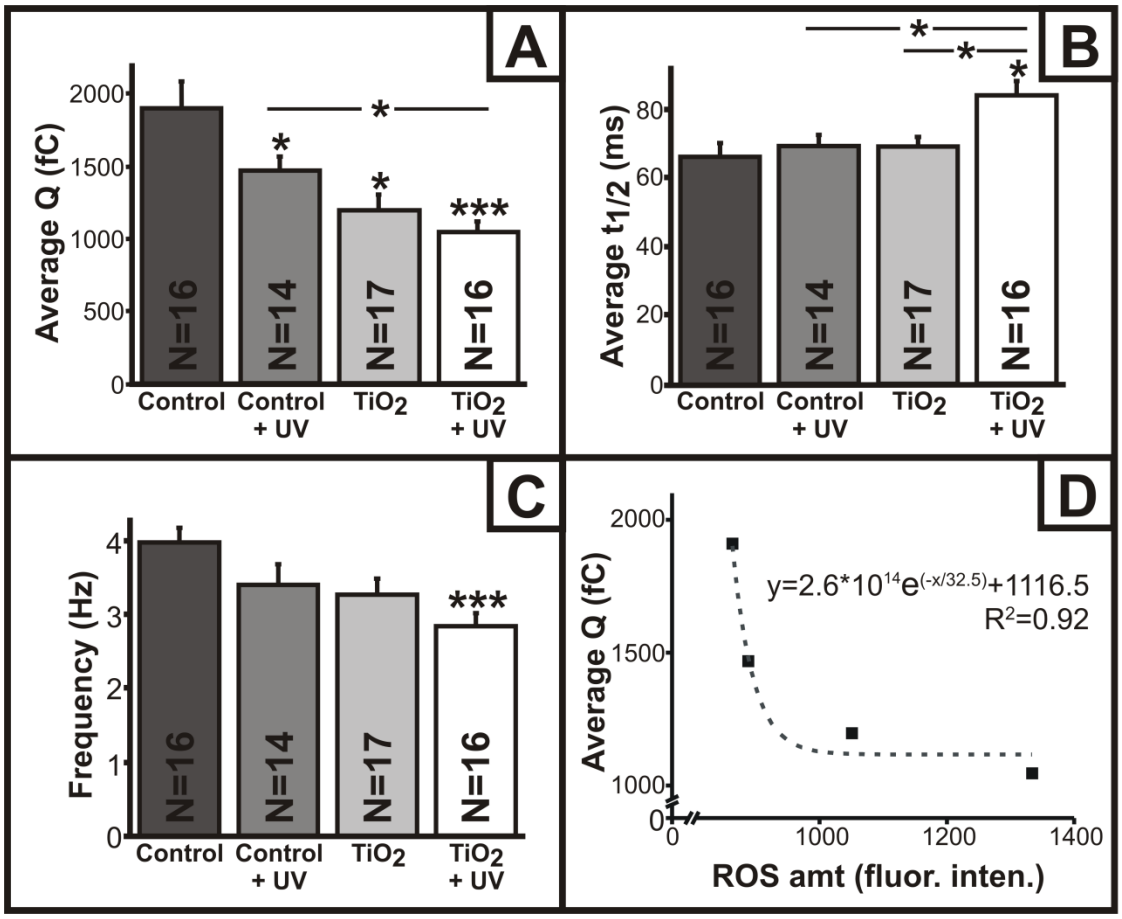

Figure 3.6 Average amperometric spike parameters from MPMCs co-cultured with 3t3s after 24 h exposure to control, control + UV light illumination, 100 µg/mL TiO_2 nanoparticles, and 100 µg/mL TiO_2 + UV light illumination. (A) All experimental conditions cause a significant decrease in Q as compared to the control, and a significant difference also arises between the control and nanoparticle exposures that were illuminated with UV light. (B) Cells exposed to nanoparticles + UV light had a significantly larger $t_{1/2}$ than any other culture condition and (C) also exhibited a significant decrease in frequency as compared to the control. (D) The correlation between average Q and fluorescence intensity from the DCFDA assay shows an exponential decay. Error bars represent SEM, * indicates $p<0.05$, and ***$p<0.001$.

It is evident that TiO_2 nanoparticle-induced oxidative stress correlates to perturbations in exocytotic cell function. However, it is beyond the scope of this work to determine if the ROS directly causes the changes in exocytosis or if the increased oxidative stress occurs in parallel with perturbations in granule release, which could be caused by changes in signaling pathways or other upstream phenomena. Scientific precedent reveals that a consecutive increase in ROS leading directly to exocytotic impairment is plausible. Herein, we will present suggestions for how the occurrence of ROS could cause specific cellular biophysical changes as we have measured in the CFMA results. Future work will aim to prove or disprove these proposed impacts. Assuming that ROS is induced close to where the nanoparticle is internalized, the greatest amount of ROS would occur within the MPMC secretory granules (based on microscopy data seen in section 2.3.2).[8] ROS could particularly affect the number of molecules being released and the kinetics of individual granule release. That is, ROS within the granule may cause a decrease in average Q per spike, or the number of molecules released per granule, because serotonin has been shown to act as an antioxidant[38] and would be easily degraded by ROS before being released or reaching the microelectrode. Figure 3.7 demonstrates the antioxidant capability of serotonin, where increasing concentrations of serotonin were reacted with ~60 mM hypochlorite, a ROS molecule, for 1 h, after which the hypochlorite amount was significantly decreased (as measured using the DCFDA assay). Based on the number of molecules secreted per mast cell granule, we can approximate the concentration of serotonin per granule to be ~150 mM, and since at 5 mM serotonin, there is minimal hypochlorite remaining in this well plate assay, it can be concluded that TiO_2 nanoparticle-induced ROS would likely react with some of the

serotonin present in the granule, causing a decrease in the number of molecules secreted, but not totally deplete the highly concentrated intragranular serotonin, even at high ROS concentrations.

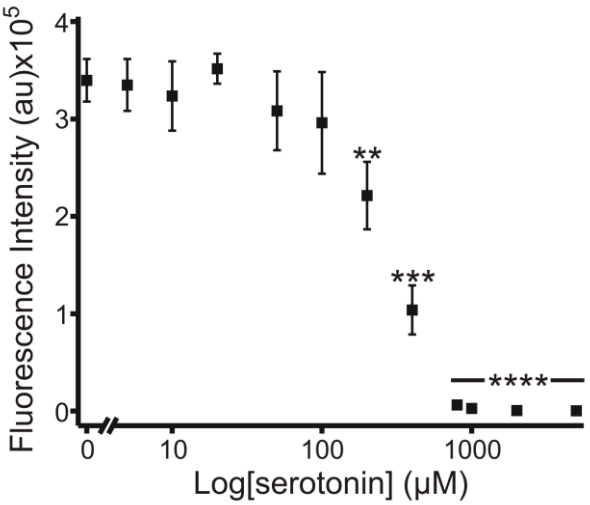

Figure 3.7 In a well-plate, a solution of serotonin acts as an antioxidant, where increasing concentrations of serotonin decrease the hypochlorite concentration (initial concentration=67 mM), as measured with DCFDA fluorescence intensity (n=3). Regression analysis indicates a significant trend ($p<0.001$). Significant reduction in fluorescence intensity starts at 200 μM as compared to the control. Significant differences are indicated where $^{**}p<0.01$, $^{***}p<0.001$, and $^{****}p<0.0001$, as compared to the control. X-axis is represented as the log of serotonin concentration.

As to the possible direct effect of ROS on the kinetics of granule secretion, the majority of the granule is comprised of a heparin-like biopolymer, which has been shown to depolymerize in the presence of ROS, particularly ·OH.[39, 40] This depolymerization would interrupt the natural organization and electrostatic repulsion of the highly negatively charged heparin and therefore decrease the driving force that causes the biopolymer to unfold during exocytosis, thereby increasing the time it takes for the granule to fully release its contents (i.e. $t_{1/2}$). While ROS may be initiated within the granule, there is evidence that some oxidative species are membrane permeable and

therefore may cross into the cytoplasm.[41] A study by Pariente and coworkers demonstrated that ROS within the cytoplasm causes damage to actin filament reorganization, a critical component needed for granule trafficking and docking.[42] Therefore, ROS permeating into the cytoplasm from the granule, or other oxidative stress the cell experiences as a result of internalizing TiO_2 nanoparticles, could cause a decrease in the efficiency of granule trafficking as evident by the decrease in the amperometric spike frequency. Future experiments will test the depolymerization and cytoskeletal impacts of nanoparticle-induced ROS.

In an attempt to mitigate the nanoparticle-induced ROS and work towards understanding if the correlation of ROS and altered exocytosis is serial or parallel in nature, cells were exposed to NAC, a commonly used antioxidant,[43, 44] as nanoparticles were introduced to the MPMC/3t3 cell co-culture. If the ROS directly alters chemical secretion behavior, cells exposed to a sufficient concentration of NAC, even with TiO_2 nanoparticle exposure, would not exhibit increased oxidative stress and, therefore, altered exocytosis. The DCFDA assay was performed as described above, where cells were exposed to varying concentrations of TiO_2 nanoparticles with a portion exposed to UV light. Additionally, a subset of cells were exposed to 1 mM NAC, and results reveal that, while NAC attenuates the ROS induced by UV light exposure, it does not mitigate the dose-dependent, nanoparticle-induced ROS (Figure 3.8A). This may be due to a difference in ROS generation mechanism/species. CFMA results correlate with the ROS results (Figure 3.8B and 3.8C), where Q decreases and $t_{1/2}$ increases upon exposure to TiO_2 nanoparticles and UV light are not recovered in the presence of NAC. Control cells exposed to UV light plus NAC resulted in recovery of both Q and $t_{1/2}$, indicating that the

nanoparticle-induced perturbation is not alleviated. It is possible that over a shorter exposure time (i.e. less than 24 h) the NAC could deplete some of the ROS as demonstrated by other TiO_2 nanoparticle toxicity studies,[43] but the data presented herein indicate that the intracellular oxidative stress caused by nanoparticles is difficult to relieve, making ROS production a likely mode of nanoparticle toxicity, though it does not distinguish if the correlation is serial or parallel.

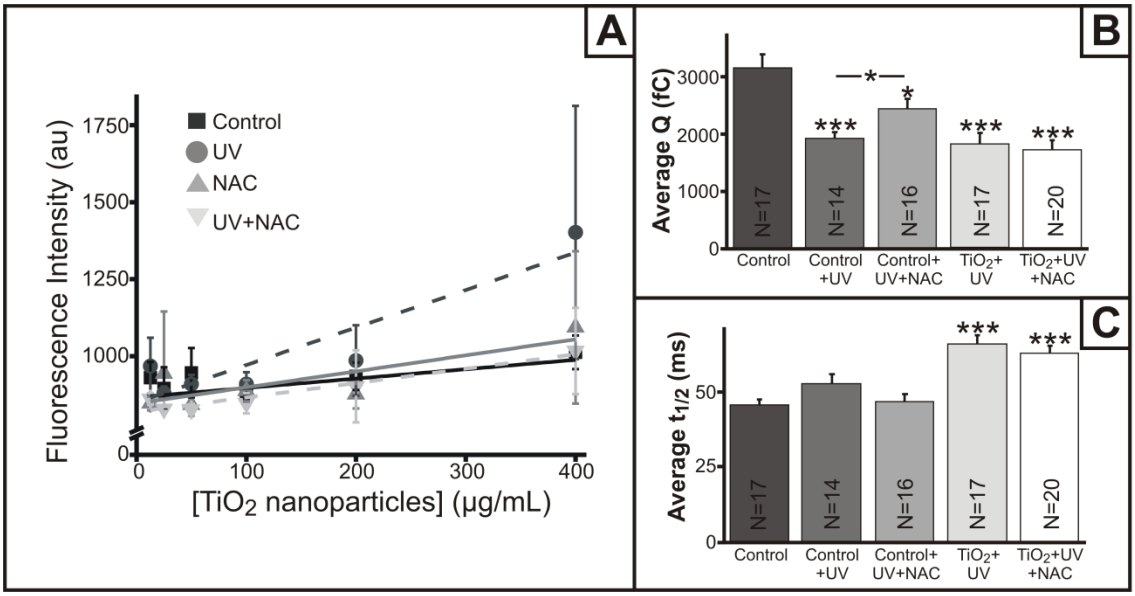

Figure 3.8 NAC, an antioxidant, does not stop nanoparticle-induced oxidative stress. (A) ROS produced from cells exposed to TiO_2, UV light, and/or NAC. In this plot, MPMC/3t3 co-culture is exposed to TiO_2 nanoparticles in varying concentrations and some to 20 min UV light (dashed lines). Regression analysis indicates significant trends ($p<0.05$) for all culture conditions (control – black solid line; UV exposure – dark gray dashed line; NAC exposure - medium gray solid line; UV and NAC exposure – light gray dashed line) and that the trend for cells exposed to UV light is significantly different ($p<0.05$) than the trend for the other three conditions. CFMA results correlate with ROS results where the TiO_2 nanoparticle-induced ROS is not ameliorated by added NAC, and in turn, correlates with perturbed exocytotic cell function. (B) Average Q is significantly decreased in cells exposed to UV light and TiO_2 + UV light though cells exposed only to UV light experienced a recovery after exposure to NAC. (C) The average $t_{1/2}$ significantly increased in cells exposed to TiO_2 + UV light and this perturbation in function is not recovered upon addition of NAC as the average Q is significantly less and the average $t_{1/2}$ is significantly more than the control. Error bars in B and C represent SEM and *$p<0.05$, **$p<0.01$,***$p<0.001$.

3.4 Conclusions

To safely design engineered nanomaterials, it is critical to understand the mechanism by which nanoparticles and cells interact. This work demonstrates that, upon exposure to TiO_2 nanoparticles, cells exhibit increased intracellular ROS amounts in a dose-dependent manner. Additionally, nanoparticle exposure followed by subsequent UV light illumination causes a further increase in the ROS present within the cell. This increase in cellular ROS correlates with perturbations in exocytotic cell function, with decreasing number of molecules released, increasing time for granule content release, and decreasing granule trafficking and docking frequency as intracellular ROS increases. While other modes of toxicity may also be involved, it is clear that ROS is a large contributor to cellular dysfunction. It is not currently possible to distinctly demonstrate whether the nanoparticle-induced ROS increase causes the change in exocytotic behavior or simply occurs coincidentally; however, evidence presented herein supports the former and inspires further work. Either way, future nanoparticle design work is aimed at fabricating TiO_2 nanoparticles that limit the ROS generated upon cellular introduction.

Chapter Four

Impact of TiO_2 Nanoparticles on Growth, Biofilm Formation, and Flavin Secretion in *Shewanella oneidensis*

This work completed in collaboration with I.L Gunsolus, B.M. Meyer, C.J. Christenson, and C.L. Haynes.

4.1 Introduction

While nanoscale particles occur naturally and have been used intentionally for centuries, release of engineered nanoparticles into the environment via direct application (e.g. pesticides), waste water effluent and sludge, and product degradation, among other routes, is of concern due to the increasing production and use of these materials and their novel physical and chemical properties. Therefore, it has become increasingly important to characterize the fate, transformation, and toxicity of engineered nanoparticles in ecological systems. The work presented herein focuses on titanium dioxide (TiO_2) nanoparticles due primarily to their high commercial production rate; global production increased to 5000 tons in 2010[1] and is projected to increase to 2.5 million tons by 2025.[2] TiO_2 nanoparticles are manufactured in a variety of forms, the most common being E171 (food additive),[1] T-Eco (sunscreens),[3] and Evonik Aeroxide® P25 (National Institute of Standards and Technology (NIST) established standard for TiO_2 nanoparticles).

Released engineered nanoparticles will potentially impact organisms on all levels of the food chain, but the most widespread consequences will result from impacts exerted on low trophic level organisms like bacteria, which play critical roles in the ecosystem. A mechanistic understanding of nanoparticle-induced bacterial toxicity has implications for understanding ecosystem health in general. *Shewanella oneidensis* MR-1 provides an excellent model system for understanding nanotoxicity as these bacteria are distributed world-wide in a variety of environments and are important for geochemical nutrient cycling.[4] Additionally, this bacterium has also been utilized in previous nanotoxicity studies as an environmentally relevant model.[5, 6] Because *S. oneidensis* is an

aquatic organism, there is a high likelihood that these bacteria will interact with nanoparticles entering the environment via the routes described above.

Much of the work to date studying the bacterial toxicity of engineered nanoparticles has focused mainly on changes in viability and/or growth,[7-9] but elucidation of toxicity mechanisms requires assessment of cell function changes. Toward understanding the mechanism of interaction, some strategies that have been employed thus far include study of nanoparticle uptake/association and post-exposure bacterial morphology,[10] membrane integrity and properties,[10-12] and oxidative stress.[10, 13] While elucidating the mechanism of nanoparticle-bacteria interaction is an area of increasing research, critical gaps remain in the understanding of bacterial function following nanoparticle interaction.

To address these gaps, we examine the effects of nanoparticle exposure on both a general bacterial function (biofilm formation) and a *S. oneidensis*-specific function (flavin secretion). Biofilms are composed of microorganisms embedded within a self-produced biopolymer matrix, and formation of these biofilms is a critical function for bacteria. Many of the important environmental functions performed by bacteria, including organic material production and degradation, toxic material degradation, and biogeochemical cycling of biogenic elements like nitrogen, oxygen, and phosphorous require cooperative metabolic functioning, as occurs in biofilms.[14] Biofilms serve a range of functions, both beneficial and detrimental to humans, which include acting as a food source for aquatic invertebrate, removing organic matter during sewage treatment, and biofouling. For *S. oneidensis,* formation of biofilms is important for their interaction with metals and metal oxides.[15] Beyond their importance to bacterial function, biofilms

represent the most common arrangement of bacteria in the environment, and so studying the impact of nanoparticles on biofilm formation allows generalizable understanding of nanoparticle toxicity.

The main function of *S. oneidensis* in the geochemical cycle is as a metal reducer, a function which is performed by the secretion of electron shuttling molecules. More specifically, *S. oneidensis* secretes flavin mononucleotide from the periplasmic space, which is readily converted into riboflavin, and these are extracellularly reduced using electrons donated by organic carbon oxidation within the cell.[4] This function serves both to transform metals and as a method of respiration for *S. oneidensis* when oxygen content is limited.

Herein, we aim to understand the mechanism of toxicity of TiO_2 nanoparticles in a variety of forms (synthesized, Aeroxide P25, and T-Eco) on *S. oneidensis* by characterizing the nanoparticle impact on the generalizable function of biofilm formation and the species-specific function of metal reduction. Quartz crystal microbalance (QCM) will be used to monitor biofilm formation and growth, which has been used previously in the study of bacterial biofilms,[16-18] and high performance liquid chromatography (HPLC) will be used to analyze riboflavin secretion from *S. oneidensis* suspensions. These assessments of functional changes as a result of TiO_2 nanoparticle exposure reveal new insights regarding the mechanism of nanoparticle-bacteria interaction.

4.2 Methods

4.2.1 Nanoparticles

Three types of TiO_2 nanoparticles were utilized in this study, acid-catalyzed TiO_2 nanoparticles synthesized in house (as-syn), Evonik Aeroxide® Degussa P25 (P25 - The Cary Company, Addison, IL) and Eusolex® T-Eco (T-Eco - EMD Chemicals Inc, Gibbstown, NJ). As-syn nanoparticles were synthesized and characterized as previously described,[19] and were chosen because of the controlled crystallinity and controlled surface chemistry that in-house synthesis affords. Two commercially available TiO_2 nanoparticles, P25 and T-Eco, were chosen because P25 is often used as a "model" TiO_2 nanoparticle in toxicity studies and T-Eco has been shown to be most similar to nanoparticles present in cosmetics, including sunscreens.[3] Both commercial nanoparticles' size and crystallinity have been characterized within the literature.[3, 20] Nanoparticle characteristics previously reported have been compiled in Figure 4.1.

Beyond previous characterization, the hydrodynamic size, stability, and ζ-potential of 25 μg/ml nanoparticle suspensions in water and Luria-Bertani (LB) broth, bacterial growth broth, was examined using Brookhaven Instruments Corporation dynamic light scattering (DLS) and ZetaPALS Zeta Potential Analyzer (Holtsville, NY). Additionally, transmission electron microscopy (TEM) images were taken on a JEOL 1200 EXII (JEOL, Tokyo, Japan) at 80 kV.

4.2.2 Bacteria Culture and Nanoparticle Exposure

Shewanella oneidensis MR-1 were generously gifted from the lab of Jeff Gralnick at the University of Minnesota. The following method was employed to culture bacteria

that were subsequently used in nanoparticle toxicity experiments. All bacteria culture and nanotoxicity experiments were performed in LB broth (BD Difco™, BD Diagnostics, Franklin Lakes, NJ) or agar (BD Difco™) plates with LB broth nutrients. *S. oneidensis*, stored at -80 °C, were inoculated onto a LB broth agar plate and incubated at 30 °C for 18-24 h, or until visible colony formation. Colonies were transferred to LB broth in sterile culture tubes with 1 colony placed in 5 mL of LB broth and allowed to come to stationary phase (~18-24 h). At this point, the bacteria were used for toxicity assessments and will herein be referred to as bacterial suspension. Typically, the bacterial suspension was at a cell density of 10^9 cells/ml as measured by the OD at 600 nm, where 1 absorbance unit equals 10^9 cells/mL. Nanoparticle exposures were conducted on the bacterial suspension in a range of 1-100 μg/ml TiO_2 nanoparticles from a suspension of nanoparticles in LB broth. These concentrations were chosen as they fall within the range of predicted environmental concentrations for the release of TiO_2 from waste water effluent.[21]

4.2.3 Viability Assay

Viability of *S. oneidensis* after exposure to TiO_2 was assessed using the fluorescent staining kit LIVE/DEAD® Baclight™ (Life Technologies, Grand Island, NY) where live cells are stained with SYTO-9 fluorescent tag and dead cells are stained with propidium iodide. Cells were diluted to a density of 10^8 cells/mL with LB broth and exposed to varying concentrations (1-100 μg/mL) of as-syn or 25 μg/mL P25/T-Eco TiO_2 nanoparticles for 24 h (at 30 °C and shaking at 200 RPM), with each condition cultured in triplicate and periodic assessment of viability over the 24 h exposure. To perform the

viability assay, the staining solution was prepared as specified by the manufacturer (kit L7012). Periodically, 0.5 mL aliquots of the samples were centrifuged at 500g for 10 minutes and pelleted cells were resuspended in a HEPES (4-(2-hydroxyethyl)-1-piperazineethanesulfonic acid) buffer solution with mineral additives to avoid extracellular nucleic acids in the LB broth that bind the fluorescent stain molecules. HEPES buffer, modeled after *Shewanella sp.* basal medium described in Balch *et al.*, consisted of 100 mM HEPES (Sigma Aldrich, St. Louis, MO), 7.8 mM $NaCH_3CO_2$ (EMD Chemicals Inc, Gibbstown, NJ), 1.3 mM $K_2HPO_4 \cdot 3H_2O$ (Mallinckrodt, Phillipsburg, NJ), 1.7 mM KH_2PO_4(JT Baker, Phillipsburg, NJ), 1.7 mM $(NH_4)_2SO_4$ (Fisher Chemical, Fairlawn, NJ), 1 mM $MgSO_4$ (Sigma Aldrich, St. Louis, MO), 9.5 μM $ZnCl_2$ (Sigma Aldrich, St. Louis, MO), 1.9 μM $NiCl_2$ (Sigma Aldrich, St. Louis, MO), 0.5 μM $Na_2MoO_4 \cdot 2H_2O$ (Sigma Aldrich, St. Louis, MO), 0.4 μM $Na_2WO_4 \cdot 2H_2O$ (Alfa Aesar, Ward Hill, MA), 0.2 μM $AlK(SO_4)_2 \cdot 12H_2O$ (Mallinckrodt, Phillipsburg, NJ), 1.8 μM $FeSO_4 \cdot 7H_2O$ (Fisher Chemical, Fairlawn, NJ), 13.5 μM $MnSO_4 \cdot H_2O$ (Mallinckrodt, Phillipsburg, NJ), 0.2 μM $CuSO_4 \cdot 5H_2O$ (Spectrum Chemical, Redondo Beach, CA), and 3.25 μM $CoSO_4 \cdot 7H_2O$ (Fisher Chemical, Fairlawn, NJ), adjusted to pH 7.2 with NaOH (Mallinckrodt, Phillipsburg, NJ).[22] 100 μL of the resuspended bacteria were plated on a 96 well plate, mixed with 100 μL of the staining solution and incubated for 15 minutes in the dark. After incubation with the reporter molecules, fluorescence intensity was measured on a multi-well plate reader (Synergy 2, Biotek, Winooski, VT) with excitation wavelength for both molecules centered at 485 nm and the fluorescence intensity of live cell stain, SYTO-9, measured at a wavelength of 530 nm and dead cell stain, propidium iodide, measured at a wavelength of 630 nm. The

ratio of live-cell to dead-cell fluorescence intensity was compared between the control and nanoparticle-exposed bacteria. The viability measurement was repeated after 0, 1, 2, 6, and 24h of nanoparticle exposure.

4.2.4 Growth

To determine the impact of nanoparticles on bacterial growth, the optical density of bacteria was monitored over time to assess nanoparticle impact on growth rates. Cells from the bacterial suspension were diluted to 10^7 cells/ml and exposed to 0, 1, 5, 10, 25, or 100 μg/mL of either as-syn, P25, or T-Eco, and measurements of OD at λ=600 nm were periodically recorded with a Spectronic 20D (Milton Roy Company, Ivyland, PA), with samples replaced onto the shaking incubator when data were not being collected. The exponential phase of growth was determined by manual inspection of each curve, and the growth rate, in generations/h, was determined using Equation 4.1, which is based on the classic model of binary fission.

(4.1) $$growth\ rate = \frac{\log OD_2 - \log OD_1}{0.301 \times (t_2 - t_1)}$$

4.2.5 Biofilm Assessment with QCM

QCM experiments to assess biofilm formation and growth were performed on a Maxtek, Inficon R-QCM system with 1" gold contact crystals in a flow cell (Inficon, East Syracuse, NY). The system was held at 30 °C in an incubator, and continuous monitoring of frequency and resistance, which relates to crystal dissipation, was performed over the course of the experiment to better understand the change in mass on the crystal and

viscoelastic properties of the biofilm, respectively. Measurements were made on two parallel crystals, control and nanoparticle exposure conditions, with samples introduced to the flow cell using peristaltic pumps (variable flow mini-pump, Fisher Scientific, Hampton, NH). Additionally, there was a constant flow throughout the experiment. For biofilm growth experiments, LB broth introduced to the flow cell at 0.25 mL/min and the crystal was allowed to equilibrate for ~1 h. After which, aerated bacteria were introduced to the crystal for ~1 h at a flow rate of 0.25 mL/min to allow attachment. Flow was switched back to aerated broth (without bacteria) and the flow was increased to 0.75 mL/min. TiO_2 nanoparticles (25 μg/mL) were introduced either simultaneously with bacteria and/or with aerated broth.

4.2.6 HPLC Measurement of Riboflavin

Flavin secretion by *S.oneidensis*, important for heavy metal reduction function, was monitored by analyzing suspensions for riboflavin using HPLC, taking advantage of riboflavin's native fluorescence. Bacterial suspensions diluted to 10^8 cells/mL were exposed to 0-100 μg/mL as-syn or 25 μg/mL P25 or T-Eco TiO_2 nanoparticles for 24 h, and exposures were made in triplicate. A 1 mL sample was removed from each suspension and centrifuged for 15 minutes at 5000 g. Then, 200 μL of the supernatant was transferred to an amber HPLC vial with a 250 μL glass insert. HPLC analysis of riboflavin was performed on an Agilent 1200 HPLC fitted with a Zorbax Eclipse XDB-C_{18} 4.6 x 150 mm, 5 μm analytical column and Eclipse XDB-C_{18} 4.6 x 12.5 mm, 5 μm analytical guard column ahead of the fluorescence detector. Isocratic elution was performed using a 70:30 mixture of 20 mM citric acid buffer (pH 3.3):methanol as the

mobile phase. The injection volume was 30 μL, flow rate was 1 mL/minute, and detection of riboflavin was achieved with excitation and emission wavelengths of 450 nm and 530 nm, respectively. The run time was 7.25 minutes, and riboflavin elution was achieved around 6.5 minutes.

4.2.7 Extracellular Polymeric Substance Isolation and Characterization

Due to its importance in biofilms and to examine other secretion behaviors of *S. oneidensis*, the extracellular polymeric substance (EPS) was extracted and characterized for its sugar and protein content. EPS extraction and characterization was performed as described in Gong *et al.*[23] Samples were prepared in quadruplicate by diluting the bacterial suspension to 10^8 cell/mL and exposing cells to 1-100 μg/mL as-syn or 25 μg/mL P25 of T-Eco TiO_2 nanoparticles for 24 h (shaking at 200 RPM at 30 °C) followed by centrifugation of 3 mL of the samples at 1500g for 10 min. Pelleted cells were resuspended in 10 mL of an aqueous solution of 8.5% (w/w) NaCl and 0.22% (w/w) formaldehyde (JT Baker, Phillipsburg, NJ) by vortexing and placed in the refrigerator for 2 h. Cells were centrifuged at 3700g for 15 min at 4 °C, resuspended in a MQ water wash, and centrifuged again. The supernatant was removed and the EPS weight was taken. MQ water was added in the ratio of 50 mL for every 1 g EPS, samples were sonicated for 3 min and again centrifuged (3700g for 15 min at 4 °C). Cells were resuspended in 5 mL of 10 mM KCl and 10 mL of cold, 200 proof ethanol. The suspension was placed in the refrigerator overnight to allow EPS precipitation. Then, EPS was pelleted (3700g for 20 min at 4 °C) and resuspended in 10 mL MQ water.

Phenol-sulfuric acid (PSA) was used to quantify sugar content of the EPS, where 2 mL of EPS suspension was mixed with 50 μL of 80% (w/w) phenol solution (Sigma Aldrich, St. Louis, MO) and 5 mL concentrated H_2SO_4 (BDH Aristar, Radnor, PA). The mixture was allowed to incubate for 20 min in a 35 °C water bath followed by stabilization at room temperature for 4 h. The absorbance of each sample was measured at 480 nm in a 96-well plate and compared to a calibration curve made from glucose standards.

Protein quantification was performed via Lowry's method where 0.3 mL of the EPS solution was mixed with 1.5 mL alkaline copper reagent in a glass vial. The alkaline copper reagent was made by combining 2% w/w $Na_2C_4H_4O_6$, 1 mL 1% w/w $CuSO_4 \cdot 5H_2O$ and 98 mL of 2% w/w $NaCO_3$ in 10 mM NaOH. Following the copper solution addition, 75 μL Folin and Ciocalteu's phenol reagent (Sigma Aldrich, St. Louis, MO) was added, incubated for 30 min, and absorbance of the samples was measured at 500 nm. Absorbance values were compared to a calibration curve generated from bovine serum albumin (BSA) standards.

4.2.8 Uptake Assessment with TEM

Determination of TiO_2 nanoparticles internalization or association with *S. oneidensis* was completed utilizing TEM. Bacteria were cultured with 25 μg/mL as-syn TiO_2 at varying lengths of exposure, then the cells were pelleted by centrifugation (555 g for 10 min) and triple rinsed with 0.1 M sodium cacodylate buffer (Sigma Aldrich, St. Louis, MO) with centrifugation at 89 g for 5 min between each rinse. Final rinse buffer was removed and replaced with a solution of 2.5% glutaraldehyde fixative (Sigma

Aldrich, St. Louis, MO) in 0.1 M sodium cacodylate buffer. After a 1 h, the pellet was rinsed three times with sodium cacodylate buffer followed by post-fixing for 1 h in 1% osmium tetraoxide (Sigma Aldrich, St. Louis, MO) in 0.2 M sodium cacodylate buffer. The cells were dehydrated in a series of solutions with increasing ethanol in water followed by propylene oxide (Sigma Aldrich, St. Louis, MO). Propylene oxide was replaced with a 1:1 propylene oxide:Epon resin and incubated for 2 h. Finally, samples were infiltrated with 100% resin for 48 h, refreshing the resin 5 times within the 48 h period. Resin was cured for 24 h in 45 °C then 24h at 60 °C. Samples were sectioned into 60-nm-thick sections using a diamond knife on an ultramicrotome, and the sections were collected on Formvar®-coated copper TEM grids (Ted Pella Inc, Redding, CA). Sample grids were stained with uranyl acetate and lead citrate (Sigma-Aldrich, St. Louis, MO) and imaged on Jeol 1200 EXII TEM at 60 kV.

4.2.9 Reactive Oxygen Species Assays

Intracellular reactive oxygen species (ROS) were monitored using two different assays, 2',7'-dichlorodihydrofluorescein diacetate (DCFDA) and aminophenyl fluorescein (APF) (Life Technologies, Grand Island, NY). DCFDA generally is considered to react with most ROS molecules, and APF reacts more specifically with hydroxyl radical. The bacterial suspension was pelleted (1500g for 10 min), and the supernatant was decanted. Cells were resuspended in LB broth with either 10 μM DCFDA or 5 μM APF for one hour to allow cell uptake of fluorescent probe molecule. The bacterial suspension was again centrifuged (1500g for 10 min), and cells were washed 3 times with LB broth to remove extracellular DCFDA or APF. Bacteria were

exposed to as-syn TiO_2 nanoparticles in triplicate as described above in a range of 0-100 μg/mL. Periodically, a 250 μL samples was taken from each condition, placed in a 96 well plate, and the fluorescence intensity was measured at $\lambda_{excitation}$ = 485/20 nm and $\lambda_{emission}$ = 528/20 nm for both assays.

4.2.10 Quantitative Reverse Transcription Polymerase Chain Reaction (qRT-PCR)

qRT-PCR was performed on samples of *S. oneidensis* exposed to 0-100 μg/mL as-syn TiO_2 after varied amounts of time and/or 25 μg/mL P25 or T-Eco after a 24 h exposure. Primers were ordered through the BioMedical Genomics Center Oligonucleotide & Peptide Synthesis service using Integrated DNA Technologies (IDT) (Coralville, IA). Assay design was prepared using the Roche Universal Probe Library (UPL) technology. To validate the primer probe sets, a five point 1:5 dilution series of the cDNA sample was carried out. Total RNA was isolated using RNAzol® RT (Sigma Aldrich, St. Louis, MO) following manufacturer protocols. Total RNA samples were synthesized to first-strand cDNA using SuperScript® II RT from Invitrogen (Life Technologies, Grand Island, NY). Quantitative PCR was performed on the ABI 7900 HT (Life Technologies, Grand Island, NY) using 3 μLs of cDNA in duplicate. A working cocktail was made by adding 10 μM forward primer (IDT), 10 μM reverse primer (IDT), 10 μM probe (UPL), and 2.22X homebrew master mix. 3 μLs of cocktail was added to 3 μL aliquots of cDNA samples and amplified by the following parameters: 2 min activation at 60 °C and a 5 minute denaturation at 95 °C, followed by 45 cycles of 10 seconds at 95 °C and 1 minute at 60 °C.

Data analysis was performed using the Pffaffl method in which the amount of the target gene was normalized to a reference gene, gyrB, and compared to control samples. 1-way ANOVA analysis was performed to determine significant changes in gene expression levels.

4.3 Results and Discussion

4.3.1 Nanoparticle Characterization

Nanoparticle stability and ζ-potential were measured in water and LB broth to better understand the aggregation state of the nanoparticles during the toxicity experiments. These data, along with data on size and crystallinity that has been previously reported,[3, 19, 20] are summarized in Figure 4.1.

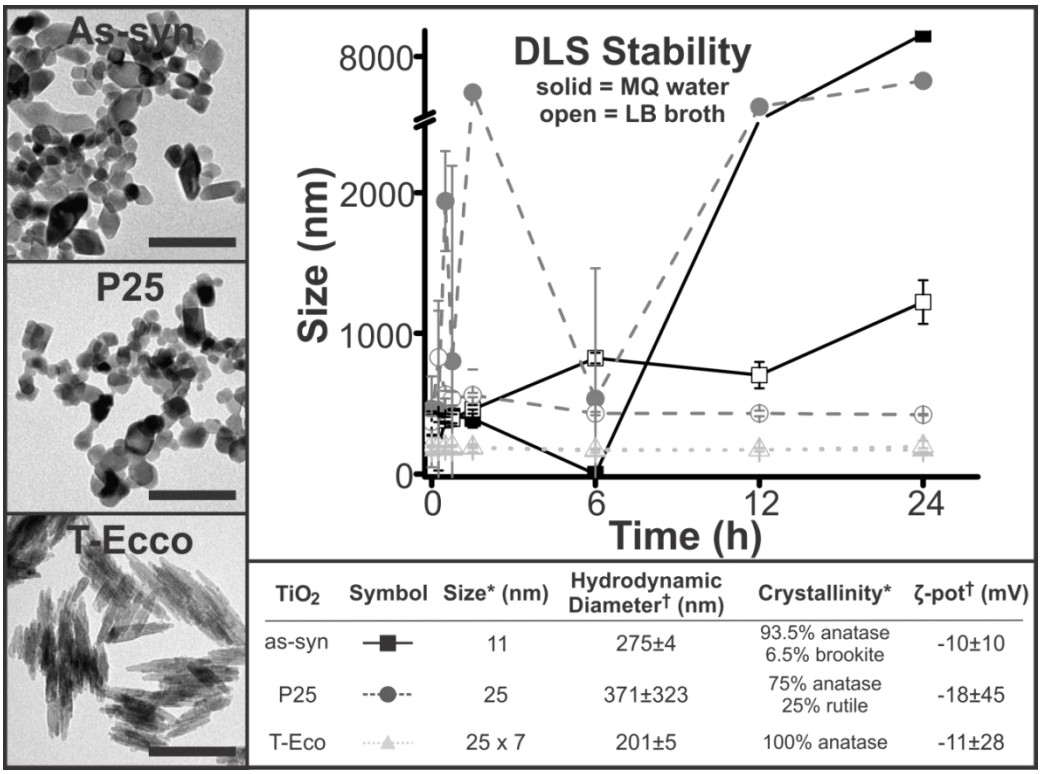

TiO_2	Symbol	Size* (nm)	Hydrodynamic Diameter† (nm)	Crystallinity*	ζ-pot† (mV)
as-syn	—■—	11	275±4	93.5% anatase 6.5% brookite	-10±10
P25	---●--	25	371±323	75% anatase 25% rutile	-18±45
T-Eco	····▲····	25 x 7	201±5	100% anatase	-11±28

Figure 4.1 Nanoparticle characteristics. * results taken from previously published work[3,19-20] † measurements taken in bacterial growth broth (LB broth). (ζ-pot = ζ-potential).

Generally, all three TiO_2 materials aggregate over 24 h, though T-Eco aggregates significantly less than as-syn and P25, possibly due to the T-Eco surface being coated with a thin layer of SiO_2. All nanoparticles in LB broth aggregated less than in water, likely because LB contains many biological macromolecules that can adsorb onto the surface and prevent aggregation.

4.3.2 TiO_2 Nanoparticles' Impact to Viability and Growth

Evaluating the viability of *S. oneidensis* after exposure to TiO_2 nanoparticles for various exposure times revealed no significant change in cell survival with increasing concentrations of as-syn TiO_2 over 24 h or with the nanoparticles of different material (see Figure 4.2), consistent with previous assessments of TiO_2 bacterial toxicity.[24, 25] There was some change in the ratio of live to dead bacteria over time (Figure 4.2B), but this was due to growth of bacteria within the experiment, and the same pattern of live/dead ratio changes were observed in all nanoparticle and control experiments.

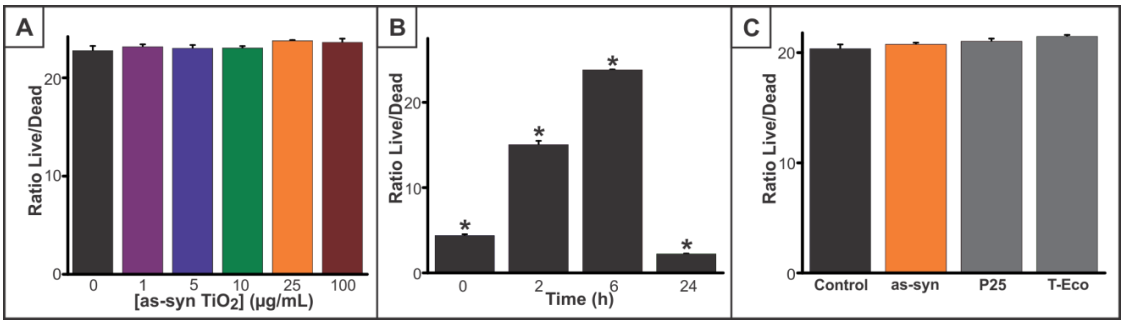

Figure 4.2 *S. oneidensis* viability after exposure to TiO_2 nanoparticles as measured with the Live/Dead Baclight™ assay. (A) Viability after 6 h exposure to varied concentrations (0-100 µg/mL) of as-syn TiO_2 nanoparticles. (B) Viability of *S. oneidensis* exposed to 25 µg/mL for varied times. *$p<0.05$ where each time point is significantly different than all other times of exposure. (C) Viability of 25 µg/mL of as-syn, P25, and T-Eco after 6 h exposure.

While viability is not altered in the presence of nanoparticles, TiO_2 caused a dose-dependent decrease in the growth rate of *S. oneidensis* (Figure 4.3A). By plotting the absorbance over time on a log scale, the exponential phase of growth was observed, and the growth or doubling rate was calculated by Equation 4.1 and quantified in the inset of Figure 4.3A. It is noted that initially, scattering from the nanoparticles contributed to the optical density measurements, so to confirm that we were observing changes as the result of slowed growth, we plotted the optical density minus the initial optical density, and differences in growth are still apparent (Figure 4.3B). A similar decrease in doubling rate was observed for all three nanoparticles, an indication that the nanoparticles are having a

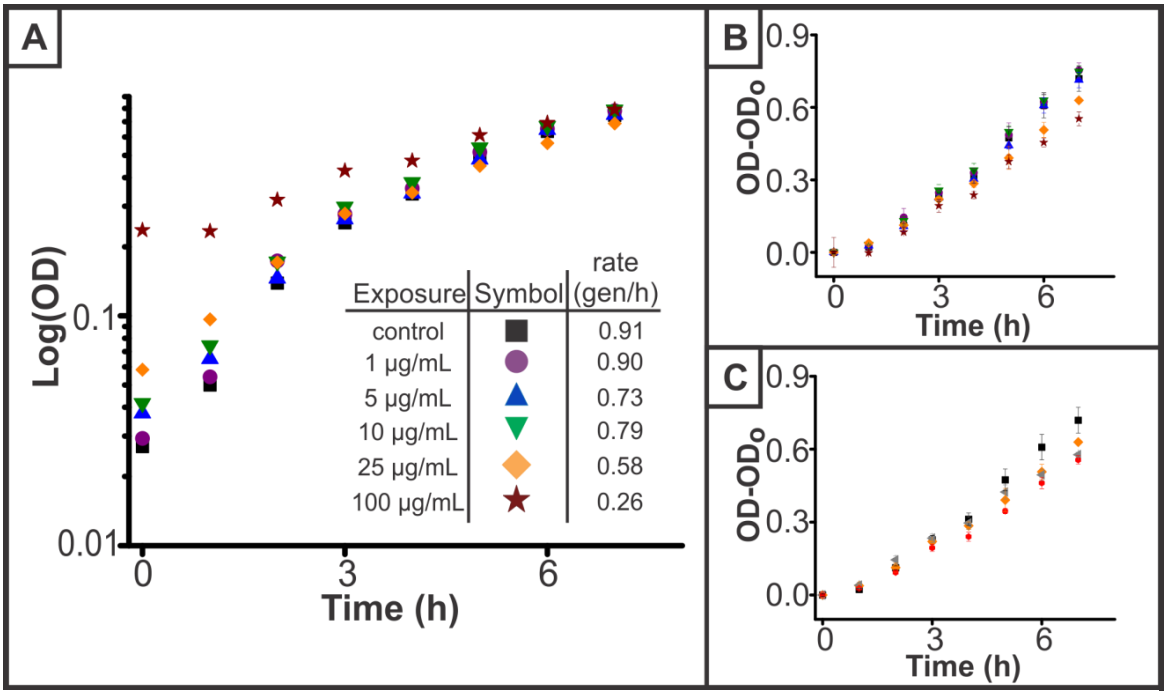

Figure 4.3 Growth of *S. oneidensis* in the presence of TiO_2 nanoparticles. (A) Exponential phase of bacteria grown in the presence of varying concentrations of as-syn TiO_2 nanoparticles. Inset indicates growth rate of bacteria as determined by Equation 4.1. (B) Exponential phase of growth with optical density at time = 0h subtracted to take into account scattering from nanoparticles. (C) Comparison of the growth of *S. oneidensis* in the presence of 25 µg/mL as-syn, P25, or T-Eco. Red pentagon=P25 and gray triangle=T-Eco.

similar impact on bacterial growth. This trend may be a result of non-specific adsorption of broth components onto the nanoparticle surface. The change of bacterial growth rate in the presence of TiO_2 nanoparticles has not been previously reported in *S. oneidensis* or other bacterial species.

4.3.3 Changes in Bacterial Functions

Moving beyond viability and growth, a functional assessment of *S. oneidensis* was performed, examining both a general bacteria and species-specific function. As mentioned previously, biofilm formation is a common function of bacteria of varied species and plays an important role in the way bacteria react to their surroundings,[26] with or without nanoparticles in this case. QCM enables measurement of biofilm growth based on the principles of the Sauerbrey equation ($\Delta m=-C\Delta f$), where changes in the resonant frequency (Δf) of a crystal are proportional to changes in mass (Δm) accounting for a crystal sensitivity factor (C). The Sauerbrey equation, however, assumes the deposited mass is rigidly bound to the crystal surface such that no damping occurs; this is not true of bacteria cells attaching to the surface. In this case, the series resonance resistance, which can be measured separately from the resonant frequency, is proportional to damping of the crystal resonance and, therefore, to the viscoelastic properties of the material deposited. A decrease in the series resonance resistance indicates a decrease in density of the deposited material. Herein, QCM measurements were used to assess both the mass of biofilm deposited on the crystal and the viscoelastic properties of the biofilm based on changes in frequency and resistance, respectively.

First, a comparison between control and 25 µg/mL as-syn TiO_2 nanoparticle-exposed cells was examined, where nanoparticles were introduced to the bacteria during the attachment phase to the QCM crystal and throughout biofilm growth (results shown in Figure 4.4). Figure 4.4A details the change in frequency of the parallel crystals. A notable characteristic of both the control and TiO_2-exposed bacteria is that the change in frequency is not linear. For control cells, an initial rapid decrease in frequency is observed as compared to the TiO_2 condition, indicating the addition of mass to the crystal, followed by a 'lag' and then further decrease in frequency. This pattern indicates that there is an initial attachment of bacteria to the crystal with a delay before the biofilm begins to grow. This pattern is in contrast to the results of biofilm formation among TiO_2-exposed bacteria, where there is a steady, but less steep change in frequency, with growth increasing after 12 h. We confirmed that the change in frequency was the result of biofilm growth or the combination of cell attachment/growth and TiO_2 deposition as

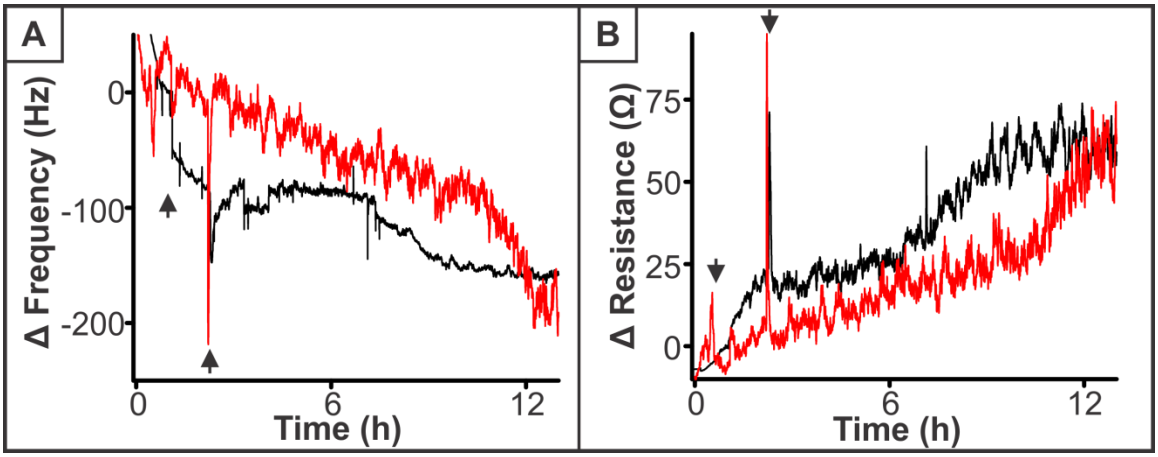

Figure 4.4 QCM response to bacterial biofilm formation and growth without (black) and with (red) exposure to 25 µg/mL as-syn TiO_2 nanoparticles. (A) Changes in deposited mass as measured by the change in frequency and (B) the viscoelastic properties as measured by changes in quartz crystal resistance. Arrows indicate the window of time where *S. oneidensis* are introduced to the QCM flow cell. Outside of this time range, flow consisted of aerated LB broth without or with TiO_2.

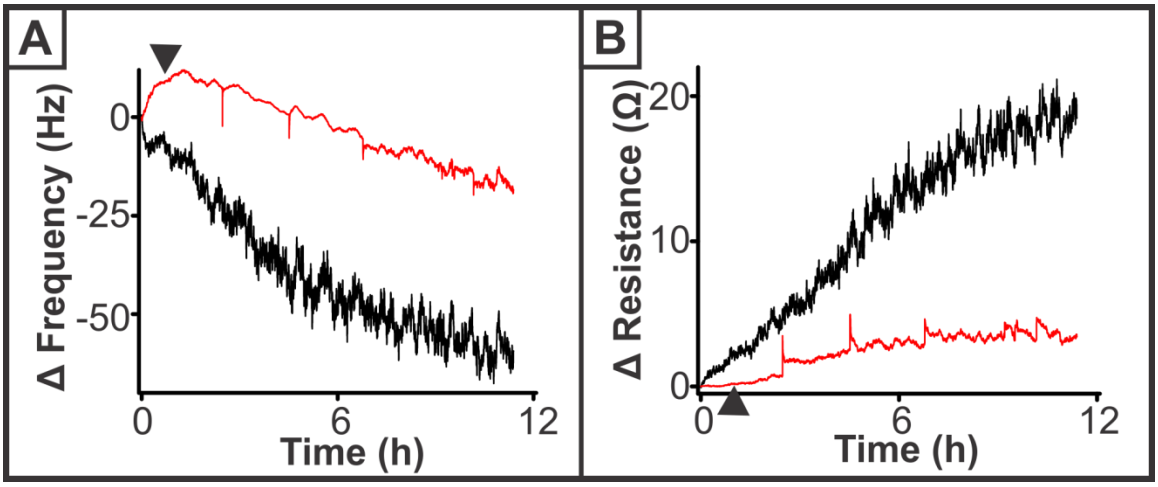

Figure 4.5 QCM drift without (black) and with (red) the presence of 25 µg/mL TiO_2 nanoparticles over the time course of a typical QCM experiment. Arrow head indicates addition of TiO_2 to LB broth with (A) showing the frequency drift and (B) indicating resistance drift.

opposed to TiO_2 nanoparticle sedimentation alone by a similar experiment, but without bacteria (Figure 4.5). This experiment showed there was drift within the system where the change in frequency becomes more negative, possibly due to adsorption of molecules from LB broth, but not deposition of TiO_2, and the drift was at most half that of the bacteria experiments. In general, QCM revealed that TiO_2 nanoparticle-exposed bacteria yield a slower change in frequency (Figure 4.4A) indicating a slower biofilm growth, which is consistent with the decrease in growth rate demonstrated above. However, the change in frequency is not linear with either control or TiO_2-exposed cells. Additionally, we considered the viscoelasticity differences between control and nanoparticle-exposed biofilms, but there was no appreciable difference in the change in resistance of the biofilm with and without nanoparticle exposure (Figure 4.4B). Another way to examine this is to plot the change in resistance divided by the change in frequency, and for both the control and TiO_2-exposed cells, there is no difference (graph not shown).

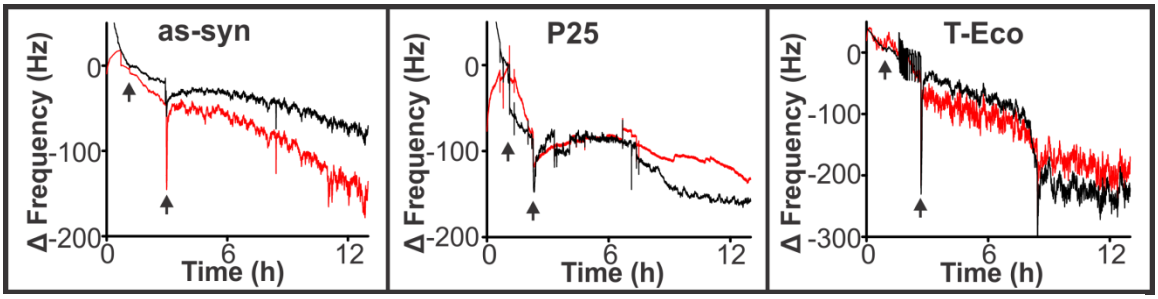

Figure 4.6 QCM analysis of bacteria exposed to 25 µg/mL as-syn, P25, or T-Eco nanoparticles during bacterial attachment, indicated by the window of time between the arrows. Red=TiO_2 exposure.

To elucidate whether the changes in biofilm growth were the result of changes in cell attachment, as opposed to simply the slowing of the rate of growth, we exposed cells to TiO_2 nanoparticles, of all three types, only during attachment and continued to monitor growth after nanoparticles were no longer present. Results varied (Figure 4.6), where as-syn TiO_2 nanoparticles seemed to promote adhesion, P25 inhibited adhesion, and T-Eco had no effect. However, the variations during attachment were small, and these differences could be due to the variations within cell populations. While it cannot be concluded that bacterial attachment is unaffected by the presence of TiO_2 nanoparticles, any nanoparticle-based impact appears to be small.

Another critical, species-specific function of *S. oneidensis* is its role as a metal reducer, where electron transfer occurs through the secreted molecule flavin mononucleotide (FMN).[27] FMN is converted to riboflavin, which was the molecule of interest in this study because FMN rapidly transforms to riboflavin even without the presence of a metal electron acceptor. Since *S. oneidensis* is responsible for metal reduction, one would predict stimulation of riboflavin secretion upon nanoparticle exposure; however, the energy required to reduce titanium (IV) likely exceeds the

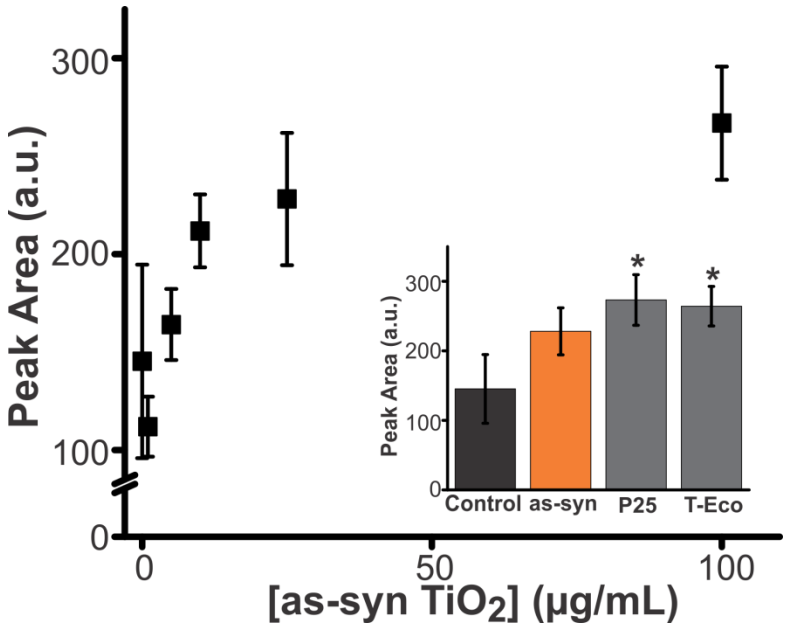

Figure 4.7 Riboflavin secretion, as measured with HPLC, is significantly increased ($p<0.05$) upon exposure to varying concentrations of as-syn TiO_2 nanoparticles. Inset includes a comparison of riboflavin secretion upon exposure to 25 µg/mL as-syn, P25, and T-Eco (*$p<0.05$ as compared to the control).

capability of the flavin reducing mechanism. Accordingly, we hypothesized that riboflavin secretion would decrease with nanoparticle exposure, correlating with the decrease in growth that was previously demonstrated.[28] After exposure to varying concentrations (0-100 µg/mL) and type of TiO_2 nanoparticles for 24 h, the extracellular riboflavin content was examined using HPLC, detecting the native fluorescence of riboflavin. Unexpectedly, extracellular riboflavin increased as a function of nanoparticle concentration (Figure 4.7), though no differences were apparent upon comparing the different TiO_2 materials. While there lacks literature precedent, this may be an indication that *S. oneidensis* flavin secretion may be activated as a response to a system stressor.

To examine if other secretion processes were affected by the presence of TiO_2, isolation and characterization of EPS for the sugar and protein content was performed as

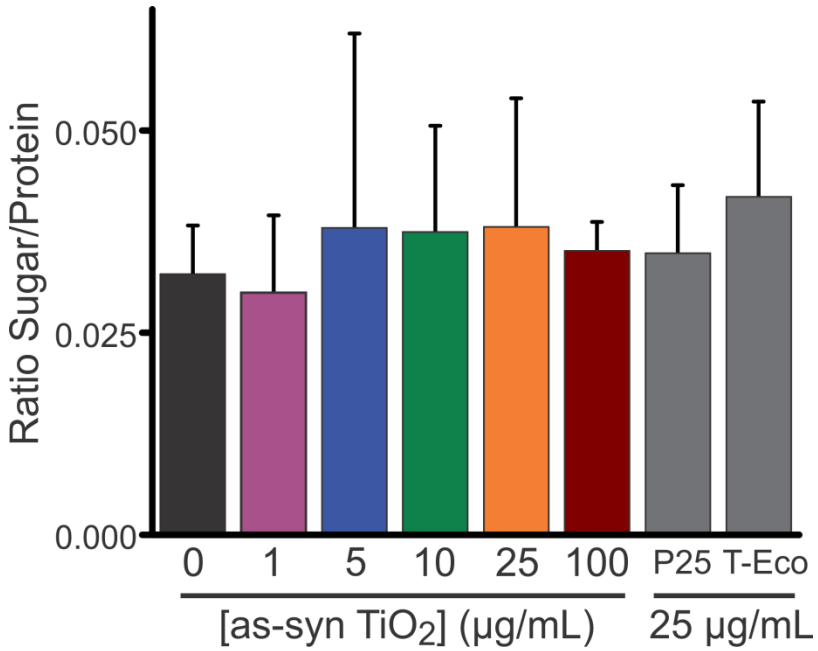

Figure 4.8 Characterization of EPS after 24 h exposure to varying concentrations and types of TiO_2 nanoparticles.

it relates both to secretion events and biofilms. That is, EPS is commonly considered to be the structural support for biofilms and is a mixture of macromolecules including secreted proteins and polysaccharides. Hessler et al. recently noted that EPS has a role in mitigating TiO_2 nanoparticle toxicity in *Pseudomonas aeruginosa* as measured by the Live/Dead Baclight™ assay.[24] In quantifying the protein and polysaccharide content of TiO_2 nanoparticle-exposed *S. oneidensis*, no change in the EPS is observed over the range of concentrations (1-100 µg/mL) or for the varied nanoparticle type after 24 h exposure (Figure 4.8). This indicates that growth and flavin secretion do not correlate to EPS production but could explain why changes in viability were not observed.

4.3.4 Mechanisms that Influence Changes in Cell Functions

Toward a mechanistic understanding of the changes in function that were observed in *S. oneidensis* after TiO_2 nanoparticle exposure, we examined nanoparticle

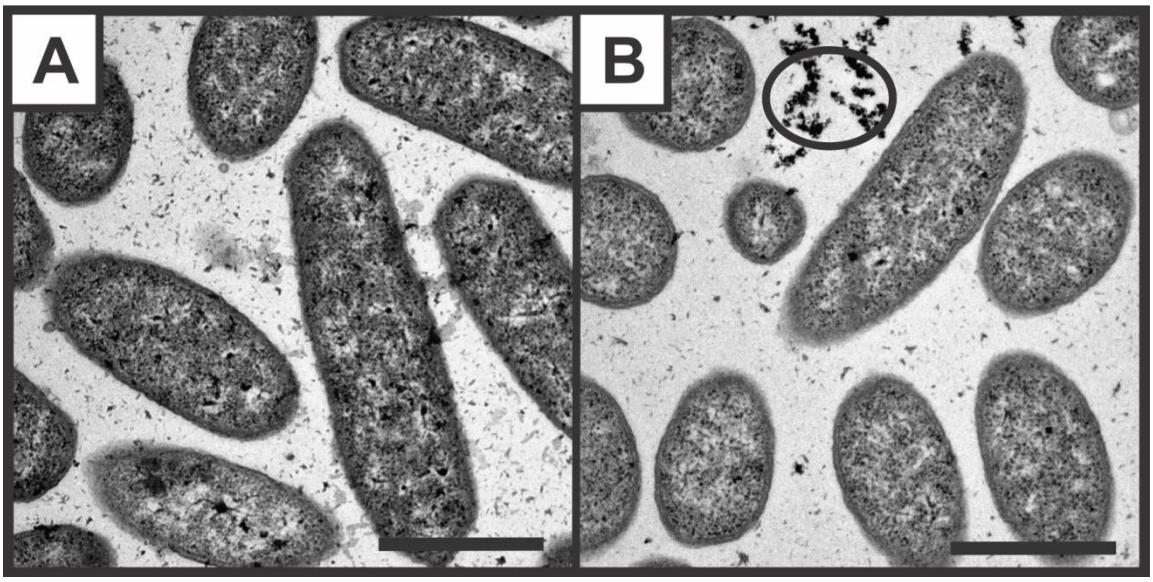

Figure 4.9 TEM images of *S. oneidensis* after 6 h incubation (A) without or (B) with 25 μg/mL as-syn TiO_2 nanoparticles. Circle indicates association of nanoparticle clusters close to bacteria. Scale bar = 1 μm

uptake or association, oxidative stress, and gene expression. Using TEM, we observed that TiO_2 nanoparticles are not internalized and do not appear to be membrane bound, though they are associated with the cells in some way as they are not washed off during rinse steps (Figure 4.9). This association was observed even after just a 2 h exposure.

Oxidative stress, or the production of ROS, is commonly considered to contribute to the mechanism of TiO_2 nanoparticle toxicity[29] and therefore, may contribute to the toxicity response measured herein (i.e. decreased growth and increased riboflavin secretion). Intracellular ROS was measured by first loading *S. oneidensis* with DCFDA or APF probe molecules, followed by exposure to varying concentrations of TiO_2 nanoparticles (0-100 μg/mL) for varying amounts of time. Over time, the intracellular ROS increases for all conditions but over the first 6 h, there is no significant difference between control and nanoparticle-exposed cells. By 24 h, a difference in ROS production is observed, but there is no trend with nanoparticle concentration, and repeated

experiments reveal that the observed differences are inconsistent (Figure 4.10). A similar response is seen with both the DCFDA and APF assays (data not shown). These results indicate that ROS levels are not correlated with measured changes in growth and riboflavin production, and observed ROS may simply be associated with normal biological processes or functions.

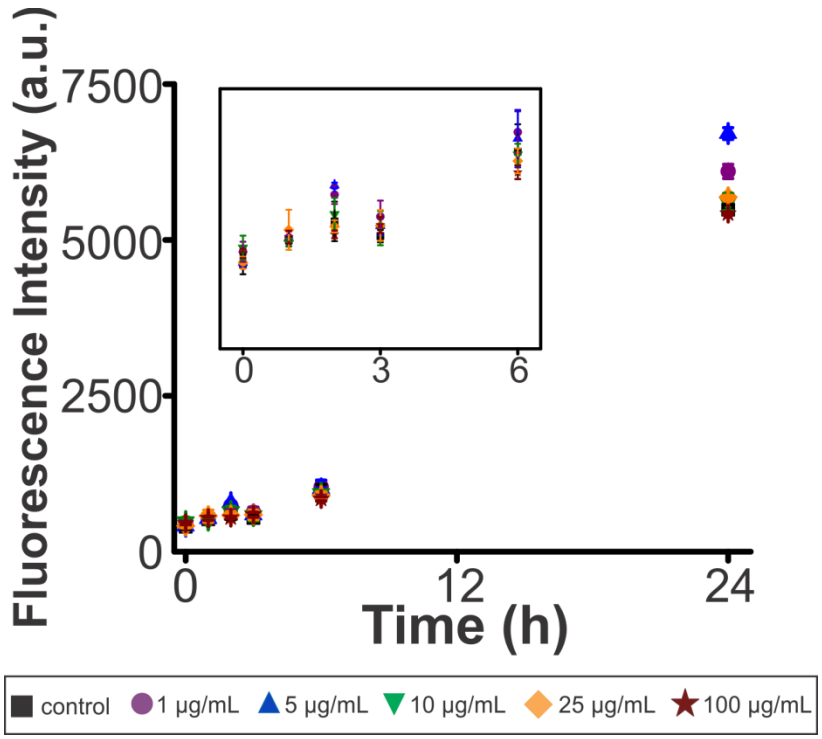

Figure 4.10 Amount of ROS over time as measured with the DCFDA assay upon exposure to varied concentrations of as-syn TiO_2 nanoparticles. Early time points (0-6 h) are illustrated in the inset.

Moving beyond uptake and oxidative stress, we examined the impact of TiO_2 nanoparticles on gene expression, which may reveal the source for the varied growth, biofilm formation and flavin secretion. Genes encoding for a variety of functions were explored using qRT-PCR after 24 h exposure to varied concentrations of as-syn TiO_2 (Figure 4.11 and Table 4.1) and 25 µg/mL P25 and T-Eco nanoparticles. Interestingly, in

all genes explored, P25 and T-Eco imparted no change in gene expression as compared to the control (data not shown) whereas as-syn nanoparticles induced some changes. Since no other toxicity assessments demonstrated a different response based on the material, it is unclear what parameters would cause P25 and T-Eco to induce varied gene expression from as-syn, though it may be the result of a different surface crystallinity (P25 is 25% rutile) and surface material (T-Eco has SiO_2 at the surface). Further exploration of how the chemical interface influences gene expression will be an area of future work, as it is beyond the scope of this study.

Flavin secretion by *S. oneidensis* is the main method of electron transfer in their metal reducing function, and metal reduction occurs as the result of signaling pathway that ends with the Mtr pathway.[30, 31] Genes related to this pathway studied herein include *cymA*,[32, 33] *ushA*,[27] *omcA*,[31] and *mtrA*.[30] While no significant trends are apparent for *cymA*, *mtrA*, and *ushA*, *omcA* shows significant ($p<0.05$) increase in gene expression after 24 h exposure to 10 µg/mL TiO_2 nanoparticles. While not significant, the other culture conditions are trending toward increased expression. *omcA* encodes for an outer membrane c-type cytochrome that plays a small role as a terminal reductase for metals and is also related to attachment of the cells to a solid surface.[31] Increased expression of this gene correlates with the increased riboflavin secretion by *S. oneidensis* over the 24 h exposure and also indicates that cell attachment as a biofilm may ultimately be affected, though this effect has not yet been observed. Other genes relating to biofilm formation and growth are the *mxdABCD* complex,[34, 35] and the expression of each of these genes was quantified after 24 h nanoparticle exposure. Of these, both *mxdA* (Figure 4.11) and *mxdB* (Table 4.1) showed decreased expression as compared to the control. *mxdA*

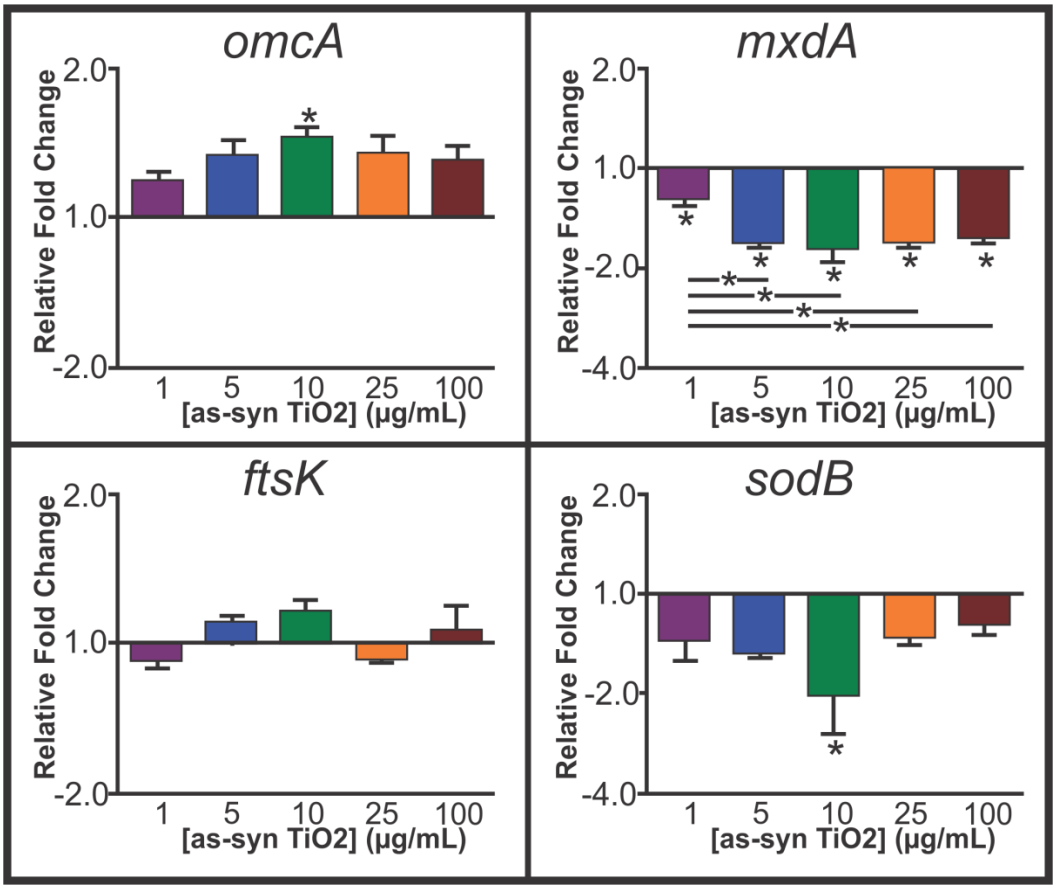

Figure 4.11 Relative fold change of genes related to flavin secretion (*omcA*), biofilms/EPS (*mxdA*), growth (*ftsK*), and cell stress (*sodB*) upon 24 h exposure to varying concentrations of as-syn TiO_2 nanoparticles (*$p<0.05$).

encodes for a diguanaylate cyclase protein and mxdB encodes for an inner membrane glycosyltransferase, both of which relate to cell attachment and synthesis of exopolymeric saccharides, which relates to EPS;[34, 35] both genes are essential for the three-dimensional growth of biofilms. Since these are both down regulated after exposure to most concentrations of nanoparticles, this may explain the decrease in growth of biofilm, as observed with QCM, because the syntheses of proteins for three dimensional growth are synthesized in lower amounts. However, the relationship of *mxdA* and *mxdB* to EPS would potentially indicate changes in the secretion profile that were not observed in the EPS characterization (Figure 4.8). It is possible that the EPS

analysis is not sensitive enough to see these changes. Alternatively, the expression of these genes at 24 h may differ from the expression at early time points. That is, gene expression may be initially stimulated upon TiO_2 nanoparticle exposure producing a level of protein that then causes a decrease in expression at the measured 24 h time point, ultimately yielding a zero net balance to the content of the EPS.

Other genes of interest included *ftsK*, responsible for chromosome partitioning proteins that relate to growth,[36] and various stress response genes. These stress response genes include *sodB* and *gst*, which code for ROS response proteins superoxide dismutase B and glutathione transferase,[37] *pspB*, which codes for cytoplasmic membrane stress indicator phage shock protein,[38] *dnaN*, responsible for DNA polymerase protein, and *radA*, which encodes for DNA repair proteins. Significant changes in gene expression were observed only for *sodB* and *pspB*. It is unsurprising to see no trend for *ftsK* expression because after 24 h, the bacterial culture has reached stationary phase, even in the presence of nanoparticles; therefore, the presence of chromosome partitioning proteins should be a steady state for all conditions. *pspB* expression levels (Table 4.1) were significantly higher for cells exposed to 25 µg/mL TiO_2 as compared to the control, indicating increased cytoplasmic membrane stress. In the case of *sodB*, there is a decreasing trend of *sodB* expression after 24 h exposure with lower nanoparticle concentrations, with a significant decrease at 10 µg/mL as-syn TiO_2 nanoparticles, though the expression is recovered at 25 and 100 µg/mL. This expression was unexpected because if oxidative stress had occurred, an increased expression would be expected. Again, the decrease may be the result of quantification of gene expression after 24 h exposure, and earlier time points may yield a different expression level. This is

particularly true for oxidative stress, as typically oxidative stress effects are observed on short time scales due to the short lifetime of the ROS molecules.[39]

Table 4.1 Relative fold change of other genes related to flavin secretion, biofilms/EPS, and cell stress investigated with qRT-PCR. Red values with a negative sign indicate a decrease in gene expression as compared to the control and black positive values are increased gene expression as compared to the control. Gray cells indicate significant ($p<0.05$) difference in expression as compared to the control.

		[as-syn TiO2] (µg/mL)				
Function	**Gene**	**1**	**5**	**10**	**25**	**100**
Flavin secretion	*mtrA*	-1.01	1.10	1.24	1.11	1.01
	cymA	1.10	1.11	1.04	1.25	1.28
	ushA	-1.13	-1.06	-1.14	1.07	1.07
Biofilms and EPS	*mxdB*	-1.37	-1.57	-1.70	-1.73	-1.56
	mxdC	-1.11	1.17	-1.14	1.20	-1.06
	mxdD	-1.16	-1.06	-1.16	-1.03	-1.10
Stress	*gst*	-1.12	1.01	1.18	1.13	1.06
	pspB	-1.04	1.18	1.07	1.62	1.34
	radA	-1.28	-1.04	-1.09	1.01	-1.14
	dnaN	-1.21	-1.01	-1.15	1.11	-1.00

To explore the impact of time on gene expression levels, we took periodic samples of *S. oneidensis* exposed 25 µg/mL as-syn TiO_2 nanoparticles and monitored expression of *omcA*, *mxdA*, *ftsK*, and *sodB* as these genes showed some interesting trends after 24 h exposure that may be related to exposure time. As seen in Figure 4.12, *sodB* showed no significant trend over time as compared to the control, supporting the previous conclusion that oxidative stress does not appear to be the root of growth and flavin secretion changes. The lack of change in *ftsK* as compared to the control indicates that this gene is not responsible for the changes in growth rate that have been observed, and further exploration is needed. Both *omcA* and *mxdA* demonstrate an initial increase in expression until 3 h, after which, expression is not different from that of the control. For *omcA*, this further supports the role TiO_2 nanoparticles play in stimulating flavin

secretion as it is stimulated within 3 h. For *mxdA*, the initial burst (until 3h) followed by return to control level at 6 h and ultimate decrease in expression after 24 h may indicate that after there is a threshold level of protein available to the bacteria, the gene expression is less. This initial burst followed by decreased expression would explain why changes in EPS were not observed. In relationship to biofilm formation and growth, the lack of difference in gene expression after 1 h could explain why only minor differences in biofilm attachment were observed (Figure 4.6) but growth of the biofilm over time was depressed.

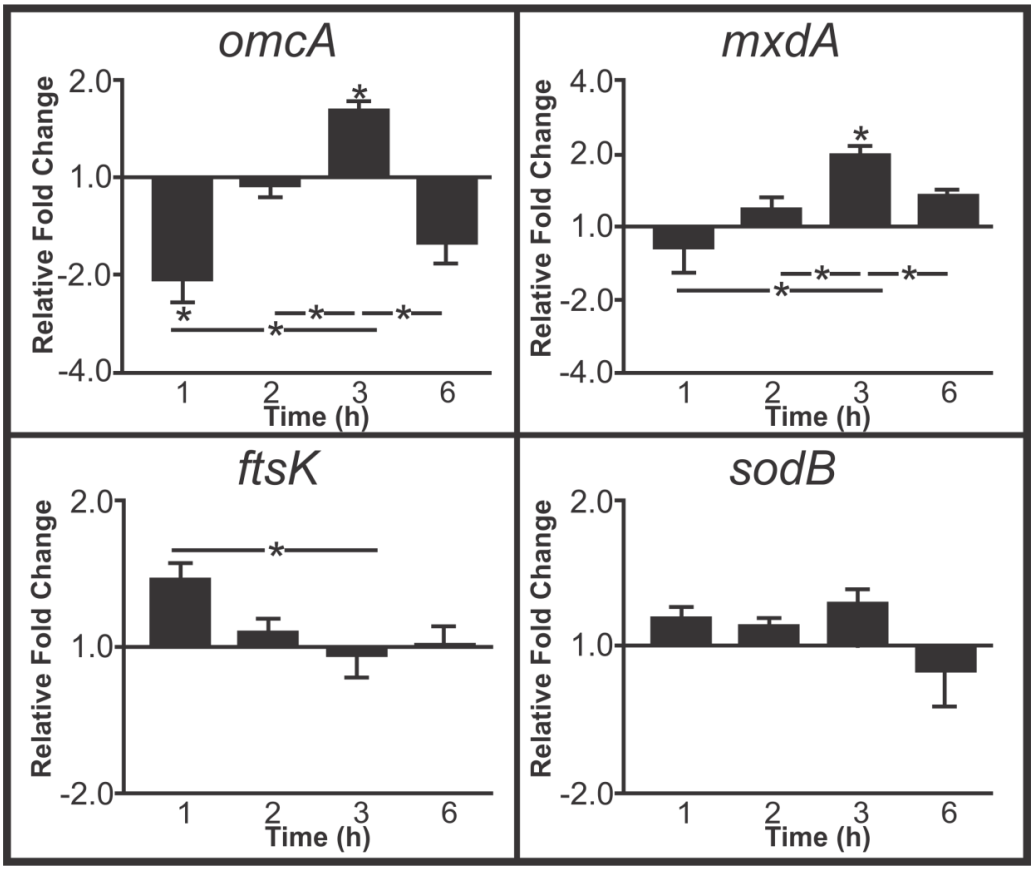

Figure 4.12 Relative fold change of genes upon exposure to 25 µg/mL as-syn TiO_2 at varying times (*p<0.05).

4.4 Conclusions

Gaining an understanding of the functional changes within a species upon exposure to nanoparticles is critical for understanding subtle changes in ecosystem health. Additionally, it aids in the development and use of nanotechnology in a sustainable way. In this study, we demonstrated that, while minimal changes in viability were observed, significant changes in bacterial growth, biofilm growth and riboflavin secretion of *S. oneidensis* occurred after exposure to TiO_2 nanoparticles. These changes were not the result of oxidative stress, but the proximity of the nanoparticles changes to gene expression that influenced bacterial function. Though there was some discrepancy in the material induced changes in gene expression, generally the type of TiO_2 nanoparticle (i.e. as-syn vs. P25 vs. T-Eco) elicits similar functional changes within *S. oneidensis*, and the discrepancies and similarities are likely the result of surface structure and will be the subject of future work.

Though the field of econanotoxicity is relatively new, this study presents an important approach to studying toxicity. That is, through a nuanced view of toxicity (i.e. functional assessment), a clear understanding of the nanoparticle impact is gained, and this yields beneficial information to inform nanoparticle design and mitigate any unintentional toxicity.

Chapter Five

Characterization of Ag^+ Dissolution from Ag Nanoparticles using Fluorous-phase Ion-selective Electrodes and Subsequent Toxicity in *Shewanella oneidensis*

This work completed in collaboration with Seyedeh M. Mousavi, Li Chen, Philippe Buhlmann, and C.L. Haynes.

5.1 Introduction

Dynamic characterization of nanoparticles is important within toxicity studies to understand how nanoparticle characteristics affect toxicity. Currently, there are a range of analytical tools employed to characterize nanoparticles at specific times in the toxicity assessment; yet, most of these tools cannot accomplish dynamic, *in situ* characterization. It is clear from the literature that nanoparticle characteristics readily change in complex environments (e.g. body or environment) due to their high surface reactivity, and these characteristics evolve over time.[1, 2] Unfortunately, the limited analytical tools for *in situ* nanoparticle characterization are impeding the fundamental understanding necessary to advance the field of nanotoxicology. One nanoparticle characteristic that is particularly important in nanotoxicology is the dissolution of nanoparticles into toxic ions.

Silver nanoparticles (Ag NPs) are considered to be the mostly widely used nanoparticle in nanoparticle-enabled consumer products, including wound dressings, toys, and clothing.[3] Primarily used as an antimicrobial agent, global production was 280 tons in 2011 and is expected to increase to 1200 tons by 2015.[4] The antimicrobial nature of Ag NPs is imparted primarily through the dissolution of Ag^+,[5] which can bind proteins and enzymes to disrupt normal cell function; [6, 7] therefore, it is critical to understand the extent and kinetics of dissolution to Ag^+ to understand Ag NP toxicity.

Due to the role of ion release in nanotoxicity, many studies have worked to characterize Ag NP dissolution. Atomic spectroscopy is commonly used for characterization, where the supernatants of nanoparticle suspensions are analyzed for the mass (inductively coupled plasma mass spectrometry (ICP-MS)), atomic emission, or atomic absorption of the atom of interest.[8-11] These techniques are highly selective and

sensitive, with picomolar detection limits. Another common method is to monitor the localized surface plasmon resonance of Ag NPs, where a decrease or shift in extinction correlates with dissolving nanoparticles, though this technique requires high concentrations of Ag NPs that may be environmentally unrealistic.[12] Both of these techniques, however, only provide a snapshot of the ion content, failing to provide real-time, *in situ* assessment of the silver ion concentration, and, in the case of atomic spectroscopies, are fairly expensive. Another disadvantage to these techniques is that they are limited in their ability to differentiate between whether the dissolved Ag is free or complexed Ag^+. It is well known that silver forms stable complexes with Lewis bases such as –SH, -NH_2 and -Cl, which are present in body fluids and cell culture media.[13] Complexation results in lowering the activity of free silver ions and can alter the bioavailability and subsequent toxicity of Ag^+. For example, increased sulfidation of Ag^+ and Ag NP can decrease bioavailability and toxicity in a variety of organisms;[2, 14, 15] therefore, understanding the species of the dissolved Ag from Ag NP is also important.

Ion-selective electrodes (ISEs) provide inexpensive, continuous, sensitive, and selective measurements of Ag^+, which make them an appealing tool for studying the kinetics of Ag NP dissolution. Additionally, ion-selective electrodes have the ability to quantitatively differentiate between free and complexed Ag^+, which could result in a more accurate assessment of Ag NP toxicity. There has been some literature precedent for use of commercially available Ag/Ag_2S ISE sensors for the study of nanoparticle dissolution, including a study using the ISE to study ion release within a cell culture.[13] While this study confirms complexation of Ag^+, lack of signal stability in the commercially available Ag/Ag_2S ISE limits the proper measurement of concentration of

Ag^+ released from dissolution of Ag NPs. Also, only five discrete measurements were recorded over 24 h, failing to provide kinetic information about nanoparticle dissolution; this was likely the result of the electrode susceptibility to biofouling. Biofouling, a common problem limiting the lifetime and response of ISEs, occurs as a result of adsorption of lipids and proteins onto the sensing membranes and extraction of lipophilic species into the sensing membrane.[16-18]

Herein, we use fluorous-phase ionophore-doped ISEs for the continuous monitoring of dissolution of citrate-capped Ag NPs in water or bacterial growth broth. Fluorous phases have extraordinarily low polarity and polarizability, and as a result, many alkanes are not miscible with perfluoroalkanes and many lipids have poor solubility in fluorous phases.[19-21] These characteristics of fluorous phases make fluorous-phase ISEs less susceptible to biofouling by limiting the extraction of neutral biomolecules into the sensing membrane.[18] In addition to lowering the susceptibility to biofouling, the silver ionophore-doped fluorous ISEs, which have been described previously by Lai *et al.*,[22] offer exceptional selectivity for Ag^+. The exceptional selectivity arises from the non-coordinating and poorly solvating properties of these fluorous phases that result from their extremely low polarity. Having all the aforementioned properties, the silver ionophore-doped fluorous-phase ISEs are an uniquely appropriate tool for continuous monitoring of Ag NP dissolution in water and the complex solution of bacterial growth broth.

Using fluorous-phase ISEs, we measured the concentration of Ag^+ and correlated this concentration with the toxicity to the bacteria *Shewanella oneidensis* MR-1. *S. oneidensis* are a minimally pathogenic bacterium found in a wide range of geographical

and ecological conditions and are notable for their role in geochemical nutrient cycling.[23] More specifically, they are metal reducers and therefore, the likelihood of interaction of *S. oneidensis* and metal nanoparticles is high, making *S. oneidensis* a relevant model species in studying Ag NP toxicity. By combining dissolution assessment with toxicity studies, this study lays the foundation for the ultimate development of an *in situ* nanoparticle characterization and toxicity assessment tool.

5.2 Methods

5.2.1 Nanoparticle Synthesis and Characterization

Citrate-capped Ag NPs were synthesized freshly for every experiment following a procedure detailed by Hackley and coworkers.[24] Prior to synthesis, glassware was cleaned with aqua regia (3:1 HCl:HNO_3) and rinsed three times with Milli-Q purified water (18MΩ·cm specific resistance, EMD Millipore, Burlington, MA). For the synthesis, 50 mL MQ water was brought to a boil and then 365 μL of 34 mM trisodium citrate dihydrate (Sigma Aldrich, St. Louis, MO) and 211 μL $AgNO_3$ (Sigma Aldrich, St. Louis, MO) were added, followed by drop-wise addition of freshly prepared 250 μL $NaBH_4$ (Sigma Aldrich, St. Louis MO). Upon addition of $NaBH_4$, the solution immediately turned yellow, and the mixture was allowed to boil for 15 min before removing the nanoparticles from heat and allowing them to come to room temperature. Nanoparticles were purified with regenerated cellulose (MWCO 50,000) centrifugal filter units (EMD Millipore, Carrigtwohill, Ireland) where 15 mL of the nanoparticle suspension were centrifuged at 1500 g for 4 min then resuspended in MQ water, with the centrifuge/resuspension steps repeated in triplicate. The concentration of

nanoparticles in the final, purified nanoparticle solution was determined via UV-vis (Ocean Optics, Dunedin, FL) using the extinction coefficient 8.7×10^8 M^{-1} cm^{-1}, as determined experimentally via correlation of absorbance values to concentrations of nanoparticles measured with ICP-MS (ICP-MS method below). Concentrations were converted to μg/mL by calculating the number of atoms per nanoparticle and converting atoms to mass using the atomic weight of Ag (107.868 g/mol). The number of atoms per nanoparticle (U) were determined based on Equation 5.1 from Marquis *et al.*,[25]

$$U = \frac{2}{3}\pi\left(\frac{D}{a}\right)^3 \quad (5.1)$$

where D is the nanoparticle diameter (11 nm) and a is the edge length of the unit cell (4.0857 Å for Ag).

Nanoparticles were characterized by transmission electron microscopy (TEM – JEOL 1200EX III, JEOL, Tokyo, Japan), UV-visible spectroscopy (USB2000, Ocean Optics, Dunedin, FL), dynamic light scattering (DLS – 90Plus, Brookhaven Instruments Corporation, Holtsville, NY), and ζ-potential measurement (ZetaPALS, Brookhaven Instruments Corporation, Holtsville, NY). The stability of the nanoparticles was monitored over 24 h with both DLS and ζ-potential in both MQ water and bacterial ferric citrate broth (described below).

5.2.2 Fluorous-phase ISE Fabrication

Ionophore-doped fluorous-phase ISEs were prepared in-house, which included preparation of the ionophore-doped fluorous membrane and assembling the electrodes.

To prepare sensing membranes, 0.5 mM ionic sites and 1.5 mM ionophore were added to the perfluoroperhydrophenanthrene (Alfa Aesar, Ward Hill, MA), and the resulting mixture, considered to be the sensing phase of the membrane, was stirred for at least 24 h to ensure complete dissolution. The ionophore, 1,3-bis(perfluorooctylethylthiomethyl)-benzene and the ionic site, sodium tetrakis[3,5-bis(perfluorohexyl)phenyl]borate, were prepared according to previously described procedures[18] and embedded on Fluoropore™ filters (porous poly(tetrafluoroethylene), 47 mm diameter, 0.45 μm pore size, 50 μm thick, 85% porosity, EMD Millipore, Bedford, MA). The Fluoropore™ filters were sandwiched between two note cards, and were cut with a 13 mm diameter hole punch to prepare the porous filter disks. The fluorous sensing phase was then applied with a micropipet onto a stack of 2 porous filter disks used to mechanically support the fluorous membrane. Full penetration of the fluorous phase into the porous supports was confirmed by a translucent appearance of the thus prepared sensing membranes.

The prepared fluorous membranes were mounted into custom machined electrode bodies made from poly(chlorotrifluoroethylene), as described previously.[18] In brief, a screw cap with a hole (8.3 mm diameter) in the center was screwed onto the electrode body, mechanically securing the sensing membrane in between the electrode body and the cap but leaving the center of the membrane exposed. The electrode bodies were then filled with 1 μM $AgCH_3CO_2$ (Sigma Aldrich, St. Louis, MO) followed by insertion of an Ag/AgCl wire. Prior to measurements, all electrodes were conditioned in a 100 mL of 0.1 mM $AgCH_3CO_2$ solution for 24 h and then conditioned in 100 mL of 1 μM $AgCH_3CO_2$ for another 24 h.

5.2.3 Fluorous-phase ISE Measurements

Potentials were monitored with an EMF 16 potentiometer (Lawson Labs, Malvern, PA) controlled with EMF Suite 1.02 software (Lawson Labs) at room temperature (25 °C) in stirred solutions. The external reference electrode consisted of a double-junction Ag/AgCl electrode with a 1 M LiOAc bridge electrolyte and a 3 M KCl reference electrolyte. All measurements were performed with 3 replicate electrodes. Calibration curves were obtained by addition of various volumes of 10 mM $AgCH_3CO_2$ to 100 mL of the solution, followed by measuring EMF at each concentration. For monitoring dissolution of nanoparticles for 24 h, 3 replicate electrodes were prepared, calibrated and placed in 100 mL of the solution. Purified Ag NPs described above were added in varying concentrations (0.3-15 µg/mL) to the solution, and the EMF was monitored for 24 hours, after which the electrodes were again calibrated to assure stability of response and sensitivity to silver ions. Ag NP dissolution was monitored in MQ water and ferric citrate bacterial growth broth.

Ferric citrate broth for bacterial culture, modified from reference 26, was made with limited chloride content to prevent AgCl complexation, and consisted of 56 mM ferric citrate (Sigma Aldrich, St. Louis, MO), 30 mM sodium lactate (from 60% solution, Spectrum Chemical, Redondo Beach, CA), 30 mM $NaHCO_3$ (Sigma Aldrich, St. Louis, MO), 5 mM NaH_2PO_4 (Sigma Aldrich, St. Louis, MO), 19 mM $(NH_4)_2SO_4$ (Fisher Chemical, Fairlawn, NJ), 1 mM KCH_3CO_2 (Mallinckrodt, Phillipsburg, NJ), and 1% mineral solution (see details below). To make the broth, ferric citrate was dissolved in MQ water by mildly heating, and then the pH was adjusted to 6.7 with NaOH (Mallinckrodt, Phillipsburg, NJ) before the other components were added, yielding a final

pH of ~7.7. The mineral solution consisted of 17.3 mM $NaCH_3CO_2$ (EMD, Gibbstown, NJ), 8.7 mM $MnSO_4 \cdot H_2O$ (Mallinckrodt, Phillipsburg, NJ), 0.9 mM $CaCl_2$ (Fisher Chemical, Fairlawn, NJ), 0.4 mM $CoCl_2 \cdot 6H_2O$ (Mallinckrodt, Phillipsburg, NJ), 0.4 mM $FeSO_4 \cdot 7H_2O$ (Fisher Chemical, Fairlawn, NJ), 0.15 mM H_3BO_3 (Mallinckrodt, Phillipsburg, NJ), 25 μM $AlK(SO_4)_2 \cdot 12H_2O$ (Mallinckrodt, Phillipsburg, NJ), 46 μM $CuSO_4 \cdot 5H_2O$ (Spectrum Chemical, Redondo Beach, CA), and 41 μM $Na_2MoO_4 \cdot 2H_2O$ (Sigma Aldrich, St. Louis, MO).

For comparison, Ag NP dissolution in MQ water and ferric citrate broth was monitored at discrete time points in parallel experiments using ICP-MS (XSeries 2, Thermo Scientific, Beverly, MA). In these experiments, aliquots were collected at 0, 2, 6, 12,and 24 h, and supernatants were separated from the nanoparticles by centrifugation at 4000 g for 10 min using centrifugal filter units. Supernatants were analyzed for mass transitions of 107 for Ag quantitation, with an indium internal standard monitored at 115.

It should be noted that the concentrations of Ag NP and measured Ag^+ were not transformed to the same units (μg/mL or M) so as to maintain the most commonly utilized description of concentration for each described in the literature. Units were reconciled, however, to determine percent dissolution.

5.2.4 Bacterial Culture

Shewanella oneidensis MR-1 were generously gifted from the Gralnick lab at the University of Minnesota. To prepare bacteria for toxicity assessments, cells stored at -80 °C were streaked onto a plate, allowing colonies to grow for ~18-24 h, upon which

colonies were transferred to Luria-Bertani (LB) growth broth (1 colony per 5 mL broth). Cells were cultured to stationary phase overnight (over 15 h) on a shaking incubator (200 rpm at 30°C), pelleted by centrifugation at 750g for 10 min, and resuspended in the ferric citrate broth. This suspension of cells was used going forward for toxicity assessments, herein referred to as "bacteria suspension," and the cell density of the bacteria suspension was consistently 10^9 cells/mL. When bacteria were not being used or measured, the suspension was maintained on the shaking incubator.

5.2.5 Bacterial Toxicity Assays

5.2.5.1 Viability

LIVE/DEAD® Baclight™ (Life Technologies, Grand Island, NY) was used to assess viability of *S. oneidensis* after exposure to varying concentrations of $AgCH_3CO_2$ (referred to as Ag^+) and Ag NPs for up to 24 h. Cells from the bacteria suspension were diluted to a density of 10^8 cells/mL with ferric citrate broth and exposed to varying concentrations (1-10 μM) of Ag^+ or (0.3-15 μg/mL) of Ag NPs with each condition cultured in triplicate and periodic assessment of viability taken over the 24 h exposure. The assay was performed as described in detail in section 4.2.3, where live cells are stained with green fluorescent molecules (SYTO-9) and dead cells stained with red fluorescent molecules (propidium iodide). Measurements were performed after 0, 2, 6, 12, and 24 h exposure, and results were analyzed by comparing the ratio of live-cell (green fluorescence) to dead-cell (red fluorescence) of the control and silver exposure conditions.

5.2.5.2 Growth

The phases of bacterial growth (lag, exponential, and stationary phases) were monitored for *S. oneidensis* after exposure to varying concentrations of Ag^+ and Ag NPs. The bacteria suspension was diluted to 10^7 cells/mL in ferric citrate broth with exposure to 1-10 μM Ag^+, 0.3-15 μg/mL Ag NPs, or water for the control with each condition in triplicate. Growth was monitored over 48 h with periodic measurement of optical density at λ=600 nm with Spectronic 20D spectrophotometer (Milton Roy Company, Ivyland, PA). The growth rate was determined from the exponential phase of growth with Equation 4.1.

5.3 Results and Discussion

5.3.1 Nanoparticle Characterization

Citrate-capped Ag NPs were chosen for the study of dissolution because citrate is one of the most widely used Ag NP capping agents. Careful characterization of the nanoparticles is important for understanding dissolution and toxicity results, and herein, Ag NPs were characterized with TEM, DLS, ζ-potential, and UV-visible spectroscopy. A summary of nanoparticle characteristics can be found in Table 5.1.

Table 5.1 Summary of Ag NP characteristics. Solution phase measurements were performed in ferric citrate growth broth.

Characteristic	**Value**
Size (as determined by TEM)	11 ± 3 nm
Hydrodynamic diameter (DLS)	112 ± 6 nm
ζ-potential	-29 ± 3 mV
LSPR (λ_{max})	389 ± 1 nm

Nanoparticles were synthesized fresh for each experiment to ensure that the nanoparticles were similar for each ISE and toxicity assessment. To confirm consistency from synthesis to synthesis, triplicate syntheses were performed and size was characterized with TEM (See Figure 5.1A for TEM image). As seen in Figure 5.1B, the distribution of sizes is consistent between preparations, with an average diameter of 11 ± 3 nm, and this consistency was verified with the localized surface plasmon resonance, as measured with UV-visible spectroscopy (Table 5.1). Further characterization of the nanoparticle stability over time was assessed with DLS in both MQ water and ferric citrate bacterial growth broth. In both water and ferric citrate broth, there is an initial increase in the aggregate size over the first 6 h, with a plateau of aggregate size at longer times. Ferric citrate broth, however, causes larger Ag NP agglomerates to form, which agrees with the correlation established in the literature where increased ionic strength, like in the broth, causes greater agglomeration/aggregation of the Ag NPs.[27]

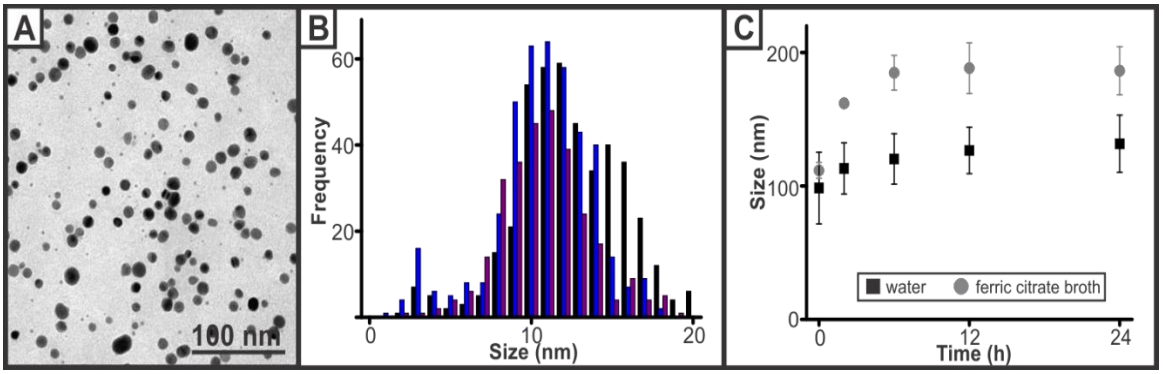

Figure 5.1 Nanoparticle characterization. (A) TEM of Ag NP (B) Histogram of sizes, as measured with ImageJ (NIH, Washington DC) from 3 separate syntheses (C) hydrodynamic diameter of 3 µg/mL Ag NP in MQ water and ferric citrate broth

5.3.2 Characterization of Dissolution with Fluorous-phase ISEs

Examination of Ag^+ dissolution kinetics and concentration were first monitored in MQ water. After calibration and equilibration, Ag NPs were added to the water and monitored over 24 h. A typical electrode response, or trace, seen in these experiments is demonstrated in Figure 5.2A (for dissolution of 3 µg/mL Ag NPs) with each color representing an individual electrode's response. The measured potential was converted to concentration of free Ag^+ using a calibration curve (Figure 5.2B). To confirm the initial burst of signal observed upon addition of Ag NPs (Figure 5.2A) was due to the increase of Ag^+ as opposed to other interferences, dissolution was monitored for 30 min from 3 µg/mL Ag NPs in MQ water, after which aliquots of 1M NaCl were added (Figure 5.2C). After each addition of NaCl, the potential immediately drops, indicating that there is a decrease in free Ag^+, a result of Ag^+ and Cl^- binding. Since the ISE is responding quickly to the change in concentration of free Ag^+, it can be concluded that the fluorous-phase ISEs have an immediate response to free Ag^+ concentrations and that the initial burst in response upon addition of Ag NP is the result of free Ag^+.

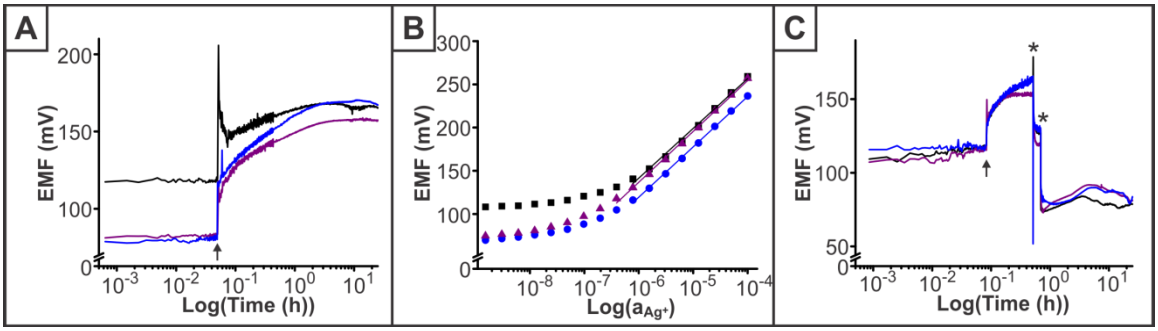

Figure 5.2 Characterization of Ag NP dissolution in MQ water with fluorous-phase ISEs. (A) Response of triplicate electrodes to Ag^+ upon addition of 3 µg/mL Ag NP (arrow) (B) Example calibration curve for Ag in water (C) Response of electrode after addition of 3 µg/mL Ag NP (arrow) followed by two additions of 1 M NaCl (asterisks), where a drop in the EMF is the result of Cl^- binding free Ag^+.

Nanoparticle dissolution was quantified for 3 different concentrations of Ag NPs, 0.3, 3, and 15 μg/mL (Table 5.2). The predicted environmental concentrations of Ag NPs that are or will be released through waste water effluent are between 0.01-18 μg/mL;[28, 29] therefore, these concentrations represent a relevant range of released engineered nanoparticles into the environment. For all nanoparticle concentrations, a similar behavior was observed, as seen in Figure 5.2A, where an initial burst of Ag^+ is observed followed by a steady increase in free Ag^+, with an eventual plateau in concentration over time. It appears that the plateaued concentration is achieved faster for lower concentrations. This burst behavior and concentration response has been observed previously in other dissolution characterization studies.[9, 30] In comparing the dissolution from Ag NPs at the 0 h measurement, both 3 and 15 μg/mL have a similar concentration, which may be an indication of some equilibrium concentration of free Ag^+ present in the purified nanoparticles that is observed at higher concentrations but not the lowest, 0.3 μg/mL Ag NP concentration.

In parallel experiments, nanoparticle dissolution was monitored with ICP-MS by analyzing the supernatant for Ag periodically throughout the 24 h dissolution experiment. Comparisons of the ISE and ICP results are shown in Table 5.2, though again, ISE measurements are continuous and the values in the table are simply taken from the larger ISE trace. Looking at the comparisons, ICP results demonstrate a similar kinetic pattern in dissolution (i.e. initial burst followed by a later plateau); yet, there are some significant differences (gray cells $p<0.05$, students pair-wise t-test) between the ISE and ICP results. Because these experiments were run in parallel and samples were not taken of the same solution, these discrepancies are likely the result of varied oxygenation

of the samples, which influences the rate of dissolution (with higher oxygen content increasing nanoparticle dissolution).[30]

Table 5.2 Concentration of Ag^+ dissolved from Ag NPs as measured over time with ISE and ICP-MS. Gray cells indicate a significant difference ($p<0.05$) between ISE and ICP-MS measurements.

	0.3 µg/mL Ag NP		3 µg/mL Ag NP		15 µg/mL Ag NP	
Time (h)	**ISE (µM)**	**ICP-MS (µM)**	**ISE (µM)**	**ICP-MS (µM)**	**ISE (µM)**	**ICP-MS (µM)**
0	0.44±0.08	0.50±0.04	1.34±0.33	1.22±0.03	1.49±0.21	1.70±0.22
2	0.75±0.10	1.32±0.18	3.28±0.58	2.78±0.02	4.76±0.45	4.65±0.22
6	0.76±0.09	1.89±0.03	3.61±0.80	4.99±0.03	6.55±0.91	7.81±0.15
12	0.78±0.10	0.95±0.2	3.59±1.00	4.29±0.08	7.59±0.93	9.59±0.27
24	0.80±0.15	1.19±0.2	3.44±0.88	3.83±0.94	8.71±1.64	10.02±0.24

To confirm that oxygen caused the difference between ICP and ISE experiments in Table 5.2 and to validate fluorous-phase ISE measurements, nanoparticle dissolution was monitored in MQ water with modulated oxygen levels. Oxygen content was modified by alternately bubbling O_2 or N_2 through the solution to intentionally alter dissolution kinetics, during which ISE measurements and ICP samples were collected. Comparisons of the ICP and ISE results can be seen in Figure 5.3, and there are no statistical differences between the ICP and ISE. Therefore, the discrepancies observed in Table 5.2 are the results of varied dissolve oxygen levels, and ISE measurements provide a level of sensitivity and selectivity similar to ICP, which is considered to be the "gold standard" for the field. From these and the previous results, we used the ISE data to calculate a percent dissolution, which equated to 16-30%, 5-13%, and 1-6% for 0.3, 3, and 15 µg/mL, respectively. These ranges represent the ranges of dissolution percentages over the entire 24 h experiment.

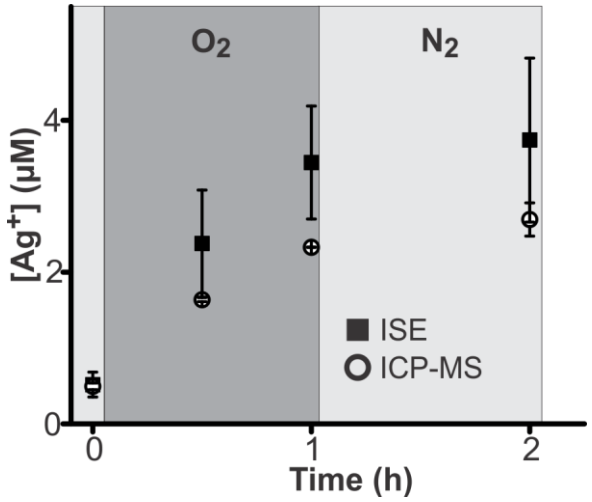

Figure 5.3 ISE and ICP measurements of 3 μg/mL Ag NP dissolution under varied oxygen content. Prior to measurement, N_2 was bubbled through the water followed by 1 h O_2 and then N_2 again.

While characterization of dissolution in water provides important information as to the response of fluorous-phase ISEs to nanoparticle dissolution, it is an unrealistic solvent for performing bacterial toxicity studies. Since Ag^+ can complex with coordinating species, possible complexation of free Ag^+ with the components of bacterial growth broth should be investigated. Because ISEs only respond to free Ag^+, the complexation of Ag^+ will be reflected in the calibrations. For obtaining calibration curves, various volumes of 10 mM $AgCH_3CO_2$ were added to 100 mL of ferric citrate broth followed by measuring the EMF values. Although the same concentration of $AgCH_3CO_2$ was added to the same volume of water and broth, the resulting calibration curves show a significant difference between the ISE response in water and broth, reflected as large differences in the intercepts of the two calibration curves (Figure 5.4). More specifically, differences in the response were caused by complexation of Ag^+ in the broth, resulting in depressed activity of Ag^+.

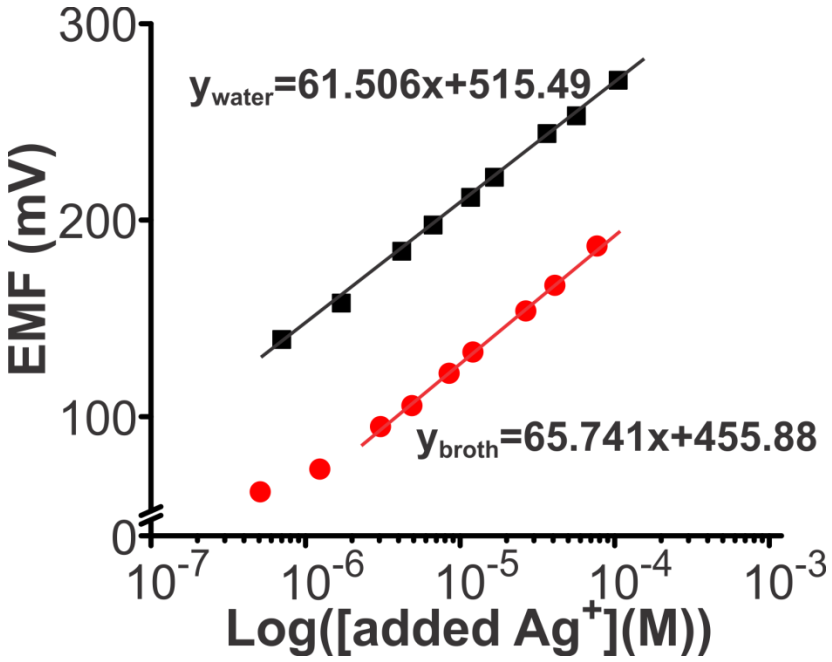

Figure 5.4 Calibration curves for Ag^+ in MQ water (black) or ferric citrate broth (red).

5.3.3 Determination of Ag Complexes in Ferric Citrate Broth

To quantify the effect of complexation on the response of the electrodes, we defined α as the ratio of activity of free Ag^+ to the sum of activities of all species containing Ag^+ (total Ag^+ content in the solution,$a_{,total,Ag+}$). As seen in Equations 5.2 and 5.3, the response of ISEs follow the Nernst equation (Equation 5.2) where $a_{,Ag+}$ is the activity of free Ag^+, $\frac{2.30\,RT}{ZF}$ (R is universal gas constant, T is temperature, F is Faraday's constant and Z is the charge of the ion detected by the ISE, which ideally should be 59 mV/decade at room temperature) is equal to S, and E^0 is the standard potential, which is constant (Equation 5.2). Replacing $a_{,Ag+}$ with $(\alpha.a_{,total,Ag+})$ results in Equation 5.3.

(5.2) $$EMF = E^o + \frac{2.30RT}{ZF} * log(a_{,Ag+})$$

(5.3) $$EMF = E^o + S * \log(\alpha) + \frac{2.30RT}{ZF} * \log(a_{,total\ Ag+})$$

In the absence of complexation, α=1, and plots of EMF vs. $a_{,Ag+}$ and EMF vs. $a_{,total\ Ag+}$ would have the same intercept. However, in the case of complexation with Ag^+, the value of α will be always smaller than 1, resulting in a lower intercept for the plot of EMF vs. $a_{,total\ Ag+}$ compared to EMF vs. $a_{,Ag+}$.

To determine the specific Ag complexes contributing to the response in ferric citrate broth (Figure 5.4), calibration curves were performed with individual components of the ferric citrate broth, with the pH adjusted similar to the broth. Based on this series of experiments, the intercept difference for calibration in ferric citrate broth and water can be explained by complexation of Ag^+ with ammonia released from the dissociation of $(NH_3)_2SO_4$, one the major components of the broth. The concentration of ammonia in the solution was measured indirectly by measuring the pH of the solution which was constant at various concentrations of Ag^+ (pH=7.7). Using the value for concentration of ammonia and the known binding constants for silver ammonia complexes, the intercept change caused by complexation with ammonia was calculated, which agrees with the experimental data. Although the intercept difference predicted by complexation with ammonia is in agreement with the observed intercept difference of calibration curves in water and broth, there are other coordinating species in the broth such as lactate and citrate anions which can contribute to complexation as well. To confirm that Ag^+ only complexes with ammonia, the ISEs were calibrated in 3 variations on the ferric citrate broth: broth lacking ferric citrate, broth lacking both sodium lactate, and broth lacking both ferric citrate and sodium lactate. All three calibration curves showed similar

intercept values, confirming that ferric lactate and sodium lactate do not interfere with complexation of Ag^+ and ammonia.

Therefore, the only species that forms a complex with silver ions in the broth is ammonia, which results in lowering the activity of Ag^+ to 5.67% of total silver activity in the solution of broth. The total Ag^+ content is distributed between free silver and silver ammonia complexes to form 83.07% $Ag(NH_3)_2^+$, 11.26% $Ag(NH_3)^+$ and 5.67% free Ag^+ (See the Appendix for a detailed calculation). To our knowledge, this is the first example of quantification of free and complexed silver species in a real-time measurement, which could contribute greatly to the understanding of Ag NP toxicity.

5.3.4 Characterization of Ag NP Dissolution in Ferric Citrate Broth

Upon characterization of the complexation, the dissolution of 3 µg/mL Ag NP was characterized in ferric citrate broth. The experimental set up was the same as that described for the MQ water studies and monitored over 24 h, followed by re-calibration of the ISEs to assure proper response. While the ISEs responded to changes in silver ions from the dissolving Ag NPs, ammonia complexation of free Ag^+ caused a decrease in signal. The measured potentials were converted to the total concentration of silver ions using the calibration curve in the broth (Figure 5.4). Figure 5.5 details the dissolution of Ag NP in broth as compared to water alongside the calculated free Ag^+ that was corrected for complexation, and the total Ag measured with ICP-MS. Comparing the results of ISE-measured dissolution in broth and water, there is clearly a higher degree of dissolution in the broth, with percentages ranging from 7-28%, depending on the time (0-24 h) in broth

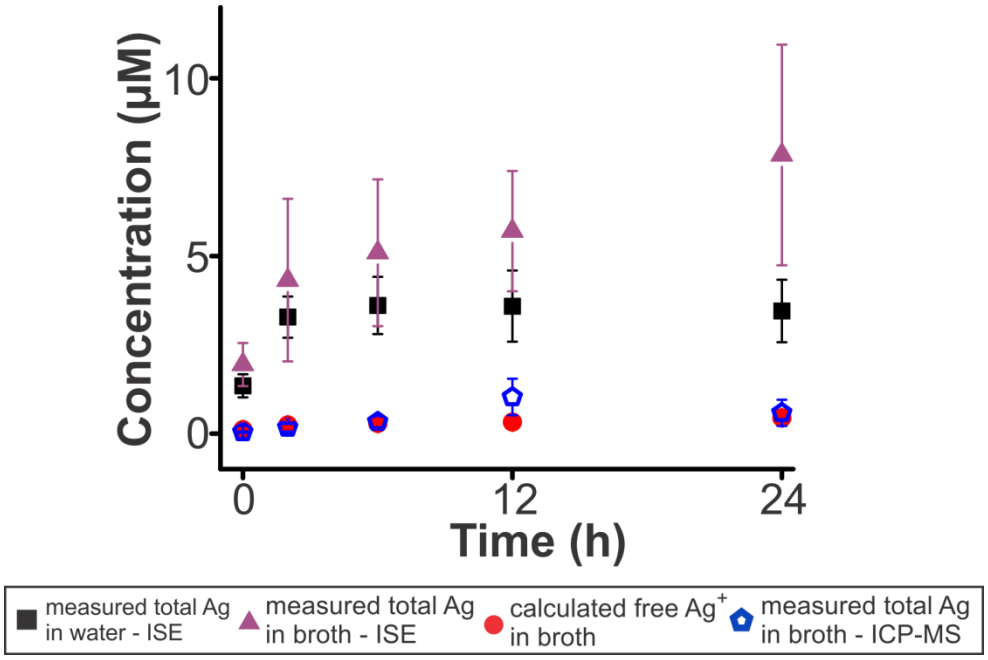

Figure 5.5 Dissolution of 3 µg/mL Ag NP in water and broth as measured with an ISE and ICP-MS. Free Ag^+ was also calculated and plotted.

as opposed to 5-13% in water, and the plateaued region is reached more slowly. This is likely the result of Le Chatelier equilibria where the decrease in free Ag^+, as the result of ammonia complexation, causes a greater percentage of the nanoparticle to dissolve. It follows that a greater percentage of dissolution would take longer to reach equilibrium, accounting for the greater time to reach the plateau. Interestingly, ICP-MS measurements follow more closely to the calculated concentration of free Ag^+. While it is possible that the parameters of Ag NP dissolution change in broth in a way that does not correlate to the method of generating the calibration curve, the differences in measured ICP-MS and ISE measurements of the total Ag is more likely the result of ICP-MS sample preparation. That is, ferric citrate broth is known to contain insoluble iron hydroxide material as the result of adjusting the pH of ferric citrate with NaOH. Since the ICP-MS sample preparation entails a filtration step, we hypothesize that some dissolved Ag

species (free or complexed) adsorbs to the precipitate and is removed from the supernatant during filtration. This will be an area of future exploration.

5.3.5 Assessment of Ag NP and Ag Ion Toxicity to *S. oneidensis*

Characterization of the dissolution in broth was used to determine relevant concentrations of ion and nanoparticle to be compared in toxicity assessments. A Live/Dead Baclight™ assay was performed to determine the viability of *S. oneidensis* after varied time (0-24 h) and concentrations of exposure to Ag^+ (1-10 μM) or Ag NPs (0.3-15 μg/mL) (Figure 5.6). Note, that the concentration of Ag^+ denotes the total Ag ion added to the broth, not just the free Ag^+ concentration that should only account for ~5% of the total Ag ion concentration. As seen in Figure 5.6, a significant decrease in the viability is observed after 6 h exposure to 4 μM Ag^+ and 15 μg/mL Ag NPs. Interestingly, at 24 h, lower concentrations of Ag^+ tend to cause an increase in viability up until 3 μM Ag^+, but viability drastically drops below the control at 4 μM Ag^+. A similar increase in viability is observed upon 24 h exposure to 0.3 μg/mL Ag NP, followed by a significant decrease in viability of *S. oneidensis* exposed to 3 and 15 μg/mL. The stimulation of *S. oneidensis* viability at lower concentrations of Ag^+ and Ag NP is likely the result of *S. oneidensis'* ability to respire a variety of metals, including Ag;[23] therefore, increased respiration stimulates growth which is measured as increased viability in this assay. It appears, however, that there is a sharp threshold whereupon the presence of Ag causes a decrease in viability because by 4 μM Ag^+ and 3 μg/mL Ag NP, a reduction in viability is observed. Comparison of bacterial viability at 3 μg/mL versus the equivalent total dissolved Ag^+ measured in ISE experiments reveals a clear

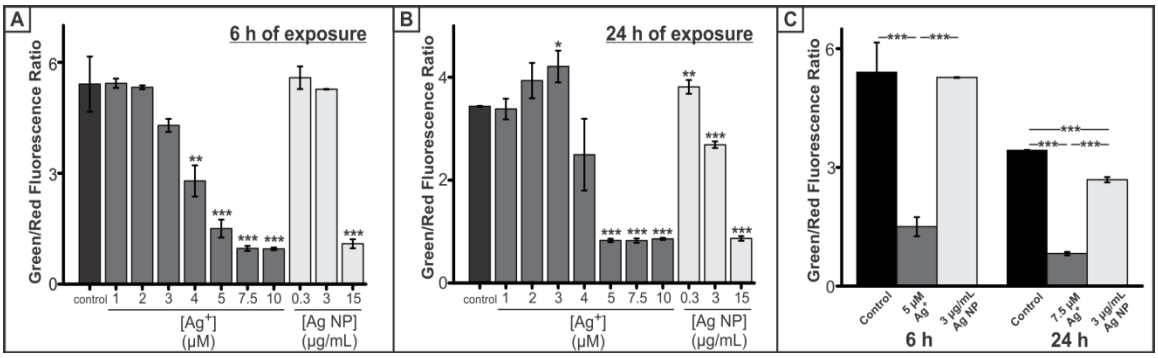

Figure 5.6 Assessment of viability of *S. oneidensis* after (A) 6 h and (B) 24 h exposure to Ag^+ and Ag NP. (C) demonstrates the comparison of Ag NP and ISE measured total dissolved Ag at the particular time point. Samples were made in triplicate and *p<0.05, **p<0.01, and ***p<0.001.

discrepancy in induced toxicity, with higher toxicity observed in the Ag^+ exposures (Figure 5.6C). One potential cause of these differences is that the duration of the ion exposure is for the entire 6 or 24 h, whereas the amount of ion released from the nanoparticle is not present at the given concentration for that entire 6 or 24 h period. Future efforts will be made to modulate the concentration of ion over the time of the toxicity experiment to better mirror the concentration measured by ISE. Another cause of the discrepancy could be that the presence of bacteria alter the dissolution parameters of the nanoparticle so that nanoparticle dissolution is decreased.

Another measurement of toxicity is the growth of the bacteria in the presence of Ag^+ and Ag NP, where growth is monitored by measurement of optical density (Figure 5.7). As in the viability assessment, 4 μM Ag^+ and higher concentrations of Ag^+ cause no growth and in fact, a decrease in optical density is observed by 3 h, indicating cell death. Lower Ag^+ and all Ag NP concentrations, however, do not arrest growth, though there is a decrease in the rate of growth (Table 5.3). Again, relating the toxicity induced by 3 μg/mL Ag NP to the measured dissolved Ag^+, there is a difference in the bacterial response. That is, most of the time during growth, *S. oneidensis* exposed to 3 μg/mL Ag

NP would be in the presence of 4 µM total dissolved Ag^+, as measured at 2 h with ISE measurements; therefore, we would expect to see a significant decrease in growth at early time points, which was not observed.

To explain the discrepancies in toxicity as observed between Ag^+ and Ag NPs, it is hypothesized that this difference indicates that amount of Ag ions is different in the broth when bacteria are present. Subsequently, a dissolution experiment of 3 µg/mL Ag NP was performed in broth and the presence of 10^8 cells/mL (data not shown). The

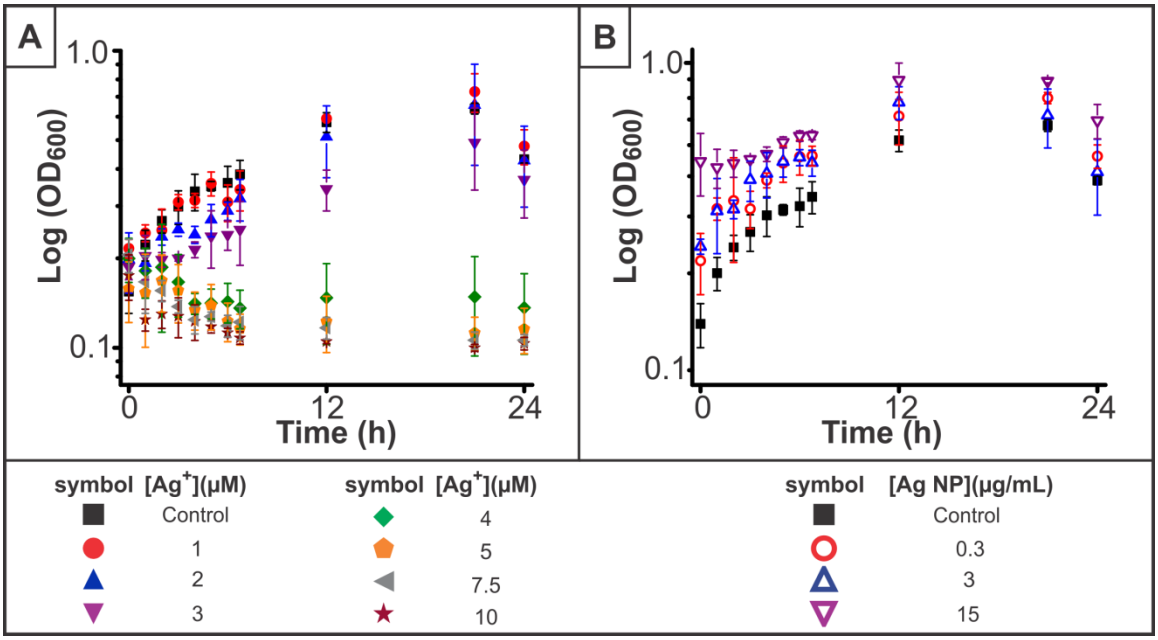

Figure 5.7 Growth curves of *S. oneidensis* in the presence of (A) Ag^+ or (B) Ag NP.

Table 5.3 Growth rate of *S. oneidensis* exposed to Ag^+ or Ag NP as determined from the exponential phase in Figure 5.7 using Equation 4.1.

Concentration Ag NP (µg/mL)	Growth rate (generations/h)	Concentrations Ag^+ (µM)	Growth rate (generations/h)
Control	0.16	1	0.12
0.3	0.09	2	0.12
3	0.09	3	0.09
15	0.09	4, 5, 7.5, and 10	no growth

dissolution kinetics were significantly different than measured in broth alone, and in fact, the measurement of free Ag^+ was below the detection limit, indicating that the bacteria alter the dissolution kinetics. This decrease in measured free Ag^+ may be the result of less toxic ion released from the nanoparticle, which could explain the differences in toxicity observed between the nanoparticle and ion concentration as measured with ISE in broth only. An alternative explanation is that the released Ag^+ is reduced/precipitated by *S. oneidensis*, decreasing the free Ag^+ in the broth that is measured by the ISE. Again, *S. oneidensis* is a known metal reducer shown to respire Ag^+,[23] reducing Ag^+ to Ag^0, and has even been shown to biosynthesize Ag NPs from Ag salts.[31] The respiration of Ag^+ from dissolved Ag NPs could explain the significant increase in viability observed after 24 h exposure to 3 μM Ag^+ as the Ag NPs are providing a usable nutrient source. While we cannot elucidate which explanation accounts for the decrease in ISE-measured Ag^+, we can conclude that these toxicity results support the literature precedent that Ag^+ is a major cause of Ag NP toxicity, as opposed to some nano-specific toxicity.[5] ISE-measured Ag^+ concentrations during Ag NP dissolution were significantly less in the presence of bacteria, which in turn resulted in a minimized toxic response from the Ag NP. The discrepancy between ISE measurements with and without the presence of bacteria highlights the importance of *in situ* measurements of nanoparticle characteristics as the toxicity profile is different from that measured *ex situ*. Future work will be aimed at performing simultaneous measurement of free Ag^+ and bacterial toxicity.

5.4 Conclusions

This works details the development of fluorous-phase ISEs for characterization of Ag NP dissolution, including the rate and extent of nanoparticle dissolution along with the characterization of the species of Ag that dissolved from the nanoparticle. One important conclusion from this study is that even in a simplified, defined bacterial culture broth, the majority of silver dissolved from Ag NP will be in a complexed form, thus affecting the bioavailability and toxicity of silver ions. In many realistic ecological compartments (e.g. rivers and oceans), complexed Ag^+ forms will be the predominant species entering the environment from Ag NP release, and having the ability to determine percentages of each complexed species is a crucial advancement to determining the impact of nanoparticles on the environment.

Considering the toxicity of Ag^+ and Ag NPs to *S. oneidensis*, it was demonstrated that total Ag^+ and Ag NP at low concentrations cause an increase in *S. oneidensis* viability but cause significant cell death above threshold concentrations; all concentrations of Ag^+ and Ag NP slow the bacterial growth rate. However, the toxicity of Ag NPs compared to *ex situ*, ISE-measured Ag^+ concentrations from said Ag NPs yielded major differences in the toxic response, which may indicate that less of the toxic species (i.e. Ag^+) were presented to *S. oneidensis*. These results illuminate the importance of moving toward *in situ* nanoparticle characterization to realistically assess nanotoxicity. Better characterization of nanoparticles will lead to a superior mechanistic view of the nano-bio interaction, which could ultimately lead to design rules for sustainable use of nanotechnology.

Chapter Six

Toward Correlation of *In Vivo* and *In Vitro* Nanotoxicology Studies in Relationship to Regulatory Guidelines

This chapter adapted from:

M.A. Maurer-Jones, C.L Haynes. Toward Correlation in *In Vivo* and *In Vitro* Nanotoxicology Studies. *Journal of Law, Medicine, and Ethics*. **2012**, (accepted).

6.1 Introduction

As illuminated in the previous chapters, my thesis research has focused on a fundamental understanding of the nanoparticle-biological interaction that may ultimately lead to sustainable, safe use of nanotechnology. Beyond the science, however, it is important to consider the ethics regarding the implementation of nanotechnology, particularly in the area of biomedical applications, one of the largest growing areas of nanotechnology research.

In the last couple years, discussions around nanoparticle therapies has focused on the question, "When have you reduced risk enough to move from bench/animal studies to "first in-human" studies?" Building applied research ethics related to nanotherapeutics requires bench and clinical scientists to have a clear vision about how to test nanotherapeutic safety, and it is clear that there is still much to be considered at the steps before "in-human" assessment. Herein, the perspective of the bench scientist is brought to bear on using *in vivo* and *in vitro* models to assess the safety of nanotherapeutics. Much of this work falls under the purview of the field of nanotoxicology that aims to understand the toxicological impact of engineered nanoscale materials. Engineered nanomaterials include a wide variety of materials that are manipulated and controlled on the nanoscale level where, typically, the nanoparticle or nanomaterial has some dimension that is less than 100 nm. These materials are of interest for a wide variety of applications, including biomedical, due to the emergent properties of the materials, where emergent properties refers to the physical and chemical characteristics that are distinctive from both those of the atoms/molecules and the bulk of the same material.

The burgeoning use of nanoscale materials for biomedical uses has yielded many promising technologies for the treatment and diagnosis of diseases, particularly cancers. The development of nanotechnology as disease therapy agents, or nanotherapeutics, has accelerated because of their potential use as drug delivery vehicles as there is preliminary evidence that nanotherapeutics efficiently traffic to the sight of treatment (e.g. a tumor) via enhanced permeability and retention and deliver a pharmaceutical payload with minimal side effects.[1] Additionally, nanoparticles can be functionalized in many different ways to simultaneously enable drug delivery and imaging, propelling the personalized medicine trend forward.[2] Currently, there are 33 products that could be classified as nanotherapeutics approved for use by the Federal Drug Administration (FDA), with hundreds more in various stages of clinical trials.[3] With the development of nano-sized therapeutics, both the expanded use and the unique properties of nanomaterials, regulatory agencies are now faced with decisions regarding the regulation of such novel technologies.

The FDA has begun to grapple with the regulatory implications of nanotherapeutics and now includes a nanoparticle size disclosure as an optional part of the approval process.[4] However, there are ongoing arguments about whether or not nanoparticles require different regulation to ensure safe use of these products or if the current mechanisms will be sufficient. This consideration is complicated by the ambiguity associated with nanoparticle characterization (e.g. how the size, surface reactivity, etc. of nanoparticle is characterized).[5]

Guidance from regulatory agencies is especially lacking at the pre-clinical stages of nanotherapeutic development, in which a suite of *in vivo* and *in vitro* assessments must

be carried out for products progressing from pre-clinical to clinical trials. *In vivo* studies are whole organism studies where nanotherapeutics are delivered via one of four pathways: inhalation, dermal, ingestion, or injection. Using a variety of techniques, typical *in vivo* assessments include the determination of physiological localization and the concentration of material in specific tissues, rate of excretion, and macroscopic tissue and organismal toxicity. *In vitro* assessments are the study of cells, either isolated from animals or an immortalized cell line, in a culture dish. In general, the use of primary cells (isolated directly from animals) will give a more realistic toxicity result because immortal cell lines transform over time; however, the use of immortal cell lines is often preferred simply because they do not require animal sacrifice. There is an abundance of *in vitro* assay options,[6-8] many of which allow researchers to probe a nanoparticle's mechanistic interaction with cells, which are fast and inexpensive to enable high-throughput cellular analysis. To be clear, *in vivo* and *in vitro* studies each have limitations (e.g. expense and dosing, respectively).[6-8] However, as both *in vivo* and *in vitro* studies provide necessary, and often complementary, information regarding the action of nanoparticle therapeutics, both *in vivo* and *in vitro* guidelines informed by oversight bodies have the potential to optimize technological progress.

Bench scientists are at the forefront of designing and creating new nanomaterials and are being pushed to assess the interaction of nanomaterials with cells, tissue, and organisms in pre-clinical studies, though these areas are outside their expertise. While contentious debate continues about whether new or additional regulation is required for nanotechnology, clear oversight guidelines will provide guidance for scientists in pre-clinical studies toward the type of toxicity testing and model systems that would enable

quick and safe development of a products.[5] The caveat to implementing new regulation beyond the current oversight is that nanoscale therapeutics must initiate a clear and unique toxicity response, where a unique response is considered to be a cellular or organismal response that has not been observed in previous toxicity studies with exposures to molecules. Herein, following the four potential routes of biomedical nanoparticle administration (i.e. inhalation, dermal, ingestion, and injection), we examine the literature to correlate pre-clinical nanotoxicology studies where *in vivo* and *in vitro* testing is employed to determine any distinctive toxicity characteristics that should be considered in the oversight of nanotherapeutics. Due to the complementary results yielded from *in vivo* and *in vitro* studies, correlating the results enables a deeper understanding of the mode of nanoparticle toxicity so that nanoparticles can be designed for optimized disease treatment and minimal unintentional toxicity. Additionally, through these correlations, there is the potential to simplify the pre-clinical stages because results from *in vitro* studies may enable generalization of the *in vivo* toxicity response, thus reducing time and cost of developing highly effective therapeutics by eliminating some of the animal testing. Figure 6.1 provides examples of results from *in vivo* and *in vitro* studies that are explored below. Within this comparison, *in vivo* studies are those where animals are exposed directly to nanoparticles, though cells/tissue may be extracted for analysis, whereas *in vitro* studies are those where the nanoparticle exposure is performed directly to isolated cells in a Petri dish. For clarity, this comparison is limited to nanotherapeutic drugs, rather than including devices and combination products.

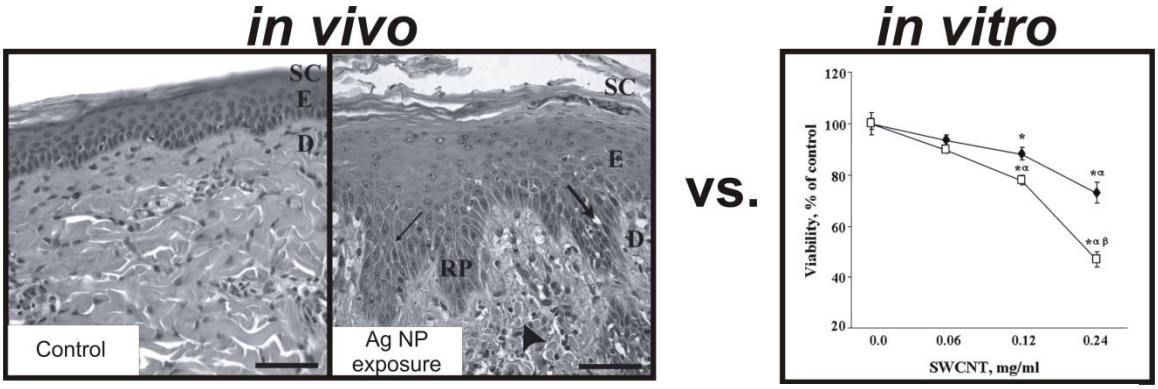

Figure 6.1 Examples of *in vivo* (histology) and *in vitro* (viability) toxicity data. *In vivo*: histological examination of porcine skin after application of silver nanoparticles (Ag NP). Abbreviations within image refer to parts of the skin that are measured as part of the histological analysis (SC-stratum corneum, E-epidermis, D-dermis, and RP-rete peg). Arrows and arrowheads indicate tissue damage (large arrows-intracellular epidermal edema, small arrows-focal areas of intracellular epidermal edema, arrowheads-perivascular inflammation). Adapted and reprinted with permission from reference 19. *In vitro*: measurement of murine epidermal cell viability after exposure to single-wall carbon nanotubes (SWCNT) as measured with the Alamar Blue assay. The SWCNT, partially purified (black circles) and unpurified (white squares), cause a dose dependent decrease in viability. *$p<0.05$ vs. control, $^{\alpha}p<0.05$ vs. 0.06mg/ml SWCNT, $^{\beta}p<0.05$ vs. 0.12mg/ml SWCNT. Reprinted with permission from reference 20

6.2 Correlation of *In Vivo* and *In Vitro* Toxicity

6.2.1 Inhalation

Currently, there is no nanotherapeutic on the market that has an inhalable delivery mechanism; however, there are a number of products in various stages of clinical trials for such diseases as bronchiolitis (i.e. severe airway damage/inflammation)[9] or lung tumors,[10] and it is conceivable that the treatment of lung diseases like asthma could include a nanoparticle-loaded inhaler. Though literature precedent is lacking regarding inhaled nanotherapies, there has been extensive work aimed at understanding the *in vivo* and *in vitro* correlation of inhaled nanoparticles from the occupational health perspective.[11] *In vivo* studies employ a variety of model animals, but primarily have

focused on mice and rats, exposing the animals to varying concentrations of various nanoparticles using either the instillation (lung entry through via the throat) or inhalation (lung entry through the nasal passage) mode of nanoparticle introduction. For *in vitro* studies, researchers commonly use the immortal (i.e. self-propagating) human lung cell lines A549 and BEAS-2B.[8]

While *in vitro* assays modeling inhaled nanoparticle toxicity use a wide variety of assays, *in vivo* studies focus on extracted bronchoalveolar lavage fluid (BALF), or fluid that is retrieved from the lungs, after a nanoparticle exposure, examining molecular markers of oxidative stress and/or inflammation. Often, markers measured within the BALF can be directly measured and compared to the same marker in the *in vitro* assays.[12-15] During oxidative stress, generated free radicals, or reactive oxygen species, overwhelm the system's innate ability to cope, which potentially leads to tissue damage. For example, Horie *et al.* studied instilled nickel oxide nanoparticles on rats and demonstrated that there were elevated levels of hydroperoxy octadecadienoate (tHODE), an indicator of oxidative stress within the lungs. This increase in tHODE was correlated to elevated levels of oxidative stress *in vitro* over a similar time (~24h) of exposure.[12] Warheit and coworkers demonstrated a similar correlation of *in vivo* and *in vitro* oxidative stress upon exposure to zinc oxide, though the magnitude of the oxidative stress response *in vitro* was smaller than *in vivo*;[13] this discrepancy may be a result of the difficulty in equating *in vitro* and *vivo* dose. Biochemical markers for other lung cell/tissue damage can also be studied in the BALF, as was done by Nel and co-workers to identify fibrosis (i.e. lung damage) *in vivo* and *in vitro*.[16] Beyond direct comparisons of similar markers within the BALF after *in vivo* nanoparticle exposure and *in vitro* assays,

in vivo studies also commonly utilize histology (see histology example in Figure 6.1 *in vivo* results) to examine tissue damage and compare to various *in vitro* assays that measure cell viability and/or markers of inflammation that would cause the observed histological damage.[16] The same biochemical markers are measured using similar methods (e.g. BALF and histology) to assess inflammation and oxidative stress upon exposure to inhaled molecular therapeutics.[17]

6.2.2 Dermal

As in the inhalation nanotherapies, there is yet to be a FDA approved dermal or transdermal nanotherapeutic, though there are many commercially available products that utilize topical application of nanoparticles, namely sunscreens and cosmetics, which typically use nanoparticles for UV light protection and wound dressings that use antibacterial nanoparticles. Porcine skin is the most common skin model used to test both traditional and nanoparticle products for human use and therefore, *in vivo* studies commonly use pigs. *In vitro* cell lines to model skins cells are much less common, with most studies isolating intact skin (i.e. an *ex vivo* model).[8] Alternatively, some studies that correlate *in vivo* to *in vitro* dermal toxicity make use of cell lines unrelated to the epidermis and assume generality across cell types.[18]

Histological investigation is the most common *in vivo* method for assessing toxicity, in all exposure pathways, and this is true for dermal nanoparticle studies. Skin characteristics monitored in the histological analysis after topical nanoparticle exposure have included skin thickness, abnormal tissue damage, and the presence of inflammatory lesions. Monteiro-Riviere and coworkers examined edema and

erythema, signs of inflammation, upon *in vivo* exposure of pigs to nano-silver and correlated the response to inflammatory biomolecules generated by a human skin cell line *in vitro*. Results revealed that there was microscopic evidence of inflammation after 14-day exposure *in vivo* and this correlated with inflammation biomarkers after 24 h silver nanoparticle *in vitro* exposure.[19] Similarly, Murray *et al.* related the indicators of oxidative stress and inflammation *in vitro* (e.g. interleukin secretion and free radical generation) to increased levels of cell types *in vivo* that are known to migrate to sites of inflammation.[20] While these studies show correlation of an inflammatory response *in vivo* to *in vitro*, another study using silver nanoparticles has indicated minimal skin irritation *in vivo*.[21] The varied results shown between studies are likely a result of the parameters of the experiments such as length of exposure, nanoparticle dose, and nanoparticle surface chemistry. Similar disparities in toxicity results are found when exposure time and dose are varied for dermal application of molecular therapeutics, which commonly use similar models and evaluation criteria.[22]

6.2.3 Ingestion

Ultimately, the development of oral therapies to treat chronic disease, as an alternative to injected therapies, could be greatly facilitated by nanotechnology as nanoparticles lengthen the stability of drug molecules within the digestive system and enable favorable drug absorption in the intestines.[23] However, there again is no FDA approved oral nanotherapy, though there are consistently more and more studies working to understand the relevant *in vivo* and *in vitro* toxicology correlation for this delivery mechanism. Models for *in vivo* study of ingestion are highly variable, from typical

research rodents (i.e. mice and rats) to primates, but many *in vitro* studies utilize the immortalized colon cancer cell line known as Caco-2.[8]

While research to understand the toxicology of ingested nanoparticles is being actively pursued, there is no consistent assay or method used at this point. Some *in vivo* studies explore the distribution and localization of particles throughout an organism after oral nanoparticle exposure. For example, Shuler and coworkers examined the distribution of iron from ingested iron-polymer composite nanoparticles in chickens and correlated iron amounts to *in vitro* iron transport and uptake within Caco-2 and other immortal cells.[24] In another example, Moulari et al. demonstrated localization of aminosalicylic acid-coated silica nanoparticles within inflamed colon regions of a colitis mouse model and observed the therapeutic effect the nanoparticles had on the colitis-induced inflammation. However, the parallel *in vitro* studies only examined cell viability and therefore make toxicity correlations difficult.[25] One example of a better toxicity correlation for orally administered nanoparticles is work done with a polymer nanoparticle drug delivery vehicle for doxorubicin, a common chemotherapy agent.[26] In this study, the drug-loaded nanoparticles administered orally caused reduction of breast tumors in rats and similarly caused a decrease in Caco-2 cell viability in an *in vitro* assay, showing that these nanoparticles influence cancer cells in general rather than breast cancer cells specifically.[26] While both inhaled and dermal application of therapeutics are likely to act locally, ingested therapeutics must survive both the digestive system and be successfully distributed after absorption; this inherent difference makes nanoparticles especially promising but also make toxicity considerations significantly more

complicated. So far, the most likely difference between orally administered molecular and nanoparticle therapeutics lies in the excretion routes which, in either the molecular or nanoparticle case, can only be accurately assessed using *in vivo* studies.

6.2.4 Injection

The most widely investigated exposure pathway for nanotherapeutics is injection, and all 33 currently approved FDA nanomedicines fall in this category.[3] Nanoparticle injectables have been explored because they could potentially eliminate the negative side effects of traditional injectable drugs, particularly chemotherapy, where solubility and stability of drug molecules limit their use. In fact, most of the approved nanoproducts are aimed at cancer diagnosis or therapy as are many injectable nanomaterials in development. Therefore, many of the models for *in vivo* injection nanotoxicity are implanted cancer cells to stimulate tumor development (in a variety of animals), and *in vitro* studies generally use cancerous cell lines. Though it is possible to use similar cancerous cell lines as those implanted to create the *in vivo* tumor, few studies take this route.[8] Some *in vitro* work has examined primary culture cells from blood, such as platelets or red blood cells, to determine blood compatibility.

Since a major aim of injectable nanotherapeutics has been to treat cancer (i.e. be toxic to cancer cells directly or through targeted release of a drug payload), much of the *in vivo* toxicity assessments focus on the nanoparticle uptake into tumors followed by various characterizations of the progression of cancer (e.g. measuring tumor volume) along with the systemic biodistribution of administered nanoparticles to assess clearance and potential sites of unintentional toxicity.[27-29] These *in vivo* studies are correlated with

in vitro viability assays that assess the percentage of cells, often cancer cells, that survive nanoparticle or drug-loaded nanoparticle exposure. For example, Devalapally *et al.* assessed tumor suppression in mice after intravenous administration of polymer nanoparticles loaded with tamoxifen and paclitaxel, FDA approved molecular cancer treatments, and correlated a decrease in tumor size with *in vitro* studies of decreased cell viability with the same cancer cells used to implant the tumors.[28] Singh *et al.* also examined nanotoxicity of nanoparticles after injection, though aimed at understanding unintentional consequences.[30] After injection of graphene oxide nanoparticles, *in vivo* pulmonary thromboembolism (i.e. damage due to clotting) was histologically observed in the lungs of mice, which correlated *in vitro* to a decrease in blood compatibility.[30] Injectable nanoparticles are the most advanced of the four therapeutic routes of administration, and accordingly, the effort to correlate *in vitro* and *in vivo* results are the most advanced and have been the most successful because of the aim to decrease cancer viability. As with molecular therapeutics, there is a distinct advantage because it is possible to draw human blood and assess blood compatibility without harming the research subject or having to use an animal model. Like orally administered nanotherapeutics, injectable nanoparticles may differ from molecular therapeutics in the excretion routes available; this possibility will have to be investigated using *in vivo* studies and will be an important part of in-human trials.

6.3 Conclusions and Perspective

Since the growth of nanotoxicology as a discipline (circa 2004), which has origins in the field of particle toxicology, there has been great concern that the emergent

properties of engineered nanomaterials would cause novel biological responses upon exposure. Most would argue there are challenges in understanding nanoparticle toxicity that arise from the characterization of nanomaterials, both pre-treatment and during exposure to biological environments.[5, 31] For example, nanomaterials have been shown to elicit a different level of toxicity based on their size, but the molecular complexity of a biological environment can influence effective nanoparticle size. Based on studies in simulated biological environments, the nanomaterials are often transformed so that the effective size, or the size the cells or organism sees, is larger than originally intended.[2] Other characteristics, such as adsorbed molecules on the nanoparticle surface[32] and material integrity,[33] are also easily transformed within the body and have a significant influence on toxicity. The gap in measurement technology that that makes dynamic, *in situ* measurements of nanoparticle characteristics currently impossible has been a great impediment to understanding and correlating *in vitro* and *in vivo* toxicity results.

The question still remains whether nanoparticles cause a unique biological response that should inform our regulatory actions. In examining the correlation between *in vivo* and *in vitro* studies above, there is yet to be evidence that the body's toxicity response to nanoparticles is different than other molecular toxicants or larger, micron-sized, particles that are already approved by the FDA. One agreement that seems to arise from these comparisons is that oxidative stress and/or inflammation can be correlated between Petri dish and whole organism studies, but this is also seen with other non-nanoparticle toxicants/therapeutics.[34] While nanotherapeutics have not yet induced a unique toxicity response, the lack of novelty may be an artifact of the discrepancies

between *in vivo* and *in vitro* nanotoxicity comparisons, such as the dose and duration of nanoparticle exposure or the differences in model systems (i.e. cancerous cell lines versus healthy animals). That is, there may be nuanced toxicity modes induced by nanoparticles that are not observed because the dose *in vitro* is not relevant *in vivo* or the *in vitro* cancer cell line does not behave in a way the mimics a whole organism. These discrepancies are exacerbated by the fact that the field is relatively new. Many of the literature studies currently available, including some highlighted here, are aimed at showing promising results of a particular nanotherapeutic and therefore only perform standard pre-clinical toxicity evaluations. Generally, the standard toxicity evaluations do not attempt to achieve *in vivo* and *in vitro* correlation and are not aimed at elucidating mechanisms of nanoparticle toxicity. Clearly, more fundamental studies on this topic, for both nanoscale and molecular therapeutics, would benefit the field of toxicity at large.

It is clear that we, as bench scientists, are still struggling with the basic science in defining nanotoxicity and have left many gaps in correlating *in vivo* and *in vitro* data. However, striving for correlation among *in vivo* and *in vitro* data to achieve a better understanding of toxicity is not novel to nanoparticle toxicants. Molecular toxicology has been grappling with similar problems and have been working on solutions that could inform regulation.[35] This supports the idea of a "new toxicology" that has been introduced by Philbert and coworkers, whose work is speaking directly to emerging, sophisticated materials,[31] but applies to molecular therapeutics as well. Based on the current state of the literature, it seems that, so far, there are no unique biomarkers or characteristics of nanoparticle toxicity, and thus, we see no justification for novel regulatory procedures at this point. The most likely candidate for distinct behavior lies in

the fact that intact nanoparticles will likely be excreted through different routes than their molecular counterparts; this should be investigated systematically, but is impossible until the first in-human trials are performed.

Chapter Seven

Toxicity of Nanoparticles to Brine Shrimp Laboratory – An Introduction to Nanotoxicity and Interdisciplinary Science

This chapter adapted from:

M.A. Maurer-Jones, S.A. Love, S. Meierhofer, B.J. Marquis, Z. Liu, C.L. Haynes. Toxicity of Nanoparticles to Brine Shrimp: An Introduction to Nanotoxicity and Interdisciplinary Science. *Journal of Chemical Education*. **2012**, (accepted).

7.1 Introduction for Instructors

In modern science, the traditional disciplinary boundaries are increasingly blurred, where chemists study toxicology or material scientists work on cancer research. Interdisciplinary research can propel innovation with different perspectives contributing to important scientific and technological problems. One new field of research that benefits from an interdisciplinary approach is the field of nanotoxicology.

Nanoparticles are frequently, but not strictly, defined as particles with at least one dimension less than 100 nm. Because of their unique physical and chemical properties, which differ from atoms or bulk of the same material, nanomaterials have been increasingly incorporated into commercially available products, including silver nanoparticles in clothing to prevent odor and titanium dioxide in cosmetics as a sunscreen. This increased use necessitates the understanding of the possible toxicity these nanoparticles pose for humans and the environment. As such, numerous scientists, including chemists, material scientists, biologists and toxicologists, have undertaken the study of the impacts of nanoparticles in biological and environmental models to better understand and hopefully predict their potential toxicity.[2]

In the experiment detailed herein, nanotoxicology is used as a platform to introduce chemistry students to interdisciplinary, collaborative science, including aspects from chemistry, materials science, toxicology, and statistics while also exposing them to an area of cutting-edge research.

As is often the case in toxicology, a model organism is used to examine potential toxicity effects. Here students utilize a simple aquatic organism, brine shrimp, as the model of study because they are simple to hatch, grow, and maintain.[1] While there are

many indicators of toxicity, viability is most commonly explored. Viability, the toxicity measure that students will use in this experiment, can be defined as the ability of a cell or organism to survive exposure to a toxicant or the number/percentage of organisms living versus dead. Students are tasked to examine brine shrimp survival after exposure to Ag or Au nanoparticles (that they have synthesized) at a variety of concentrations. By varying the concentrations within this experiment, the students can then perform meaningful statistical analysis of their data. Pooling of the class' replicate data allows students to practically apply these tools, leading to an understanding of differences in toxicity and when scientific data reveal statistical significance.

During development, this experiment was tested with chemistry students in a Woodbury, MN high school. An analysis of student comprehension, based on student's paired pre- and post-experiment responses, is included herein; these data influenced the experimental procedure presented.

7.2 Methods

In this experiment, the students synthesize nanoparticles, perform a serial dilution of nanoparticle suspension, do a live/dead brine shrimp assessment, and analyze the resulting data. In the interest of time and conservation of materials, it is best performed in groups of 2 or 4 (2 pairs of lab partners) so that the work is divided. This experiment was designed with high-school students in mind, but would also be applicable to an introductory level chemistry or environmental science class, providing that the lab met multiple days in a week as students need 2 or 3 consecutive days to complete all

components. Herein, we describe the components of the experiment, including our vision for the division of tasks with the student worksheet.

7.2.1 Nanoparticle Synthesis

Both Au and Ag syntheses will be performed by the students using stock solutions, which should be prepared beforehand. With the exception of sodium borohydride ($NaBH_4$) that must be made on the day of nanoparticle synthesis, all stock solutions may be prepared and stored for 4-6 months provided that they are kept in the dark or in dark bottles. They may even last longer, but should be tested before use if stored for longer. Transmission electron microscopy (TEM) images of prepared nanoparticles can be seen in Figure 7.1.

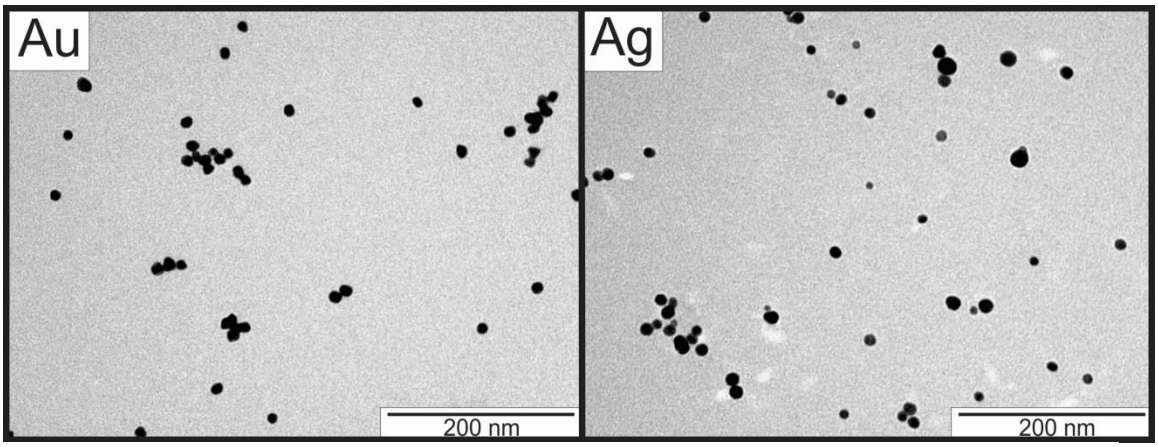

Figure 7.1 TEM images of Au and Ag nanoparticles that will be prepared by the students within this experiment.

7.2.1.1 Au

Students will synthesize citrate-reduced Au nanoparticles from sodium citrate and $HAuCl_4$ stock solutions as modified from the previously published method.[3] In glass

vials, students add 15 mL of 1.1 mM $HAuCl_4$ stock solution and begin heating on medium-high heat, stirring the solution with either a magnetic stir bar or every 30 seconds with a stir rod. When the $HAuCl_4$ solution is boiling, or after 10 min, add 1.5 mL of 50 mM sodium citrate stock solution. Au nanoparticles should form within a couple minutes, if not immediately, and the solution should change from colorless/light yellow to deep purple. Keep heating the Au nanoparticle solution for 10 min after the color change, making sure to stir every 30 seconds or continuously stir with stir bar. Nanoparticles can be stored for extended periods as long as they are kept from light, by storage in amber colored storage bottles or under aluminum foil.

7.3.1.2 Ag

Citrate-capped Ag nanoparticles will be synthesized by students via $NaBH_4$ reduction of $AgNO_3$ to Ag^0, modified from a previously published method.[4] In a glass vial/beaker, 13 mL of deionized water is added and heated, ideally under constant stirring, until water is beginning to boil, after which 1 mL of 7.5 mM $AgNO_3$ and 1 mL of 7.5 mM sodium citrate should be added to the vial and stirred. Next, 20 drops of 10 mM $NaBH_4$ is added, and the solution should immediately turn from colorless to yellow as the nanoparticles form. Continue to heat and stir the nanoparticle suspension for 10 minutes after color change. Unlike the other stock solutions, $NaBH_4$ solutions should be freshly prepared for each experiment. Again, nanoparticles can be stored for many weeks as long as they are kept from light.

7.3.2 Exposure Solutions and Nanoparticle Dilution

In this experiment, students will be comparing the toxicity of different concentrations of nanoparticles, along with water and metal ion (i.e. Ag^{+} or Au^{3+}) controls, on brine shrimp. To achieve the varied concentrations, a serial dilution is performed from the stock, as-synthesized particles yielding the following concentrations: 100% nanoparticles, 50% nanoparticles, 25% nanoparticles, and 12.5% nanoparticles. While the exact concentration of nanoparticles may differ in the syntheses, the concentration of the as-synthesized and diluted nanoparticles will be comparable for the toxicity assay. For those with access to a UV-visible spectroscopy instrument (e.g. a Spec20), the nanoparticle concentration can be determined using Beer's Law (Absorbance=εbc), where b is the cuvette pathlength in cm, ε is extinction coefficient of the nanoparticles, and c is the nanoparticle concentration. The extinction coefficients for Au nanoparticles (at λ=542 nm, $\varepsilon=2.4*10^{8}$ $cm^{-1}M^{-1}$) and Ag nanoparticles (at λ=390 nm, $\varepsilon=8.7*10^{8}$ $cm^{-1}M^{-1}$) are used to solve Beer's law for concentration. Table 7.1 indicates the solutions that will be prepared and subsequently incubated with the brine shrimp. Students should prepare solutions in vials/test tubes labeled a-f (see Table 7.1) and these solution can either be stored for future use or used immediately.

7.2.3 Live/Dead Brine Shrimp Assay

The brine shrimp assay entails a 24 h exposure (or longer) to control and nanoparticle solutions described above and determining if the brine shrimp are viable after exposure. Viability of the brine shrimp is assessed based on movement, where live

Table 7.1 Volumes of solutions, either synthesized nanoparticle, water, or stock solution, that are needed to make the exposure solutions in the nanoparticle dilution instructions.

Sample Label	Sample Name	Water Volume (mL)	Nanoparticles Volume (mL) - from vial X	Other specified solution Volumes
a	negative control	5	-	-
b	ion control	-	-	5 mL Ag or Au stock solution
c	100% nanoparticles	-	10 - synthesis vial	-
d	50% nanoparticles	5	5 - vial c	-
e	25% nanoparticles	5	5 - vial d	-
f	12.5% nanoparticles	5	5 - vial e	-

brine shrimp (as seen in Figure 7.2) are those that move while dead shrimp do not. 2-3 days prior to the viability experiment, brine shrimp should be hatched from eggs by placing ~0.4g eggs in 1 L of artificial sea water (35 g Instant Ocean® in 1 L deionized water) with constant aeration, either from an air pump or in a fish tank, and illuminated by a lamp to keep them warm. Brine shrimp eggs (inset on Figure 7.2) should be stored in a cool, dry space and can be stored for years.

The assay is best performed in a multi-well plate where the wells can hold at least 2 mL each, though other containment is possible. A Pasteur pipet marked with lines for measuring 0.5 and 1 mL is prepared by pre-measuring the volumes with a volumetric pipet and then taking up that volume into the Pasteur pipet and recording the height of the water with a permanent marker. While this task can be completed by the instructor prior to the students experiment, it is also possible for the students to perform this task and is diagrammed in the student worksheet. Students will measure 0.5 mL brine shrimp

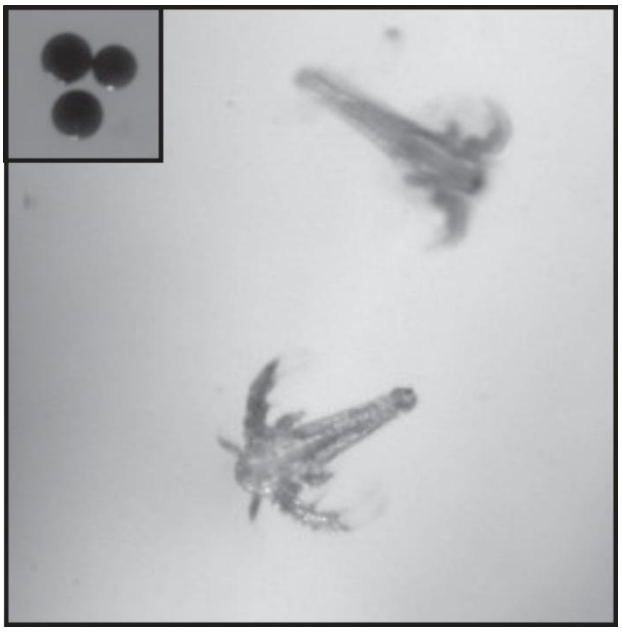

Figure 7.2 Image of brine shrimp eggs (inset) and live brine shrimp.

suspension and count the moving brine shrimp while they are still in the pipet, then transfer the brine shrimp to an empty well and record the value and the well in which it was placed. This part of the experiment has the greatest potential for error and therefore, students should take their time counting and transferring brine shrimp. It may be easier to count the moving brine shrimp by holding the pipet against a dark surface. Also, the addition of Protoslo® to the brine shrimp to slow them down can make it easier for students to count (20-30 drops Protoslo® to 20 mL brine shrimp aliquot). Students should get 15-20 brine shrimp per 0.5 mL so if the brine shrimp are too dense from the hatching solution, add artificial sea water solution (35 g Instant Ocean in 1L water) to the suspension of brine shrimp to dilute to range. Students should perform the viability in quadruplicate so that each control or nanoparticle concentration has multiple data points. This means that if a student/lab pair within a larger group is testing the viability of 3 sample solutions, they should fill a total of 12 wells.

After counting and recording the number of shrimp per well, the most time consuming portion of this experiment, students should add 1 mL serum solution (25% serum (e.g. bovine calf serum, fetal bovine serum, etc):75% artificial sea water by volume) to each well of brine shrimp to prevent nanoparticle aggregation and 1 mL of the control or nanoparticle solution to each well. Again, if a student is performing the viability assay on 3 of the solutions, only one experimental solution should be used per well across the 4 replicate wells for that condition. Upon exposure, brine shrimp should be covered with a clear cover (i.e. as commonly provided with well plates or plastic wrap), placed under a lamp, such as a desk or utility lamp, approximately 9 inches from the bulb and incubated for 24 h, after which the brine shrimp should be counted again, only counting the shrimp that are still moving (i.e. alive).

7.2.4 Data Analysis

An important component of chemistry, and science in general, is data analysis and statistics. In this experiment, students use the viability data to perform simple statistics. First, viability is calculated per well by Equation 7.1.

(7.1) $$viability\ (in\ \%) = \frac{\#\ live\ brine\ shimp\ after\ exposure}{\#\ live\ brine\ shrimp\ before\ exposure} \times 100\%$$

Once the viability is calculated per well, data can be combined for each exposure condition and students can calculate the average, standard deviation, and other statistical transformations (e.g. t-testing). Using the combined data, students can then plot the data to see a graphical representation of the class' results, making conclusions about the

relative toxicity of Au and Ag nanoparticles. Variations to the viability experiment can be performed, such as varying the time of exposure (e.g. 24 vs. 48 or 72 h) and number of replicates, depending on the aim of this experiment.

7.2.5 Hazards and Safety Considerations

$NaBH_4$ is flammable. Goggles should be worn during this experiment in addition to the optional use of gloves and lab aprons. All nanoparticle solutions, including reagents and exposed brine shrimp, should be collected and disposed in accordance with hazardous waste procedures.

7.2.6 Division of the Experiments

This experiment can be split over 2 or 3 days and as previously mentioned, it saves time and resources to split tasks over multiple people or lab pairs. Table 2 depicts how the experiment can be divided in different roles and the division of tasks per day. In groups of two (either individuals or lab pairs), we suggest students study one type of nanoparticle (i.e. Au or Ag) and the tasks of nanoparticle synthesis and dilution be split between the 2. In this configuration, each unit of the duo would study the toxicity of 3 exposure solutions for a single nanoparticle. The breakdown of tasks per day is suggested as follows for a 3 day experiment: Day 1 - nanoparticle synthesis and dilution, Day 2 - count out brine shrimp and perform exposure, Day 3 - determine number of surviving brine shrimp and data analysis. For a 2 day experiment, day 1 consists of nanoparticle synthesis, dilution, and brine shrimp counting/exposure and day 2 involves determining the number of surviving shrimp and data analysis. Because nanoparticles

can be stored, one can imagine that this experiment could also be broken over multiple weeks within a semester, performing nanoparticle synthesis in prior weeks, so long as there are 2 consecutive days for the viability assay. It may be beneficial to pre-synthesize a set of nanoparticles for the first class to use and the second class can utilize the nanoparticles made in the first class. This also enables the "diluter" role to begin at the same time as "synthesis." The student worksheet below details a 3-day experiment with students working in groups of 2 lab pairs.

Table 7.2 Suggested roles within lab groups and break down of experiments per day.

Roles	3-day	2-day
Ag Synthesizer Diluter Au Synthesizer Diluter	Day 1: nanoparticle synthesis and dilution Day 2: brine shrimp counting and exposure Day 3: counting surviving brine shrimp and data analysis	Day 1: nanoparticle synthesis, dilution, shrimp counting and exposure Day 2: counting surviving brine shrimp and data analysis

7.3 Student Worksheet

Name _____
Lab Partner_____

Nanoparticle (circle one): Au Ag
Group role (circle one): nanoparticle synthesis dilution
Exposure conditions (circle three): a b c d e f

Nanoparticle Toxicity to Brine Shrimp

Description: It is critical to determine the toxicity of substances to determine their safety. This lab is designed to assess the toxicity of gold (Au) and silver (Ag) nanoparticles on brine shrimp viability. Viability is a term to describe whether an

organism is alive or dead. That is, if an organism is living, it is said to be viable. In this lab, brine shrimp are a model organism to perform initial assessment of nanoparticle toxicity. If the nanoparticles are found to be non-toxic, scientists would likely move to toxicity assessment in an organism higher in the food chain.

Experimental Outcomes:

- Synthesize nanoparticles and prepare nanoparticle solutions
- Perform brine shrimp toxicity test with nanoparticles
- Analyze toxicity results for statistical significance

Instructions: You will be working with your lab partner and 2 other lab groups. Each trio of lab partners will be working with one type of nanoparticle (Au or Ag), and each lab pair will use that nanoparticle to perform brine shrimp toxicity tests. In addition, each lab group pair will have a group role within the trio of lab partners: nanoparticle synthesis, nanoparticle dilution, or data collection. The instructions for each role are listed below. You are responsible for answering the questions within the procedure section that you complete (i.e. answer the Au synthesis questions if that is your role, but you do not need to complete the questions in the dilution/data collection sections). Additionally, there are questions at the end of each day's procedure that everyone must answer.

NOTE: Please remember to circle the nanoparticle your group will be working with and the group role that you have at the top of this page.

Procedure – Day 1

Safety:

equipment:	goggles (optional: gloves and lab apron)
procedures:	wash hands completely after lab
	rinse skin with water upon contact with chemicals
disposal:	unused nanoparticles in "Noble Metal" waste container

Au Nanoparticle Synthesis

Responsible parties_____ *(only complete if this is <u>your</u> role)*

Supplies:

- goggles
- gloves (optional)
- 20 mL graduated cylinder
- glass vial
- hot plate
- thermometer
- glass stir rod *
- timer
- 15 mL Gold (Au) stock solution
- 1.5 mL 50 mM sodium citrate solution for Gold
- tongs, test tube holder, or "hot hands"

* hot plate w/magnetic stir bars may be used

Method:

1. Add 15.0 mL Au stock solution to glass vial using a graduated cylinder
   Actual volume of Au stock solution measured: _____mL

2. Heat Au solution to approximately 140°C (medium high heat) on hot plate.
   Actual solution temperature: _____
   What color is the solution before heating?_____

3. Stir solution with stir rod every 30 seconds for the duration of the synthesis

4. When Au solution is boiling (or after 10 minutes), add 1.5 mL sodium citrate stock solution using a graduated cylinder
   Actual volume of sodium citrate measured: _____mL
   What color is the solution after addition of sodium citrate?_____
   When did the solution change colors? (immediately? after some time?)_____

5. Keep Au nanoparticle solution heating for 10 minutes after color change, making sure to stir every 30 seconds

6. Remove synthesized Au nanoparticles from heat and give vial to the lab pair with the "dilution" role

Silver (Ag) Nanoparticle Synthesis

Responsible parties_____ *(only complete if this is <u>your</u> role)*

Supplies:

- goggles
- gloves (optional)
- 20 mL graduated cylinder
- glass vial
- hot plate
- thermometer
- glass stir rod *
- timer
- 13 mL deionized water
- 1 mL 7.5 mM Silver (Ag) stock solution WARNING: Ag stock solution will stain hands and clothing
- 1 mL 7.5 mM sodium citrate stock solution
- 1 mL 10 mM Sodium borohydride
- tongs, test tube holder, or "hot hands"

* hot plate w/magnetic stir bars may be used

Method:

1. Add 13 mL deionized water to glass vial using a graduated cylinder
   Actual volume of water added: _____mL

2. Heat water on hot plate until small bubbles begin forming on side of vial (beginning to boil)

3. Add 1 mL Ag stock solution and 1 mL sodium citrate stock solution to hot water using a pipette
   What color is the solution?_____

4. Add magnetic stir bar to glass vial and begin stirring the solution

5. Add 1 mL (20 drops) sodium borohydride solution to vial
   What color is the solution after addition of $NaBH_4$?_____

6. Keep Ag nanoparticle solution boiling for 10 minutes after color change, making sure to stir vigorously and continuously

7. Remove synthesized Ag nanoparticles from heat and give vial to the lab pair with the "dilution" role

Dilution of Gold (Au) Nanoparticles

Responsible parties_____ *(only complete if this is <u>your</u> role)*

Supplies:

- goggles
- gloves (optional)
- permanent marker
- 6 empty vials w/ covers
- 10 mL graduated cylinder
- 20 mL deionized water
- 5 mL Gold stock solution
- 10 mL Gold nanoparticles

Method:

1. Label vials a-f

2. Vial a: add 5 mL deionized water with a graduated cylinder

3. Vial b: add 5 mL Au or Ag stock solution with a graduated cylinder

4. Vial c: add 10 mL synthesized Au or Ag nanoparticles with graduated cylinder

5. Vial d: add 5 mL of solution from vial c + 5 mL deionized water with a graduated cylinder and stir

6. Vial e: add 5 mL of solution from vial d + 5 mL deionized water with a graduated cylinder and stir

7. Vial f: add 5 mL of solution from vial e + 5 mL deionized water with a graduated cylinder and stir

8. Keep vials for Day 2 Viability Assay.

What is the concentration of vial d as compared to vial c?_____
What is the concentration of vial e as compared to vial d?_____
What is the concentration of vial e as compared to vial c?_____
What is the concentration of vial f as compared to vial c?_____

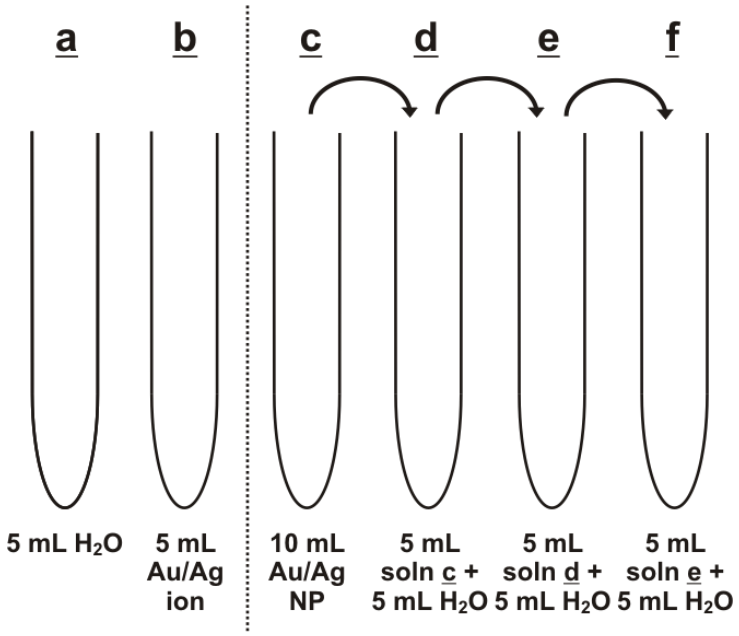

Dilution of Silver (Ag) Nanoparticles
Responsible parties_____ *(only complete if this is your role)*
Supplies:
- goggles
- gloves (optional)
- permanent marker
- 6 empty vials w/ covers
- 10 mL graduated cylinder
- 20 mL deionized water
- 5 mL Silver stock solution WARNING: Ag stock solution will stain hands and clothing

- 10 mL Silver nanoparticles

Method:

1. Label vials a-f
2. Vial a: add 5 mL deionized water with a graduated cylinder
3. Vial b: add 5 mL Au or Ag stock solution with a graduated cylinder
4. Vial c: add 10 mL synthesized Au or Ag nanoparticles with graduated cylinder
5. Vial d: add 5 mL of solution from vial c + 5 mL deionized water with a graduated cylinder and stir
6. Vial e: add 5 mL of solution from vial d + 5 mL deionized water with a graduated cylinder and stir
7. Vial f: add 5 mL of solution from vial e + 5 mL deionized water with a graduated cylinder and stir
8. Keep vials for Day 2 Viability Assay.

What is the concentration of vial d as compared to vial c?_____
What is the concentration of vial e as compared to vial d?_____
What is the concentration of vial e as compared to vial c?_____
What is the concentration of vial f as compared to vial c?_____

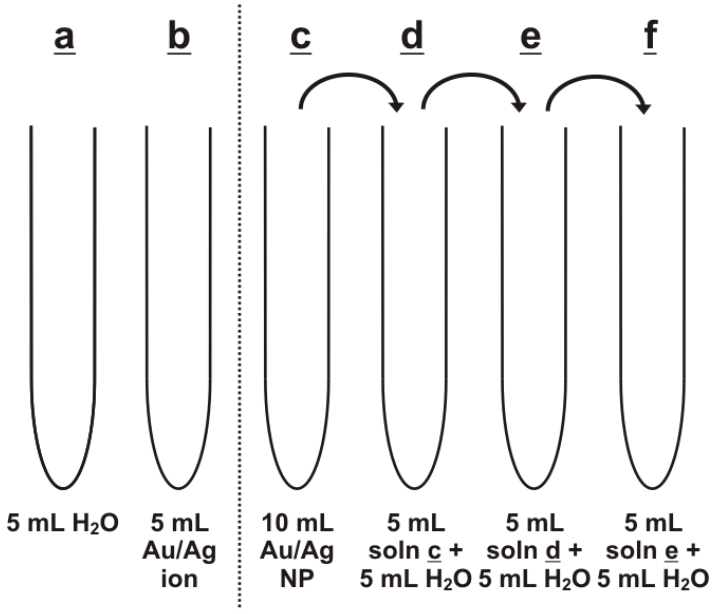

Within the duo of lab groups, one lab pair should get vials a, d, f and one should get vials b, c, and e to perform brine shrimp viability assay

Questions: (These questions have multiple components. Make sure to answer all parts of the question before day 2 of the procedure.)

1. What are nanoparticles? What are two chemical and/or physical properties that differ between the Au and Ag nanoparticles?

2. What type of dilution is used to make the nanoparticle solutions with varying concentrations? Describe a different dilution scheme/method to arrive at the same concentrations.
3. Why do we want to test varying concentrations of the nanoparticle solutions?
4. Assume the synthesized nanoparticle solution is 100 nM (nanomolar, 10^{-9} M). Based on the dilution factors, what is the concentration of nanoparticles in vial c, d, e, and f? (You may need to get dilution factors from members within the group)

Procedure – Day 2

Safety:

equipment:	goggles (optional: gloves)
procedures:	wash hands completely after lab rinse with water upon chemical contact
disposal:	unused brine shrimp in 10% bleach for 30 minutes, then down drain unused nanoparticles in "Noble Metal" waste container unused serum solution down the drain

Viability Assay (everyone completes)
Part A: Mark Pasteur pipette with .5 mL and 1 mL markings
Supplies:

- water
- volumetric pipet
- small beaker
- Pasteur pipet
- Protoslo® Quieting Solution (if desired)

Method:

1. Add 0.5 mL water to small beaker using volumetric or transfer pipet

2. Pipet all 0.5 mL of water into Pasteur pipet and mark the meniscus location on the pipet ensuring that there are no bubbles in the water-filled region of the pipet (see pictorial depiction)

3. Dispose of water but save pipet with the 0.5 mL marked upon it.

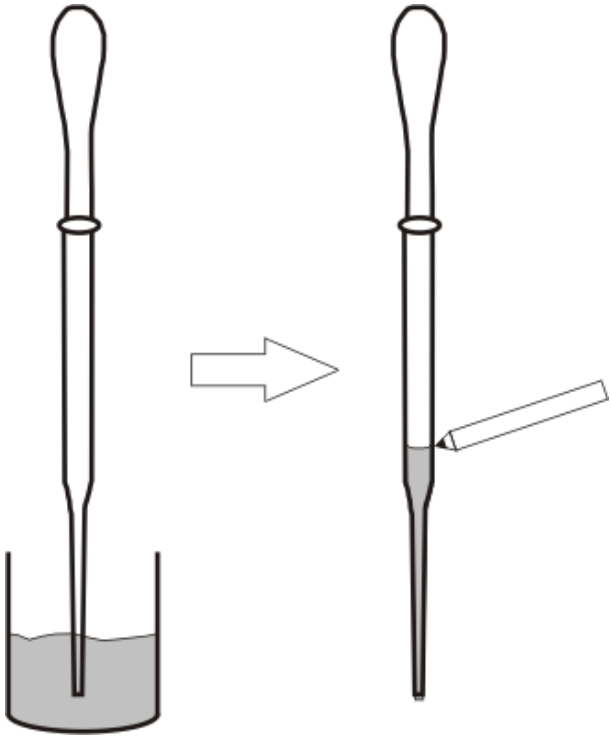

4. Add 1 mL water to the same small beaker

5. Pipet all 1 mL of water into the *same* Pasteur pipet and mark the meniscus location on the pipet as done above

6. Dispose of water. Pipet should now have a 0.5 and 1 mL marks on it and will be used to measure out solutions for the brine shrimp assay

Part B: Count and record living brine shrimp in 12 spot wells

Supplies:

- Pasteur pipet with .5 mL and 1.0 mL markings
- pipet bulb or aid
- 6 mL brine shrimp

Method:

1. Pipet up 0.5 mL brine shrimp into glass Pasteur pipet

2. Count brine shrimp that are moving while in the pipet. Tip: it may be easier to see brine shrimp by holding pipet against a dark surface

3. Following counting, put brine shrimp into one well of a 24-well plate

4. Record the number of shimp below in the appropriate circle corresponding to the location of the brine shrimp in 24 well plate (shown below)

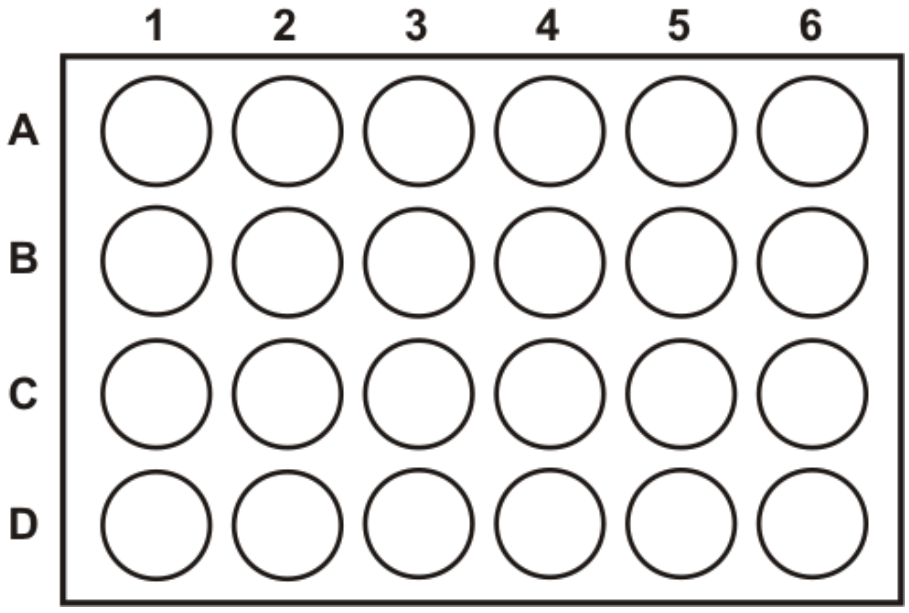

5. Repeat steps 7-10 until 3 columns (a total of 12 wells) contain brine shrimp

Part C: Nanoparticle exposure of brine shrimp

Supplies:

- 15 mL serum solution
- synthesized nanoparticle solutions
- incandescent 40 watt lamp
- ring stand
- pipet
- noble metal waste container

Methods:

1. Add 1 mL 25% serum solution to each well of brine shrimp

2. You will be given 3 exposure conditions per lab group, (as described in #8 of the dilution instructions), so 4 wells will be replicates of a single condition

3. Add 1 mL exposure solution (control, ion, or nanoparticles) to each well and label the well plate above with which solution (a-f) was placed in the well

4. Place well plate under lamp approximately 9 inches from the bulb with the wells covered

5. Rinse pipet out with water and save for tomorrow

6. Dispose of remaining nanoparticle and ion solutions (vials b-f) in the designated waste container

After exposure to nanoparticle solutions, the brine shrimp will be incubated for ~24 hours before you do the viability test in tomorrow's class to see what fraction of brine shrimp survive exposure.

Questions:

1. Hypothesize what will happen to the brine shrimp after exposure to all the exposure conditions. That is, predict whether the shrimp with live or die upon exposure to solutions a-f.

Procedure – Day 3

Safety:

equipment: goggles (optional: gloves)
procedures: wash hands completely after lab
rinse with water upon contact with chemicals

disposal: Add 10% bleach to brine shrimp solution, then dispose in the "Noble Metal" waste container

Part D: Brine shrimp viability assessment (everyone completes)

Supplies:

- bleach
- noble metal waste container
- pipet
- calculator

Method:

1. Pull all solution from one well in the plate into glass Pasteur pipet

2. Count brine shrimp that are still moving in pipet as well as any moving shrimp that are left behind in the well. Do NOT include shrimp that are not moving (dead shrimp) in your count

3. Record your brine shrimp count in the appropriate circle below for all 12 wells

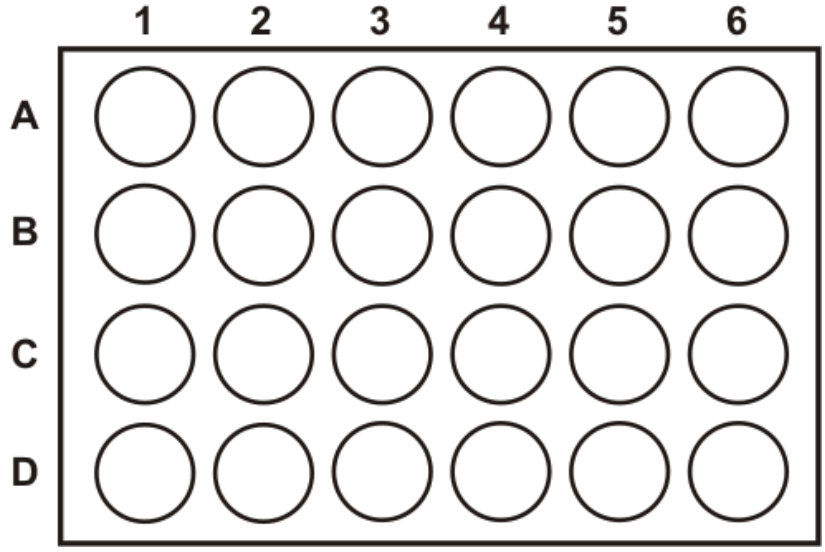

4. Using the values from yesterday (see the values you put into the well plate diagram yesterday), determine the fraction of brine shrimp that are alive today and convert it to a decimal fraction. For example, if yesterday in well 1A you had 20 brine shrimp alive and today you had 15 alive in well 1A, your fraction would be 15/20 and the decimal fraction would be 0.75.

5. Record the decimal fraction value in the correct well in the well-plate diagram below

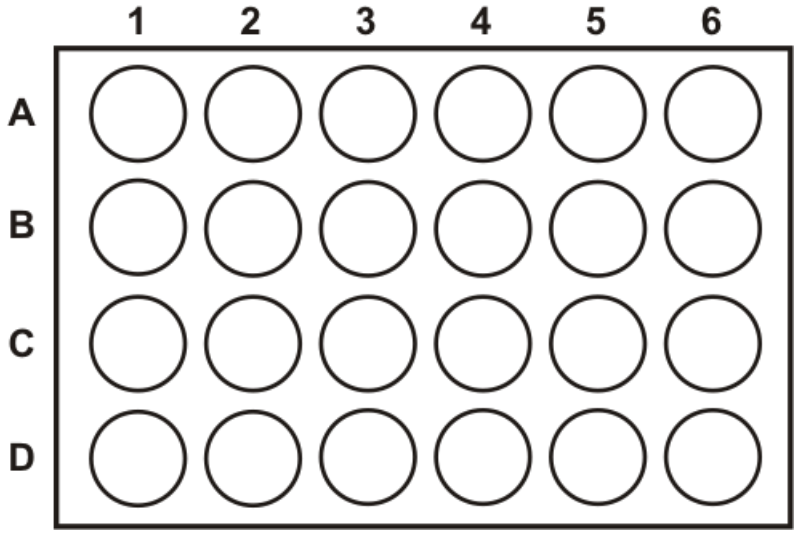

6. Determine average decimal fraction for each exposure condition you performed
   Exposure Condition (e.g. a or e): _____ Average: _____
   Exposure Condition:_____ Average: _____
   Exposure Condition:_____ Average: _____

7. CLEAN UP: Upon completion of the viability assay, discard all well contents into the designated waste container (Add 10% bleach to brine shrimp, then dispose in the noble metal waste container)

Data Collection

1. Collect decimal fraction for all wells of each culture condition from your own data and the others in your duo

2. Pool data with that of other duos that used the same nanoparticle (Au or Ag). Record the values on the class data graph

3. Determine the class average for each exposure condition (a-f) of the nanoparticle you worked with

Nanoparticle used: _____
Class average for vial a (control): _____
Class average for vial b (ion): _____
Class average for vial c :_____
Class average for vial d:_____
Class average for vial e : _____
Class average for vial f:_____

Concluding Questions

1. Why do we include the ion exposure as one of the conditions? Why do we include the water exposure?

2. What does a viability decimal fraction of 1 mean? What does a viability decimal

fraction of 0 mean? Considering the data from your entire trio, did the exposure to nanoparticles affect brine shrimp viability?

3. How consistent was the data within your given group? Across groups? How might we represent this variability mathematically?

4. Do you think brine shrimp are a good model to predict human nanoparticle toxicity?

7.4 Results and Discussion

Three classes of high school chemistry students, two standard and one advanced placement level, performed this experiment during development. The students were given the following five question test, both prior to and following the experiment, to assess their level of comprehension of the core themes (interdisciplinary science, nanotoxicology, and statistics) presented:

1. A nanoparticle is a very small particle. What does the prefix nano mean?
2. Why would we worry about toxicity?
    Where can you find nanoparticles?
    To your knowledge, have you encountered nanoparticles before now?
    How might you be exposed?
3. How do you determine safety of a chemical/technology?
4. Viability means the measure of organisms that survive exposure to a toxic substance. If after expose to the substance, the viability is 70%±5%. What does the ±5% mean?
5. What fields of science ask questions related to toxicity?

Pre-laboratory discussions were led by the experiment developers, in lieu of the high school teacher introductory lecture. Direct comparisons were made between the pre- and post-tests of individual students in each class; differences in responses (i.e.: changes between incorrect/correct and qualitative/quantitative answer) to the five posed questions

were assessed and tabulated for all anonymous, paired (pre- and post- experimental testing) responses. For question one, students were asked to define the "nano" prefix: responses ranged from qualitative (i.e.: very small, tiny) to quantitative (i.e.: correct 10^{-9} and incorrect 10^{9}). The most common error was an inversion in scale for those giving quantitative responses, for both the pre- and post-test responses. Overall, student comprehension shifted to more quantitative responses when students responded differently on the post-test. For question two, students were asked about their exposure to nanoparticles. Students largely (>65%) responded that they had been exposed to nanoparticles in the pre-test: post-testing showed students who had answered negatively changed their answers to affirmative responses. Question three asked students to describe safety determinations (for a chemical or technology); typical responses included testing (involving either animals or people) and experimentation for both pre- and post- test responses. The students were asked to interpret data suggesting viability of 70% ± 5% in question four: responses ranged from "give or take", error/% error/range of error, and specifically stated ranges. Students responses were largely unchanged from pre- and post-testing, while the roughly 5% that did respond differently provided more descriptive, appropriate responses (e.g. percent error became percent range of live brine shrimp). To assess the students understanding of interdisciplinary science, students were asked which fields of science ask questions related to toxicity. Student responses included various fields from physical and biological sciences, medicine, and a more general response of "all fields". Upon post-testing, student responses included similar branches of science but typically included more disciplines in their answers (e.g. toxicology became toxicology, chemistry, biology). The experiment was successfully completed in the

laboratory classroom and based on their pre- and post-testing answers, the students showed improvement in their understanding of nanotoxicology and interdisciplinary science: limited improvement was seen from the statistic question, where student responses were largely unchanged after performing the experiment.

The described trial, with high school students, informed the final version of the experiment described in the methods section; changes were made to the division of experiments and the Ag nanoparticle synthesis. Additionally, this beta-test illuminated the multi-component nature of nanotoxicity studies. That is, this experiment has many components, and depending on pre-laboratory preparation and lecture, the emphasis could be placed preferentially on one area or another. Clearly, based on the pre- and post-test question results above, our emphasis was placed largely on nanoparticles, nanotoxicity and the advantages of interdisciplinary science, which is the bias of our academic research. However, we envision this experiment to be useful for a lot of different learning outcomes, depending on where emphasis is placed by the instructor.

7.5 Classroom Science Standards

The high school national science education standards (NSES) addressed by this activity include “Science as Inquiry,” “Physical Science,” “Science and Technology,” and “History and Nature of Science.” More details on specific national standards can be found in Table 7.3.

Table 7.3 National Science Education Standards (NSECs), grade 9-12, fulfilled by this experiment

Science as Inquiry	**12 ASI**	Abilities necessary to do scientific inquiry	12ASI1.2	Design and conduct scientific investigations
Science as Inquiry	**12 ASI**	Abilities necessary to do scientific inquiry	12ASI1.3	Use technology and mathematics to improve investigations and communications
Science as Inquiry	**12 ASI**	Abilities necessary to do scientific inquiry	12ASI1.6	Communicate and defend a scientific argument
Physical Science	**12BPS**	Structure and properties of matter	12BPS1.1	Matter is made of minute particles called atoms, and atoms are composed of even smaller components
Science in Personal and Social Perspectives	**12FSPSP**	Natural and human-induced hazards	12FSPSP5.4	Natural and human induced hazards present the need for humans to assess potential danger and risk
Science in Personal and Social Perspectives	**12FSPSP**	Science and technology in local, national, and global challenges	12FSPSP6.4	Individuals and society must decide on proposals involving new research and the introduction of new technologies into society

7.6 Conclusions

This experiment was designed to be flexible for a variety of instructional aims (e.g. emphasis on statistical analysis in chemistry) and can be used fully or only partially (e.g. only nanoparticle synthesis or only viability assay). Through this experiment, students are exposed to the fields of nanotechnology and nanotoxicology, with hands-on

experience with basic chemical, material, toxicological, and statistical principles. Beyond scientific principles, this experiment encourages class-wide collaboration and allows all students to contribute to the group data.

Bibliography

Chapter 1 References

1. G. Oberdörster, A. Maynard, K. Donaldson, V. Castranova, J. Fitzpatrick, K. Ausman, J. Carter, B. Karn, W. Kreyling, D. Lai, *et al. Part. Fibre Toxicol.* **2005**, 2, 8.
2. Nanoscience and Nanotechnologies: Opportunities and Uncertainties. The Royal Academy of Science Policy Section and The Royal Academy of Engineering; London, **2004**.
3. C. O. Robichaud, A. E. Uyar, M. R. Darby, L. G. Zucker and M. R. Wiesner. *Environ. Sci. Technol.* **2009**, 43, 4227-4233.
4. M. C. Stensberg, Q. Wei, E. S. McLamore, D. M. Porterfield, A. Wei and M. S. Sepúlveda. *Nanomedicine.* **2011**, 6, 879-898.
5. G. Oberdörster, J. Ferin, G. Finkelstein, P. Wade and N. Corson. *J. Aerosol Sci.* **1990**, 21, 384-387.
6. A. P. Gondikas, E. K. Jang and H. Hsu-Kim. *J. Colloid Interface Sci.* **2010**, 347, 167-171.
7. A. Nel. *Science* **2005**, 308, 804-806.
8. A. D. Maynard, D. B. Warheit and M. A. Philbert. *Toxicol. Sci.* **2011**, 120, S109-S129.
9. G. Oberdörster, E. Oberdörster and J. Oberdörster. *Environ. Health Perspect.* **2005**, 113, 823-839.
10. B. J. Marquis, M. A. Maurer-Jones, K. L. Braun and C. L. Haynes. *Analyst* **2009**, 134, 2293-2300.
11. M. L. Etheridge, S. A. Campbell, A. G. Erdman, C. L. Haynes, S. M. Wolf and J. McCullough. *Nanomedicine: Nanotechnology, Biology and Medicine* **2012**, (in press).
12. E. Lechtman, N. Chattopadhyay, Z. Cai, S. Mashouf, R. Reilly and J. P. Pignol. *Phys. Med. Biol.* **2011**, 56, 4631.
13. B. Gulson, M. McCall, M. Korsch, L. Gomez, P. Casey, Y. Oytam, A. Taylor, M. McCulloch, J. Trotter, L. Kinsley, *et al. Toxicol. Sci.* **2010**, 118, 140-149.
14. S. H. Liou, T. C. Tsou, S. L. Wang, L. A. Li, H. C. Chiang, W. F. Li, P. P. Lin, C. H. Lai, H. L. Lee, M. H. Lin, *et al. J.Nanopart. Res.* **2012**, 14, 878.
15. M. Methner, C. Beaucham, C. Crawford, L. Hodson and C. Geraci. *J. Occup. Env. Hyg.* **2012**, 9, 543-555.
16. S. Ham, C. Yoon, E. Lee, K. Lee, D. Park, E. Chung, P. Kim and B. Lee. *J. Nanopart. Res.* **2012**, 14.
17. K. Donaldson, P. J. A. Borm, G. Oberdörster, K. E. Pinkerton, V. Stone and C. L. Tran. *Inhalation Toxicol.* **2008**, 20, 53-62.
18. R. Duffin, L. Tran, D. Brown, V. Stone and K. Donaldson. *Inhalation Toxicol.* **2007**, 19, 849-856.
19. Project on Emerging Nanotechnologies. http://www.nanotechproject.org (October 2012).
20. N. C. Mueller and B. Nowack. *Environ. Sci. Technol.* **2008**, 42, 4447-4453.
21. F. Gottschalk, R. W. Scholz and B. Nowack. *Environmental Modelling and Software* **2010**, 25, 320-332.
22. G. E. Batley, J. K. Kirby and M. J. McLaughlin. *Acc. Chem. Res.* **2012**, (in press).

23. S. J. Klaine, P. J. J. Alvarez, G. E. Batley, T. F. Fernandes, R. D. Handy, D. Y. Lyon, S. Mahendra, M. J. McLaughlin and J. R. Lead. *Environ. Toxicol. Chem.* **2008**, 27, 1825-1851.
24. F. Gottschalk, T. Sonderer, R. W. Scholz and B. Nowack. *Environ. Sci. Technol.* **2009**, 43, 9216-9222.
25. F. Gottschalk and B. Nowack. *J. Environ. Monit.* **2011**, 13, 1145-1155.
26. S. A. Blaser, M. Scheringer, M. MacLeod and K. Hungerbühler. *Sci. Total Environ.* **2008**, 390, 396-409.
27. R. Arvidsson, S. Molander, B. A. Sandén and M. Hassellöv. *Human and Ecological Risk Assessment: An International Journal* **2011**, 17, 245-262.
28. A. Praetorius, M. Scheringer and K. Hungerbühler. *Environ. Sci. Technol.* **2012**, 46, 6705-6713.
29. M. A. Kiser, P. Westerhoff, T. Benn, Y. Wang, J. Pérez-Rivera and K. Hristovski. *Environ. Sci. Technol.* **2009**, 43, 6757-6763.
30. P. Westerhoff, G. Song, K. Hristovski and M. A. Kiser. *J. Environ. Monit.* **2011**, 13, 1195-1203.
31. S. A. Love, M. A. Maurer-Jones, J. W. Thompson, Y. S. Lin and C. L. Haynes Assessing Nanoparticle Toxicity. *Annual Review of Analytical Chemistry,* Vol 5; **2012**; pp 181-205.
32. C. I. L. Justino, T. A. Rocha-Santos and A. C. Duarte. *TrAC Trends in Analytical Chemistry* **2011**, 30, 554-567.
33. A. A. Keller, H. Wang, D. Zhou, H. S. Lenihan, G. Cherr, B. J. Cardinale, R. Miller and Z. Ji. *Environ. Sci. Technol.* **2010**, 44, 1962-1967.
34. A. M. El Badawy, K. G. Scheckel, M. Suidan and T. Tolaymat. *Sci. Total Environ.* **2012**, 429, 325-331.
35. I. Chowdhury, Y. Hong and S. L. Walker. *Colloids and Surfaces A: Physicochemical and Engineering Aspects* **2010**, 368, 91-95.
36. C. Levard, E. M. Hotze, G. V. Lowry and G. E. Brown. *Environ. Sci. Technol.* **2012**, 46, 6900-6914.
37. A. E. Nel, L. Maedler, D. Velegol, T. Xia, E. M. V. Hoek, P. Somasundaran, F. Klaessig, V. Castranova and M. Thompson. *Nat. Mater.* **2009**, 8, 543-557.
38. M. Mahmoudi, I. Lynch, M. R. Ejtehadi, M. P. Monopoli, F. B. Bombelli and S. Laurent. *Chem. Rev.* **2011**, 111, 5610-5637.
39. J. Buffle, K. J. Wilkinson, S. Stoll, M. Filella and J. Zhang. *Environ. Sci. Technol.* **1998**, 32, 2887-2899.
40. T. S. Radniecki, D. P. Stankus, A. Neigh, J. A. Nason and L. Semprini. *Chemosphere* **2011**, 85, 43-49.
41. J. Liu, S. Legros, G. Ma, J. G. C. Veinot, F. von der Kammer and T. Hofmann. *Chemosphere* **2012**, 87, 918-924.
42. J. A. Nason, S. A. McDowell and T. W. Callahan. *J. Environ. Monit.* **2012**, 14, 1885-1892.
43. R. Tantra, J. Tompkins and P. Quincey. *Colloids and Surfaces B: Biointerfaces* **2010**, 75, 275-281.
44. H. Zhang, J. A. Smith and V. Oyanedel-Craver. *Water Res.* **2012**, 46, 691-699.
45. A. P. Gondikas, A. Morris, B. C. Reinsch, S. M. Marinakos, G. V. Lowry and H. Hsu-Kim. *Environ. Sci. Technol.* **2012**, 46, 7037-7045.

46. Y. Yin, J. Liu and G. Jiang. *ACS Nano* **2012**, 6, 7910-7919.
47. A. Nel, T. Xia, L. Mädler and N. Li. *Science* **2006**, 311, 622-627.
48. M. Rudolph, J. Erler and U. A. Peuker. *Colloids and Surfaces A: Physicochemical and Engineering Aspects* **2012**, 397, 16-23.
49. F. He, W. Wang, J.-W. Moon, J. Howe, E. M. Pierce and L. Liang. *ACS Appl. Mater. Interfaces* **2012**, 4, 4373-4379.
50. Z.-M. Xiu, Q.-B. Zhang, H. L. Puppala, V. L. Colvin and P. J. J. Alvarez. *Nano Lett.* **2012**, 12, 4271-4275.
51. I. A. Mudunkotuwa and V. H. Grassian. *J. Environ. Monit.* **2011**, 13, 1135-1144.
52. H. C. Fischer and W. C. Chan. *Curr. Opin. Biotechnol.* **2007**, 18, 565-571.
53. K. J. Lee, P. D. Nallathamby, L. M. Browning, C. J. Osgood and X. H. N. Xu. *ACS Nano* **2007**, 1, 133-143.
54. M. Fresta, G. Fontana, C. Bucolo, G. Cavallaro, G. Giammona and G. Puglisi. *J. Pharm. Sci.* **2001**, 90, 288-297.
55. C. M. Sayes, A. A. Marchione, K. L. Reed and D. B. Warheit. *Nano Lett.* **2007**, 7, 2399-2406.
56. Z. Chen, H. A. Meng, G. M. Xing, C. Y. Chen, Y. L. Zhao, G. A. Jia, T. C. Wang, H. Yuan, C. Ye, F. Zhao, *et al. Toxicol. Lett.* **2006**, 163, 109-120.
57. P. C. Gokhale, C. Zhang, J. T. Newsome, J. Pei, I. Ahmad, A. Rahman, A. Dritschilo and U. N. Kasid. *Clin. Cancer Res.* **2002**, 8, 3611-3621.
58. I. Dransfield, A. M. Buckle, J. S. Savill, A. McDowall, C. Haslett and N. Hogg. *J. Immunol.* **1994**, 153, 1254-1263.
59. S. Bruckner, S. Rhamouni, L. Tautz, J. B. Denault, A. Alonso, B. Becattini, G. S. Salvesen and T. Mustelin. *J. Biol. Chem.* **2005**, 280, 10388-10394.
60. H. Dumortier, S. Lacotte, G. Pastorin, R. Marega, W. Wu, D. Bonifazi, J. P. Briand, M. Prato, S. Muller and A. Bianco. *Nano Lett.* **2006**, 6, 1522-1528.
61. C. M. Sayes, K. L. Reed and D. B. Warheit. *Toxicol. Sci.* **2007**, 97, 163-180.
62. B. J. Marquis and C. L. Haynes. *Biophys. Chem.* **2008**, 137, 63-69.
63. R. Brayner, R. Ferrari-Iliou, N. Brivois, S. Djediat, M. F. Benedetti and F. Fiévet. *Nano Lett.* **2006**, 6, 866-870.
64. D. A. Pelletier, A. K. Suresh, G. A. Holton, C. K. McKeown, W. Wang, B. Gu, N. P. Mortensen, D. P. Allison, D. C. Joy, M. R. Allison, *et al. Appl. Environ. Microbiol.* **2010**, 76, 7981-7989.
65. Y. Yang, J. M. Mathieu, S. Chattopadhyay, J. T. Miller, T. Wu, T. Shibata, W. Guo and P. J. J. Alvarez. *ACS Nano* **2012**, 6, 6091-6098.
66. C. L. Arnaout and C. K. Gunsch. *Environ. Sci. Technol.* **2012**, 46, 5387-5395.
67. X. Fang, R. Yu, B. Li, P. Somasundaran and K. Chandran. *J. Colloid Interface Sci.* **2010**, 348, 329-334.
68. Y. Ge, J. P. Schimel and P. A. Holden. *Environ. Sci. Technol.* **2011**, 45, 1659-1664.
69. A. Pradhan, S. Seena, C. Pascoal and F. Cássio. *Microb. Ecol.* **2011**, 62, 58-68.
70. P. Das, C. J. Williams, R. R. Fulthorpe, M. E. Hoque, C. D. Metcalfe and M. A. Xenopoulos. *Environ. Sci. Technol.* **2012**, 46, 9120-9128.
71. K. Birbaum, R. Brogioli, M. Schellenberg, E. Martinoia, W. J. Stark, D. Günther and L. K. Limbach. *Environ. Sci. Technol.* **2010**, 44, 8718-8723.

72. W. Du, Y. Sun, R. Ji, J. Zhu, J. Wu and H. Guo. *J. Environ. Monit.* **2011**, 13, 822-828.
73. Y. Ma, L. Kuang, X. He, W. Bai, Y. Ding, Z. Zhang, Y. Zhao and Z. Chai. *Chemosphere* **2010**, 78, 273-279.
74. J. H. Priester, Y. Ge, R. E. Mielke, A. M. Horst, S. C. Moritz, K. Espinosa, J. Gelb, S. L. Walker, R. M. Nisbet, Y. J. An, *et al. Proc. Natl. Acad. Sci. U.S.A.* **2012**, 109, E2451-2456.
75. T. Sabo-Attwood, J. M. Unrine, J. W. Stone, C. J. Murphy, S. Ghoshroy, D. Blom, P. M. Bertsch and L. A. Newman. *Nanotoxicology* **2012**, 6, 353-360.
76. H. Zhu, J. Han, J. Q. Xiao and Y. Jin. *J. Environ. Monit.* **2008**, 10, 713-717.
77. M. Wang, L. Chen, S. Chen and Y. Ma. *Ecotoxicol. Environ. Saf.* **2012**, 79, 48-54.
78. D. Lin and B. Xing. *Environ. Pollut.* **2007**, 150, 243-250.
79. D. H. Atha, H. Wang, E. J. Petersen, D. Cleveland, R. D. Holbrook, P. Jaruga, M. Dizdaroglu, B. Xing and B. C. Nelson. *Environ. Sci. Technol.* **2012**, 46, 1819-1827.
80. J. H. Postlethwait, S. L. Johnson, C. N. Midson, W. S. Talbot, M. Gates, E. W. Ballinger, D. Africa, R. Andrews, T. Carl, J. S. Eisen, *et al. Science* **1994**, 264, 699-703.
81. M. Kasahara, K. Naruse, S. Sasaki, Y. Nakatani, W. Qu, B. Ahsan, T. Yamada, Y. Nagayasu, K. Doi, Y. Kasai, *et al. Nature* **2007**, 447, 714-719.
82. J. M. Oades. *Geoderma* **1993**, 56, 377-400.
83. B. J. Marquis, S. A. Love, K. L. Braun and C. L. Haynes. *Analyst* **2009**, 134, 425-439.
84. T. Yu, K. Greish, L. D. McGill, A. Ray and H. Ghandehari. *ACS Nano* **2012**, 6, 2289-2301.
85. M. Horie, H. Fukui, K. Nishio, S. Endoh, H. Kato, K. Fujita, A. Miyauchi, A. Nakamura, M. Shichiri, N. Ishida, *et al. J. Occup. Health* **2011**, 53, 64-74.
86. E. K. Rushton, J. Jiang, S. S. Leonard, S. Eberly, V. Castranova, P. Biswas, A. Elder, X. Han, R. Gelein, J. Finkelstein, *et al. Journal of Toxicology and Environmental Health-Part a-Current Issues* **2010**, 73, 445-461.
87. J. P. M. Almeida, A. L. Chen, A. Foster and R. Drezek. *Nanomed.* **2011**, 6, 815-835.
88. T. Mosmann. *J. Immunol. Methods* **1983**, 65, 55-63.
89. D. A. Scudiero, R. H. Shoemaker, K. D. Paull, A. Monks, S. Tierney, T. H. Nofziger, M. J. Currens, D. Seniff and M. R. Boyd. *Cancer Res.* **1988**, 48, 4827-4833.
90. T. F. Slater, B. Sawyer and U. Straeuli. *Biochim. Biophys. Acta* **1963**, 77, 383-393.
91. G. Punshon, D. S. Vara, K. M. Sales, A. G. Kidane, H. J. Salacinski and A. M. Seifalian. *Biomaterials* **2005**, 26, 6271-6279.
92. D. Hughes and H. Mehmet *Cell Proliferation & Apoptosis*; BIOS Scientific: Oxford, **2003**.
93. P. L. T. Huong, A. H. J. Kolk, T. A. Eggelte, C. P. H. J. Verstijnen, H. Gilis and J. T. Hendriks. *J. Immunol. Methods* **1991**, 140, 243-248.
94. H. M. Evans and W. Schulemann. *Science* **1914**, 39, 443-454.

95. M. Huang, E. Khor and L. Y. Lim. *Pharm. Res.* **2004**, 21, 344-353.
96. C. Zhang, B. Wangler, B. Morgenstern, H. Zentgraf, M. Eisenhut, H. Untenecker, R. Kruger, R. Huss, C. Seliger, W. Semmler, *et al. Langmuir* **2007**, 23, 1427-1434.
97. K. Kostarelos, L. Lacerda, G. Pastorin, W. Wu, S. Wieckowski, J. Luangsivilay, S. Godefroy, D. Pantarotto, J. P. Briand, S. Muller, *et al. Nat. Nanotechnol.* **2007**, 2, 108-113.
98. I. Nicoletti, G. Migliorati, M. C. Pagliacci, F. Grignani and C. Riccardi. *J. Immunol. Methods* **1991**, 139, 271-279.
99. E. S. Kaneshiro, M. A. Wyder, Y. P. Wu and M. T. Cushion. *J. Microbiol. Methods* **1993**, 17, 1-16.
100. E. Bonfoco, D. Krainc, M. Ankarcrona, P. Nicotera and S. A. Lipton. *Proc. Natl. Acad. Sci. U.S.A.* **1995**, 92, 7162-7166.
101. M. van Engeland, L. J. W. Nieland, F. C. S. Ramaekers, B. Schutte and C. P. M. Reutelingsperger. *Cytometry* **1998**, 31, 1-9.
102. T.-J. Fan, L.-H. Han, R.-S. Cong and J. Liang. *Acta Biochim. Biophys. Sin.* **2005**, 37, 719-727.
103. G. P. Studzinski *Apoptosis : A Practical Approach*; Oxford University Press: Oxford ; New York, **1999**.
104. O. Ostling and K. J. Johanson. *Biochem. Biophys. Res. Commun.* **1984**, 123, 291-298.
105. Y. Gavrieli, Y. Sherman and S. A. Bensasson. *J. Cell Biol.* **1992**, 119, 493-501.
106. D. A. Bass, J. W. Parce, L. R. Dechatelet, P. Szejda, M. C. Seeds and M. Thomas. *J. Immunol.* **1983**, 130, 1910-1917.
107. S. L. Hempel, G. R. Buettner, Y. Q. O'Malley, D. A. Wessels and D. M. Flaherty. *Free Radic. Biol. Med.* **1999**, 27, 146-159.
108. E. H. W. Pap, G. P. C. Drummen, V. J. Winter, T. W. A. Kooij, P. Rijken, K. W. A. Wirtz, J. A. F. Op den Kamp, W. J. Hage and J. A. Post. *FEBS Lett.* **1999**, 453, 278-282.
109. K. M. Robinson, M. S. Janes and J. S. Beckman. *Nat. Protoc.* **2008**, 3, 941-947.
110. K. M. Robinson, M. S. Janes, M. Pehar, J. S. Monette, M. F. Ross, T. M. Hagen, M. P. Murphy and J. S. Beckman. *Proc. Natl. Acad. Sci. U.S.A.* **2006**, 103, 15038-15043.
111. J. M. Gutteridge and G. J. Quinlan. *J. Appl. Biochem.* **1983**, 5, 293-299.
112. M. A. Baker, G. J. Cerniglia and A. Zaman. *Anal. Biochem.* **1990**, 190, 360-365.
113. Y. Sun, L. W. Oberley and Y. Li. *Clin. Chem.* **1988**, 34, 497-500.
114. E. Engvall and P. Perlmann. *Immunochemistry* **1971**, 8, 871-874.
115. C. A. Dinarello. *Chest* **2000**, 118, 503-508.
116. I. J. Elenkov, D. G. Iezzoni, A. Daly, A. G. Harris and G. P. Chrousos. *Neuroimmunomodulation* **2005**, 12, 255-269.
117. A. L. Neal. *Ecotoxicology* **2008**, 17, 362-371.
118. D. Y. Lyon and P. J. J. Alvarez. *Environ. Sci. Technol.* **2008**, 42, 8127-8132.
119. C. O. Dimkpa, J. E. McLean, D. W. Britt and A. J. Anderson. *Nanotoxicology* **2012**, 6, 635-642.
120. I. M. Sadiq, N. Chandrasekaran and A. Mukherjee. *Current Nanoscience* **2010**, 6, 381-387.

121. N. S. Wigginton, T. A. de, F. Piccapietra, J. Dobias, V. J. Nesatyy, M. J. F. Suter and R. Bernier-Latmani. *Environ. Sci. Technol.* **2010**, 44, 2163-2168.
122. Y. Yang, J. Wang, H. Zhu, V. L. Colvin and P. J. Alvarez. *Environ. Sci. Technol.* **2012**, 46, 3433-3441.
123. G. Jiang, Z. Shen, J. Niu, Y. Bao, J. Chen and T. He. *J. Environ. Monit.* **2011**, 13, 42-48.
124. P. Begum, R. Ikhtiari and B. Fugetsu. *Carbon* **2011**, 49, 3 9 0 7 –3 9 1 9.
125. C. Wang, L. Wang, Y. Wang, Y. Liang and J. Zhang. *Environ. Earth Sci.* **2012**, 65, 1643-1649.
126. J. P. Bohnsack, S. Assemi, J. D. Miller and D. Y. Furgeson. *Methods in Molecular Biology* **2012**, 926, 261-316.
127. X. Y. Yang, A. P. Gondikas, S. M. Marinakos, M. Auffan, J. Liu, H. Hsu-Kim and J. N. Meyer. *Environ. Sci. Technol.* **2012**, 46, 1119-1127.
128. J. L. Ferry, P. Craig, C. Hexel, P. Sisco, R. Frey, P. L. Pennington, M. H. Fulton, I. G. Scott, A. W. Decho, S. Kashiwada, *et al. Nat. Nanotechnol.* **2009**, 4, 441-444.
129. D. A. Giljohann, D. S. Seferos, P. C. Patel, J. E. Millstone, N. L. Rosi and C. A. Mirkin. *Nano Lett.* **2007**, 7, 3818-3821.
130. P. V. Asharani, L. W. Yi, Z. Y. Gong and S. Valiyaveettil. *Nanotoxicology* **2011**, 5, 43-54.
131. T. P. Dasari and H.-M. Hwang. *Sci. Total Environ.* **2010**, 408, 5817-5823.
132. J. P. Ryman-Rasmussen, J. E. Riviere and N. A. Monteiro-Riviere. *J. Investig. Dermatol.* **2007**, 127, 143-153.
133. E. Chnari, J. S. Nikitczuk, K. E. Uhrich and P. V. Moghe. *Biomacromolecules* **2006**, 7, 597-603.
134. H. Babich and E. Borenfreund. *Fundam. Appl. Toxicol.* **1988**, 10, 295-301.
135. T. Laaksonen, H. Santos, H. Vihola, J. Salonen, J. Riikonen, T. Heikkila, L. Peltonen, N. Kurnar, D. Y. Murzin, V. P. Lehto, *et al. Chem. Res. Toxicol.* **2007**, 20, 1913-1918.
136. R. Rallo, B. France, R. Liu, S. Nair, S. George, R. Damoiseaux, F. Giralt, A. Nel, K. Bradley and Y. Cohen. *Environ. Sci. Technol.* **2011**, 45, 1695-1702.
137. A. D. Maynard, R. J. Aitken, T. Butz, V. Colvin, K. Donaldson, G. Oberdörster, M. A. Philbert, J. Ryan, A. Seaton, V. Stone, *et al. Nature* **2006**, 444, 267-269.
138. B. J. Marquis, M. A. Maurer-Jones, O. H. Ersin, Y. -S. Lin, C. L. Haynes. *J. Nanopart. Res.* **2011**, 13, 1389-1400.

Chapter 2 References

1. M. A. Maurer-Jones, K. C. Bantz, S. A. Love, B. J. Marquis and C. L. Haynes. *Nanomedicine* **2009**, 4, 219-241.
2. B. J. Marquis, S. A. Love, K. L. Braun and C. L. Haynes. *Analyst* **2009**, 134, 425-439.
3. N. Lewinski, V. Colvin and R. Drezek. *Small* **2008**, 4, 26-49.
4. C. M. Sayes, K. L. Reed, S. Subramoney, L. Abrams and D. B. Warheit. *J. Nanopart. Res.* **2009**, 11, 421-431.

5. J. Seagrave, J. D. McDonald and J. L. Mauderly. *Exp. Toxicolog. Pathol.* **2005**, 57, 233-238.
6. M. Fisichella, H. Dabboue, S. Bhattacharyya, M.-L. Saboungi, J.-P. Salvetat, T. Hevor and M. Guerin. *Toxicol. In Vitro* **2009**, 23, 697-703.
7. N. A. Monteiro-Riviere, A. O. Inman and Dh. *Carbon* **2006**, 44, 1070-1078.
8. S. P. Low, K. A. Williams, L. T. Canham and N. H. Voelcker. *Biomaterials* **2006**, 27, 4538-4546.
9. B. J. Marquis, A. D. McFarland, K. L. Braun and C. L. Haynes. *Anal. Chem.* **2008**, 80, 3431-3437.
10. B. J. Marquis, M. A. Maurer-Jones, K. L. Braun and C. L. Haynes. *Analyst* **2009**, 134, 2293-2300.
11. R. C. Lin and R. H. Scheller. *Ann. Rev. Cell Dev. Bi.* **2000**, 16, 19-49.
12. C. Benoist and D. Mathis. *Nature* **2002**, 420, 875-878.
13. M. Kovarova and J. Rivera. *Curr. Med. Chem.* **2004**, 11, 2083-2091.
14. B. J. Marquis and C. L. Haynes. *Biophys. Chem.* **2008**, 137, 63-69.
15. Project on Emerging Nanotechnologies. http://nanotechproject.org/ (October 2012).
16. B. G. Trewyn, S. Giri, I. I. Slowing and V. S. Y. Lin. *Chem. Comm.* **2007**, 3236-3245.
17. I. I. Slowing, B. G. Trewyn, S. Giri and V. S. Y. Lin. *Adv. Funct. Mat.* **2007**, 17, 1225-1236.
18. I. I. Slowing, J. L. Vivero-Escoto, C.-W. Wu and V. S. Y. Lin. *Adv. Drug Deliver. Rev.* **2008**, 60, 1278-1288.
19. G. Oberdörster, A. Elder and A. Rinderknecht. *J. Nanosci. Nanotechno.* **2009**, 9, 4996-5007.
20. D. B. Warheit, K. L. Reed and C. M. Sayes. *Inhal. Toxicol.* **2009**, 21, 61-67.
21. S. P. Hudson, R. F. Padera, R. Langer and D. S. Kohane. *Biomaterials* **2008**, 29, 4045-4055.
22. Z. Tao, B. B. Toms, J. Goodisman and T. Asefa. *Chem. Res. Toxicol.* **2009**, 22, 1869-1880.
23. A. J. Di Pasqua, K. K. Sharma, Y.-L. Shi, B. B. Toms, W. Ouellette, J. C. Dabrowiak and T. Asefa. *J. Inorg. Biochem.* **2008**, 102, 1416-1423.
24. I. I. Slowing, C.-W. Wu, J. L. Vivero-Escoto and V. S. Y. Lin. *Small* **2009**, 5, 57-62.
25. G. J. Nohynek, J. Lademann, C. Ribaud and M. S. Roberts. *Crit. Rev. Toxicol.* **2007**, 37, 251-277.
26. X. Shen, L. Zhu, G. Liu, H. Yu and H. Tang. *Environ. Sci.Technol.* **2008**, 42, 1687-1692.
27. C. Kormann, D. W. Bahnemann and M. R. Hoffmann. *Environ. Sci. Technol.* **1991**, 25, 494-500.
28. B. O'Regan and M. Graetzel. *Nature* **1991**, 353, 737-740.
29. D. Kuciauskas, M. S. Freund, H. B. Gray, J. R. Winkler and N. S. Lewis. *J. of Phys. Chem. B* **2001**, 105, 392-403.
30. T. C. Long, N. Saleh, R. D. Tilton, G. V. Lowry and B. Veronesi. *Environ. Sci. Technol.* **2006**, 40, 4346-4352.

31. U. Heinrich, R. Fuhst, S. Rittinghausen, O. Creutzenberg, B. Bellmann, W. Koch and Levsen. *Inhal. Toxicol.* **1995**, 7, 533-556.
32. C.-Y. Jin, B.-S. Zhu, X.-F. Wang and Q.-H. Lu. *Chem. Res. Toxicol.* **2008**, 21, 1871-1877.
33. W. Stöber, A. Fink and E. Bohn. *J. Colloid Interface Sci.* **1968**, 26, 62-69.
34. Y.-S. Lin and C. L. Haynes. *Chem.Mater.* **2009**, 21, 3979-3986.
35. Y.-S. Lin and C. L. Haynes. *J. Am. Chem. Soc.* **2010**, 132, 4834-4842.
36. S. L. Isley and R. L. Penn. *J. Phys. Chem. C* **2008**, 112, 4469-4474.
37. H. M. Rietveld. *J. Appl. Crystallogr.* **1969**, 2, 65-71.
38. C. M. Sayes, R. Wahi, P. A. Kurian, Y. P. Liu, J. L. West, K. D. Ausman, D. B. Warheit and V. L. Colvin. *Toxicol. Sci.* **2006**, 92, 174-185.
39. K. T. Kawagoe, J. B. Zimmerman and R. M. Wightman. *J. Neurosci. Meth.* **1993**, 48, 225-240.
40. H. Zhang and J. F. Banfield. *J. Mater. Chem.* **1998**, 8, 2073-2076.
41. D. H. Everett *Basic Principles of Colloid Science*; Royal Society of Chemistry: London, **1988**.
42. G. Oberdörster, A. Maynard, K. Donaldson, V. Castranova, J. Fitzpatrick, K. Ausman, J. Carter, B. Karn, W. Kreyling, D. Lai, *et al. Part. Fibre Toxicol.* **2005**, 2, 8.
43. A. M. Alkilany, P. K. Nagaria, C. R. Hexel, T. J. Shaw, C. J. Murphy and M. D. Wyatt. *Small* **2009**, 5, 701-708.
44. X. He, H. Nie, K. Wang, W. Tan, X. Wu and P. Zhang. *Anal. Chem.* **2008**, 80, 9597-9603.
45. F. Lu, S.-H. Wu, Y. Hung and C.-Y. Mou. *Small* **2009**, 5, 1408-1413.
46. Z. Pan, W. Lee, L. Slutsky, R. A. F. Clark, N. Pernodet and M. H. Rafailovich. *Small* **2009**, 5, 511-520.
47. H.-M. Liu, S.-H. Wu, C.-W. Lu, M. Yao, J.-K. Hsiao, Y. Hung, Y.-S. Lin, C.-Y. Mou, C.-S. Yang, D.-M. Huang, *et al. Small* **2008**, 4, 619-626.
48. Z. Tao, M. P. Morrow, T. Asefa, K. K. Sharma, C. Duncan, A. Anan, H. S. Penefsky, J. Goodisman and A.-K. Souid. *Nano Lett.* **2008**, 8, 1517-1526.
49. H.-J. Eom and J. Choi. *Toxicol. In Vitro* **2009**, 23, 1326-1332.
50. R. Duffin, L. Tran, D. Brown, V. Stone and K. Donaldson. *Inhal. Toxicol.* **2007**, 19, 849-856.
51. D. Napierska, L. C. J. Thomassen, V. Rabolli, D. Lison, L. Gonzalez, M. Kirsch-Volders, J. A. Martens and P. H. Hoet. *Small* **2009**, 5, 846-853.
52. M. Horie, K. Nishio, K. Fujita, S. Endoh, A. Miyauchi, Y. Saito, H. Iwahashi, K. Yamamoto, H. Murayama, H. Nakano, *et al. Chem. Res. Toxicol.* **2009**, 22, 543-553.
53. T. C. Theoharides, D. Kempuraj, M. Tagen, P. Conti and D. Kalogeromitros. *Immunol. Rev.* **2007**, 219, 204.
54. H. L. Karlsson, J. Gustafsson, P. Cronholm and L. Moeller. *Toxicol. Lett.* **2009**, 188, 112-118.
55. B. Fahmy and S. A. Cormier. *Toxicol. In Vitro* **2009**, 23, 1365-1371.
56. C.-Y. Wang, H. Groenzin and M. J. Shultz. *J. Am. Chem. Soc.* **2004**, 126, 8094-8095.
57. A. Vittadini, M. Casarin and A. Selloni. *Theor. Chem. Acc.* **2007**, 117, 663-671.

58. L. T. Zhuravlev. *Langmuir* **1987**, 3, 316-318.

Chapter Three

1. B. J. Marquis, M. A. Maurer-Jones, O. E. Ersin, Y. S. Lin and C. L. Haynes. *J. Nanopart. Res.* **2011**, 13, 1389-1400.
2. W. Gorski, C. A. Aspinwall, J. R. T. Lakey and R. T. Kennedy. *J. Electroanal. Chem.* **1997**, 425, 191-199.
3. E. M. Akirav, J. Lebastchi, E. M. Galvan, O. Henegariu, M. Akirav, V. Ablamunits, P. M. Lizardi and K. C. Herold. *Proc. Natl. Acad. Sci. U.S.A.* **2011**, 108, 19018-19023.
4. A. E. Bishop, R. Pietroletti, C. W. Taat, W. H. Brummelkamp and J. M. Polak. *Virchows Arch. A Pathol. Anat. Histopathol.* **1987**, 410, 391-396.
5. S. N. Abraham and A. L. St. John. *Nat. Rev. Immunol.* **2010**, 10, 440-452.
6. K. Pihel, E. R. Travis, R. Borges and R. M. Wightman. *Biophys. J.* **1996**, 71, 1633-1640.
7. P. S. Cahill, Q. D. Walker, J. M. Finnegan, G. E. Mickelson, E. R. Travis and R. M. Wightman. *Anal. Chem.* **1996**, 68, 3180-3186.
8. M. A. Maurer-Jones, Y. S. Lin and C. L. Haynes. *ACS Nano* **2010**, 4, 3363-3373.
9. B. J. Marquis, A. D. McFarland, K. L. Braun and C. L. Haynes. *Anal. Chem.* **2008**, 80, 3431-3437.
10. B. J. Marquis, M. A. Maurer-Jones, K. L. Braun and C. L. Haynes. *Analyst* **2009**, 134, 2293-2300.
11. S. A. Love and C. L. Haynes. *Anal. Bioanal. Chem.* **2010**, 398, 677-688.
12. Project on Emerging Nanotechnologies. http://nanotechproject.org/ (October 2012).
13. G. J. Nohynek, J. Lademann, C. Ribaud and M. S. Roberts. *Crit. Rev. Toxicol.* **2007**, 37, 251-277.
14. A. L. Pruden and D. F. Ollis. *Environ. Sci. Technol.* **1983**, 17, 628-631.
15. N. Serpone, A. Salinaro and A. Emeline Deleterious effects of sunscreen titanium dioxide nanoparticles on DNA: efforts to limit DNA damage by particle surface modification. In *Nanoparticles and Nanostructured Surfaces: Novel Reporters with Biological Applications,* 1 ed.; SPIE: San Jose, CA, USA, 2001; pp 86-98.
16. I. P. Parkin and R. G. Palgrave. *J. Mater. Chem.* **2005**, 15, 1689-1695.
17. S. C. Hayden, N. K. Allam and M. A. El-Sayed. *J. Am. Chem. Soc.* **2010**, 132, 14406-14408.
18. I.-S. Kim, M. Baek and S.-J. Choi. *J. Nanosci. Nanotechnol.* **2010**, 10, 3453-3458.
19. C. M. Sayes, R. Wahi, P. A. Kurian, Y. Liu, J. L. West, K. D. Ausman, D. B. Warheit and V. L. Colvin. *Toxicol. Sci.* **2006**, 92, 174-185.
20. H. Yin, P. S. Casey, M. J. McCall and M. Fenech. *Langmuir* **2010**, 26, 15399-15408.
21. L. W. Zhang, J. Yang, A. R. Barron and N. A. Monteiro-Riviere. *Toxicol. Lett.* **2009**, 191, 149-157.

22. S. Sohaebuddin, P. Thevenot, D. Baker, J. Eaton and L. Tang. *Part. Fibre Toxicol.* **2010**, 7, 22.
23. B. C. Schanen, A. S. Karakoti, S. Seal, D. R. Drake Iii, W. L. Warren and W. T. Self. *ACS Nano* **2009**, 3, 2523-2532.
24. B. Vileno, M. Lekka, A. Sienkiewicz, S. Jeney, G. Stoessel, J. Lekki, L. Forro and Z. Stachura. *Environ. Sci. Technol.* **2007**, 41, 5149-5153.
25. H.-J. Eom and J. Choi. *Toxicol. In Vitro* **2009**, 23, 1326-1332.
26. M. J. Akhtar, M. Ahamed, S. Kumar, H. Siddiqui, G. Patil, M. Ashquin and I. Ahmad. *Toxicology* **2010**, 276, 95-102.
27. K. Matsui, M. Karasaki, M. Segawa, S. Y. Hwang, T. Tanaka, C. Ogino and A. Kondo. *MedChemComm* **2010**, 1, 209-211.
28. Z. Pan, W. Lee, L. Slutsky, R. A. F. Clark, N. Pernodet and M. H. Rafailovich. *Small* **2009**, 5, 511-520.
29. L. K. Limbach, R. Bereiter, E. Müller, R. Krebs, R. Gälli and W. J. Stark. *Environ. Sci. Technol.* **2008**, 42, 5828-5833.
30. K.-H. Liao, Y.-S. Lin, C. W. Macosko and C. L. Haynes. *ACS Appl. Mater. Interfaces* **2011**, 3, 2607-2615.
31. L. K. Limbach, Y. Li, R. N. Grass, T. J. Brunner, M. A. Hintermann, M. Muller, D. Gunther and W. J. Stark. *Environ. Sci. Technol.* **2005**, 39, 9370-9376.
32. G. Oberdörster. *J. Intern. Med.* **2009**, 267, 89-105.
33. E. C. Cho, Q. Zhang and Y. Xia. *Nat. Nanotechnol.* **2011**, 6, 385-391.
34. B. J. Marquis, Z. Liu, K. L. Braun and C. L. Haynes. *Analyst* **2011**, 136, 3478-3486.
35. S. Barillet, A. Simon-Deckers, N. Herlin-Boime, M. Mayne-L'Hermite, C. Reynaud, D. Cassio, B. Gouget and M. Carriere. *J. Nanopart. Res.* **2010**, 12, 61-73.
36. M. Horie, K. Nishio, K. Fujita, H. Kato, S. Endoh, M. Suzuki, A. Nakamura, A. Miyauchi, S. Kinugasa, K. Yamamoto, *et al. Toxicol. In Vitro* **2010**, 24, 1629-1638.
37. S. M. Hussain, K. L. Hess, J. M. Gearhart, K. T. Geiss and J. J. Schlager. *Toxicol. In Vitro* **2005**, 19, 975-983.
38. M. L. C. Bernheim, A. Ottolenghi and F. Bernheim. *Biochim. Biophys. Acta* **1957**, 23, 431-432.
39. D. D. Metcalfe, H. L. Thompson, S. J. Klebanoff and W. R. Henderson, Jr. *Biochem. J.* **1990**, 272, 51-57.
40. C. Rota, L. Liverani, F. Spelta, G. Mascellani, A. Tomasi, A. Iannone and E. Vismara. *Anal. Biochem.* **2005**, 344, 193-203.
41. M. N. Moller, J. R. Lancaster, Jr. and A. Denicola. *Curr. Top. Membr.* **2008**, 61, 23-42.
42. J. A. Rosado, A. González, G. M. Salido and J. A. Pariente. *Cell. Signal.* **2002**, 14, 547-556.
43. C. Xue, W. Liu, J. Wu, X. Yang and H. Xu. *Toxicol. In Vitro* **2011**, 25, 110-116.
44. R. K. Srivastava, Q. Rahman, M. P. Kashyap, M. Lohani and A. B. Pant. *PLoS One* **2011**, 6, e25767.

Chapter Four

1. A. Weir, P. Westerhoff, L. Fabricius, K. Hristovski and N. von Goetz. *Environ. Sci. Technol.* **2012**, 46, 2242-2250.
2. C. O. Robichaud, A. E. Uyar, M. R. Darby, L. G. Zucker and M. R. Wiesner. *Environ. Sci. Technol.* **2009**, 43, 4227-4233.
3. Z. Lewicka, A. Benedetto, D. Benoit, W. Yu, J. Fortner and V. Colvin. *J. Nanopart. Res.* **2011**, 13, 3607-3617.
4. H. H. Hau and J. A. Gralnick. *Annu. Rev. Microbiol.* **2007**, 61, 237-258.
5. B. Wu, R. Huang, M. Sahu, X. Feng, P. Biswas and Y. J. Tang. *Sci. Total Environ.* **2010**, 408, 1755-1758.
6. B. Wu, W.-Q. Zhuang, M. Sahu, P. Biswas and Y. J. Tang. *Sci. Total Environ.* **2011**, 409, 4635-4639.
7. K. Li and Y. Chen. *J. Hazard. Mater.* **2012**, 209-210, 264-270.
8. Z.-M. Xiu, Q.-B. Zhang, H. L. Puppala, V. L. Colvin and P. J. J. Alvarez. *Nano Lett.* **2012**, 12, 4271-4275.
9. D. A. Pelletier, A. K. Suresh, G. A. Holton, C. K. McKeown, W. Wang, B. Gu, N. P. Mortensen, D. P. Allison, D. C. Joy, M. R. Allison, *et al. Appl. Environ. Microbiol.* **2010**, 76, 7981-7989.
10. A. l. Simon-Deckers, S. Loo, M. Mayne-L'hermite, N. Herlin-Boime, N. Menguy, C. C. Reynaud, B. Gouget and M. Carrière. *Environ. Sci. Technol.* **2009**, 43, 8423-8429.
11. D. Y. Lyon and P. J. J. Alvarez. *Environ. Sci. Technol.* **2008**, 42, 8127-8132.
12. M. Li, S. Pokhrel, X. Jin, L. Mädler, R. Damoiseaux and E. M. V. Hoek. *Environ. Sci. Technol.* **2011**, 45, 755-761.
13. D. Y. Lyon, L. Brunet, G. W. Hinkal, M. R. Wiesner and P. J. J. Alvarez. *Nano Lett.* **2008**, 8, 1539-1543.
14. M. E. Davey and G. A. O'Toole. *Microbiol. Mol. Biol. Rev.* **2000**, 64, 847-867.
15. E. Marsili, D. B. Baron, I. D. Shikhare, D. Coursolle, J. A. Gralnick and D. R. Bond. *Proc. Natl. Acad. Sci. U.S.A.* **2008**, 105, 3968-3973.
16. D. E. Nivens, J. Q. Chambers, T. R. Anderson and D. C. White. *Anal. Chem.* **1993**, 65, 65-69.
17. A. L. Schofield, T. R. Rudd, D. S. Martin, D. G. Fernig and C. Edwards. *Biosens. Bioelectron.* **2007**, 23, 407-413.
18. V. Reipa, J. Almeida and K. D. Cole. *J. Microbiol. Methods* **2006**, 66, 449-459.
19. M. A. Maurer-Jones, Y.-S. Lin and C. L. Haynes. *ACS Nano* **2010**, 4, 3363-3373.
20. P. O. Vasiliev, B. Faure, J. B. S. Ng and L. Bergström. *J. Colloid Interface Sci.* **2008**, 319, 144-151.
21. F. Gottschalk, R. W. Scholz and B. Nowack. *Environmental Modelling and Software* **2010**, 25, 320-332.
22. W. E. Balch, G. E. Fox, L. J. Magrum, C. R. Woese and R. S. Wolfe. *Microbiol. Rev.* **1979**, 43, 260-296.
23. A. S. Gong, C. H. Bolster, M. Benavides and S. L. Walker. *Environ. Eng. Sci.* **2009**, 26, 1523-1532.
24. C. M. Hessler, M.-Y. Wu, Z. Xue, H. Choi and Y. Seo. *Water Res.* **2012**, 46, 4687-4696.

25. M. Heinlaan, A. Ivask, I. Blinova, H.-C. Dubourguier and A. Kahru. *Chemosphere* **2008**, 71, 1308-1316.
26. H. Bandara, O. L. T. Lam, L. J. Jin and L. Samaranayake. *Crit. Rev. Microbiol.* **2012**, 38, 217-249.
27. E. D. Covington, C. B. Gelbmann, N. J. Kotloski and J. A. Gralnick. *Mol. Microbiol.* **2010**, 78, 519-532.
28. C. H. von, J. Ogawa, S. Shimizu and J. R. Lloyd. *Appl. Environ. Microbiol.* **2008**, 74, 615-623.
29. G. Jiang, Z. Shen, J. Niu, Y. Bao, J. Chen and T. He. *J. Environ. Monit.* **2011**, 13, 42-48.
30. D. Coursolle and J. A. Gralnick. *Frontiers in Microbiology* **2012**, 3, 56.
31. D. Coursolle, D. B. Baron, D. R. Bond and J. A. Gralnick. *J. Bacteriol.* **2010**, 192, 467-474.
32. C. R. Myers and J. M. Myers. *J. Bacteriol.* **1997**, 179, 1143-1152.
33. S. J. Marritt, T. G. Lowe, J. Bye, D. G. G. McMillan, L. Shi, J. Fredrickson, J. Zachara, D. J. Richardson, M. R. Cheesman, L. J. C. Jeuken, *et al. Biochem. J.* **2012**, 444, 465-474.
34. K. M. Thormann, S. Duttler, R. M. Saville, M. Hyodo, S. Shukla, Y. Hayakawa and A. M. Spormann. *J. Bacteriol.* **2006**, 188, 2681-2691.
35. R. M. Saville, N. Dieckmann and A. M. Spormann. *FEMS Microbiol. Lett.* **2010**, 308, 76-83.
36. J. S. McLean, G. E. Pinchuk, O. V. Geydebrekht, C. L. Bilskis, B. A. Zakrajsek, E. A. Hill, D. A. Saffarini, M. F. Romine, Y. A. Gorby, J. K. Fredrickson, *et al. Environ. Microbiol.* **2008**, 10, 1861-1876.
37. D. K. Thompson, A. S. Beliaev, C. S. Giometti, S. L. Tollaksen, T. Khare, D. P. Lies, K. H. Nealson, H. Lim, J. Yates, C. C. Brandt, *et al. Appl. Environ. Microbiol.* **2002**, 68, 881-892.
38. R. Bencheikh-Latmani, S. M. Williams, L. Haucke, C. S. Criddle, L. Wu, J. Zhou and B. M. Tebo. *Appl. Environ. Microbiol.* **2005**, 71, 7453-7460.
39. M. P. Lesser. *Annu. Rev. Physiol.* **2006**, 68, 253-278.

Chapter Five

1. G. E. Batley, J. K. Kirby and M. J. McLaughlin. *Acc. Chem. Res.* **2012** (in press).
2. G. V. Lowry, B. P. Espinasse, A. R. Badireddy, C. J. Richardson, B. C. Reinsch, L. D. Bryant, A. J. Bone, A. Deonarine, S. Chae, M. Therezien, *et al. Environ. Sci. Technol.* **2012**, 46, 7027-7036.
3. T. M. Benn and P. Westerhoff. 2008.
4. M. C. Stensberg, Q. Wei, E. S. McLamore, D. M. Porterfield, A. Wei and M. S. Sepúlveda. *Nanomedicine* **2011**, 6, 879-898.
5. Z.-m. Xiu, Q.-B. Zhang, H. L. Puppala, V. L. Colvin and P. J. J. Alvarez. *Nano Lett.* **2012**, 12, 4271-4275.
6. C. Marambio-Jones and E. Hoek. *J. Nanopart. Res.* **2010**, 12, 1531-1551.

7. W. K. Jung, H. C. Koo, K. W. Kim, S. Shin, S. H. Kim and Y. H. Park. *Appl. Environ. Microbiol.* **2008**, 74, 2171-2178.
8. S. Elzey and V. Grassian. *J. Nanopart. Res.* **2010**, 12, 1945-1958.
9. J. Liu and R. H. Hurt. *Environ. Sci. Technol.* **2010**, 44, 2169-2175.
10. A. P. Gondikas, A. Morris, B. C. Reinsch, S. M. Marinakos, G. V. Lowry and H. Hsu-Kim. *Environ. Sci. Technol.* **2012**, 46, 7037-7045.
11. X. Li, J. J. Lenhart and H. W. Walker. *Langmuir* **2012**, 28, 1095-1104.
12. J. Zook, S. Long, D. Cleveland, C. Geronimo and R. MacCuspie. *Anal. Bioanal. Chem.* **2011**, 401, 1993-2002.
13. M. Koch, S. Kiefer, C. Cavelius and A. Kraegeloh. *J. Nanopart. Res.* **2012**, 14.
14. B. C. Reinsch, C. Levard, Z. Li, R. Ma, A. Wise, K. B. Gregory, G. E. Brown and G. V. Lowry. *Environ. Sci. Technol.* **2012**, 46, 6992-7000.
15. O. Choi, K. K. Deng, N.-J. Kim, L. Ross Jr, R. Y. Surampalli and Z. Hu. *Water Res.* **2008**, 42, 3066-3074.
16. M. C. Frost and M. E. Meyerhoff. *Curr. Opin. Chem. Biol.* **2002**, 6, 633-641.
17. W. K. Ward, H. M. Casey, M. J. Quinn, I. F. Federiuk and M. D. Wood. *Diabetes Technol. Ther.* **2003**, 5, 943-952.
18. P. G. Boswell and P. Buhlmann. *J. Am. Chem. Soc.* **2005**, 127, 8958-8959.
19. J. G. Riess. *Tetrahedron* **2002**, 58, 4113-4131.
20. J. J. Grec, J. G. Riess and B. Devallez. *Nouveau Journal De Chimie-New Journal of Chemistry* **1985**, 9, 109-117.
21. J. G. Riess and M. Leblanc. *Pure Appl. Chem.* **1982**, 54, 2383-2406.
22. C.-Z. Lai, M. A. Fierke, R. C. a. d. Costa, J. A. Gladysz, A. Stein and P. Bühlmann. *Anal. Chem.* **2010**, 82, 7634-7640.
23. H. H. Hau and J. A. Gralnick. *Annu. Rev. Microbiol.* **2007**, 61, 237-258.
24. S. L. Chinnapongse, R. I. MacCuspie and V. A. Hackley. *Sci. Total Environ.* **2011**, 409, 2443-2450.
25. B. J. Marquis, M. A. Maurer-Jones, K. L. Braun and C. L. Haynes. *Analyst* **2009**, 134, 2293-2300.
26. R. M. Atlas *Handbook of Microbiological Media, Third Edition*; CRC Press: **2004**
27. A. M. El Badawy, K. G. Scheckel, M. Suidan and T. Tolaymat. *Sci. Total Environ.* **2012**, 429, 325-331.
28. F. Gottschalk, T. Sonderer, R. W. Scholz and B. Nowack. *Environ. Sci. Technol.* **2009**, 43, 9216-9222.
29. S. A. Blaser, M. Scheringer, M. MacLeod and K. HungerbÃ¼hler. *Sci. Total Environ.* **2008**, 390, 396-409.
30. W. Zhang, Y. Yao, N. Sullivan and Y. Chen. *Environ. Sci. Technol.* **2011**, 45, 4422-4428.
31. A. K. Suresh, D. A. Pelletier, W. Wang, J.-W. Moon, B. Gu, N. P. Mortensen, D. P. Allison, D. C. Joy, T. J. Phelps and M. J. Doktycz. *Environ. Sci. Technol.* **2010**, 44, 5210-5215.

Chapter Six

1. J. Xie, S. Lee and X. Y. Chen. *Adv. Drug Delivery. Rev.* **2010**, 62, 1064-1079.
2. S. H. Liou, T. C. Tsou, S. L. Wang, L. A. Li, H. C. Chiang, W. F. Li, P. P. Lin, C. H. Lai, H. L. Lee, M. H. Lin, *et al. J. Nanopart. Res.* **2012**, 14.
3. M. L. Etheridge, S. A. Campbell, A. G. Erdman, C. L. Haynes, S. M. Wolf and J. McCullough. *Nanomed-Nanotechnol.* **2012**, (in press).
4. A. C. von Eschenbach Nanotechnology: A Report of the US Food and Drug Administration Nanotechnology Task Force. Rockville, MD, **2007**.
5. B. J. Marquis, M. A. Maurer-Jones, O. H. Ersin, Y. S. Lin and C. L. Haynes. *J. Nanopart. Res.* **2011**, 13, 1389-1400.
6. B. J. Marquis, S. A. Love, K. L. Braun and C. L. Haynes. *Analyst* **2009**, 134, 425-439.
7. M. A. Maurer-Jones, K. C. Bantz, S. A. Love, B. J. Marquis and C. L. Haynes. *Nanomed.* **2009**, 4, 219-241.
8. S. A. Love, M. A. Maurer-Jones, J. W. Thompson, Y. S. Lin and C. L. Haynes Assessing Nanoparticle Toxicity. *Annual Review of Analytical Chemistry*, Vol 5; **2012**; pp 181-205.
9. P. P. GmbH L-CsA in the Prevention of Bronchiolitis Obliterans Syndrome (BOS) in Lung Transplant (LT) Patients. http://www.clinicaltrials.gov/ct2/show/NCT01334892?term=NCT01334892&rank=1 (October 2012).
10. M. D. A. C. Center Aerosol L9-NC and Temozolomide in Ewing's Sarcoma. http://www.clinicaltrials.gov/ct2/show/NCT00492141?term=NCT00492141&rank=1 (October 2012).
11. G. Oberdörster, V. Stone and K. Donaldson. *Nanotoxicology* **2007**, 1, 2-25.
12. M. Horie, H. Fukui, K. Nishio, S. Endoh, H. Kato, K. Fujita, A. Miyauchi, A. Nakamura, M. Shichiri, N. Ishida, *et al. J. Occup. Health* **2011**, 53, 64-74.
13. D. B. Warheit, C. M. Sayes and K. L. Reed. *Environ. Sci. Technol.* **2009**, 43, 7939-7945.
14. L. Tabet, C. Bussy, A. Setyan, A. Simon-Deckers, M. J. Rossi, J. Boczkowski and S. Lanone. *Part. Fibre Toxicol.* **2011**, 8, 3.
15. E. K. Rushton, J. Jiang, S. S. Leonard, S. Eberly, V. Castranova, P. Biswas, A. Elder, X. Han, R. Gelein, J. Finkelstein, *et al. J. Toxicol. Env. Heal. A.* **2010**, 73, 445-461.
16. X. Wang, T. Xia, S. A. Ntim, Z. X. Ji, S. J. Lin, H. Meng, C. H. Chung, S. George, H. Y. Zhang, M. Y. Wang, *et al. ACS Nano* **2011**, 5, 9772-9787.
17. S. A. Cryan, N. Sivadas and L. Garcia-Contreras. *Adv. Drug Deliver. Rev.* **2007**, 59, 1133-1151.
18. P. S. Melo, P. D. Marcato, S. C. Hubert, I. R. Ferreira, P. L. B. de, A. B. A. Almeida, N. Duran, S. Torsoni, A. B. Seabra and O. L. Alves. *J. Phys.: Conf. Ser.* **2011**, 304, 012027/012021-012027/012028.
19. M. E. Samberg, S. J. Oldenburg and N. A. Monteiro-Riviere. *Environ. Health Perspect.* **2010**, 118, 407-413.
20. A. R. Murray, E. Kisin, S. S. Leonard, S. H. Young, C. Kommineni, V. E. Kagan, V. Castranova and A. A. Shvedova. *Toxicology* **2009**, 257, 161-171.

21. Y.-H. Park, J. N. Kim, S. H. Jeong, J. E. Choi, S.-H. Lee, B. H. Choi, J. P. Lee, K. H. Sohn, K. L. Park, M.-K. Kim, *et al. Toxicology* **2010**, 267, 178-181.
22. C. J. Mbah, P. F. Uzor and E. O. Omeje. *J. Chem. Pharm. Res.* **2011**, 3, 680-700.
23. A. des Rieux, V. Fievez, M. Garinot, Y.-J. Schneider and V. Preat. *J. Control. Release* **2006**, 116, 1-27.
24. G. J. Mahler, M. B. Esch, E. Tako, T. L. Southard, S. D. Archer, R. P. Glahn and M. L. Shuler. *Nat. Nanotechnol.* **2012**, 7, 264-U1500.
25. B. Moulari, D. Pertuit, Y. Pellequer and A. Lamprecht. *Biomaterials* **2008**, 29, 4554-4560.
26. A. K. Jain, N. K. Swarnakar, M. Das, C. Godugu, R. P. Singh, P. R. Rao and S. Jain. *Mol. Pharm.* **2011**, 8, 1140-1151.
27. W. T. Al-Jamal, K. T. Al-Jamal, P. H. Bomans, P. M. Frederik and K. Kostarelos. *Small* **2008**, 4, 1406-1415.
28. H. Devalapally, Z. Duan, M. V. Seiden and M. M. Amiji. *Clin. Cancer Res.* **2008**, 14, 3193-3203.
29. C. J. Gannon, P. Cherukuri, B. I. Yakobson, L. Cognet, J. S. Kanzius, C. Kittrell, R. B. Weisman, M. Pasquali, H. K. Schmidt, R. E. Smalley, *et al. Cancer* **2007**, 110, 2654-2665.
30. S. K. Singh, M. K. Singh, M. K. Nayak, S. Kumari, S. Shrivastava, J. J. A. Gracio and D. Dash. *ACS Nano* **2011**, 5, 4987-4996.
31. A. D. Maynard, D. B. Warheit and M. A. Philbert. *Toxicol. Sci.* **2011**, 120, S109-S129.
32. M. Lundqvist, J. Stigler, G. Elia, I. Lynch, T. Cedervall and K. A. Dawson. *Proc. Natl. Acad. Sci. U.S.A.* **2008**, 105, 14265-14270.
33. Y.-S. Lin and C. L. Haynes. *J. Am. Chem. Soc.* **2010**, 132, 4834-4842.
34. L. A. A. Gilliam and D. K. St Clair. *Antioxid. Redox Signal.* **2011**, 15, 2543-2563.
35. National Research Council. *Toxicity Testing in the 21st Century: A Vision and a Strategy*; National Academy Press: Washington DC, **2007**.

Chapter Seven

1. M.A. Lieberman. *J. Chem. Educ.* **1999**, 76, 1689-1691.
2. G. Oberdörster, E. Oberdörster, and J. Oberdörster. *Environ. Health Perspect.* **2005**, 113, 823-839.
3. B.J. Marquis, A.D. McFarland, K.L. Braun, and C.L. Haynes. *Anal. Chem.* **2008**, 80, 3431-3437.
4. S.L. Chinnapongse, R.I. MacCuspie, and V.A. Hackley. *Sci. Total Environ.* **2011**, 409, 2442-2450.

Appendix A

Calculations of Distribution Coefficients of Ag^+ and Ag-ammonia Complexes

The pH of the broth solution has measured to be 7.7 and was constant in various concentrations of Ag^+.

Using the pKa value of 9.244 for ammonia (J. F. Rubinson and K. Rubinson *Contemporary Chemical Analysis*; Prentice Hall: 1998), the concentration of ammonia is calculated. The concentration of added Ag^+ is negligible compared to concentration of NH_4^+, so $[NH_4^+]$ has been set equal to the starting concentration.

$$[NH_3][H^+]= [NH_4^+] K_a$$

$$[NH_4^+]_0 = 40mM , [H^+]=10^{-7.7}$$

$$[NH_3]= 1.143 \times 10^{-3}$$

Total silver ion content= $[Ag^+] + [AgNH_3^+] + [Ag(NH_3)_2^+]$

Total silver ion content= $[Ag^+] + ([Ag^+] [NH_3] K_{f,1}) + ([Ag^+] [NH_3]^2 K_{f,1} K_{f,2})$

Total silver ion content= $[Ag^+] (1+[NH_3] K_{f,1}+[NH_3]^2 K_{f,1} K_{f,2})$

$pK_{f,1}=3.24$ and $pK_{f,2}=3.81$ where $pK_{f,1}$ and $pK_{f,2}$ are formation constants of silver-ammonia complexes (J. A. Dean *Lange's Handbook of Chemistry, Fourteenth Edition*; McGraw-Hill: 1992)

$[Ag^+]$ / Total silver ion content= $1 / (1+[NH_3] K_{f,1}+[NH_3]^2 K_{f,1} K_{f,2})$ = **0.05667**

$[AgNH_3^+]$ / Total silver ion content = $([NH_3] K_{f,1}) / (1+[NH_3] K_{f,1}+[NH_3]^2 K_{f,1} K_{f,2})$=**0.11257**

$[Ag(NH_3)_2^+]$ / Total silver ion content = $([NH_3]^2 K_{f,1} K_{f,2}) / (1+[NH_3] K_{f,1}+[NH_3]^2 K_{f,1} K_{f,2})$ = **0.83075**

Appendix B

Curriculum Vitae

Melissa A. Maurer-Jones

University of Minnesota – Twin Cities
Department of Chemistry
207 Pleasant St SE L-18
Minneapolis, MN 55455

Email: jone1317@umn.edu
Phone: 612-626-5282

Education

Ph.D. **(2012 – expected graduation)** – Chemistry, University of Minnesota - Twin Cities, Minneapolis, MN.

Thesis: Fundamental Assessment of the Immunogenicity and Ecotoxicity of Nanoparticles

Advisor: Christy L. Haynes

M.S. **(2008)** – Chemistry, University of Minnesota - Twin Cities, Minneapolis, MN.

Advisor: Christy L. Haynes

B.S. **(2006)** – Chemistry, University of St. Thomas, St. Paul, MN.

Research Advisor: Anthony J. Borgerding

Research Experience

Graduate Assistant **(2007-present)** – Department of Chemistry, University of Minnesota.
Advisor: Christy L. Haynes

- Worked to study the impact of engineered titania and silver nanomaterials on the cellular function of immune system cells and nonpathogenic bacteria models using electrochemistry, quartz crystal microbalance, and traditional toxicological assays

Lab Analyst **(2006-2007)** – Pace Analytical Services, Inc., Minneapolis, MN

- Performed analysis of 3M product to ensure product safety, reviewed notebooks for co-workers, and maintained company instruments

Research Assistant **(2002-2006)** – Department of Chemistry, University of St. Thomas
Advisor: Anthony J. Borgerding

- Developed a microextraction tool for extracting volatile compounds from aqueous solutions

Awards and Honors

Student Exchange Award **(2012)** – American Chemical Society Division of Environmental Chemistry/Society of Environmental Toxicology and Chemistry

Doctoral Dissertation Fellowship **(2011-2012)** – University of Minnesota

American Chemical Society-Division of Analytical Chemistry **(2011)** – Summer Fellowship, American Chemical Society

Graduate Student Travel Grant **(2011)** – Society of Electroanalytical Chemistry

Graduate Research Symposium Travel Award **(2010)** – Department of Chemistry, University of Minnesota

Scholarly Travel Grant **(2009)** – Graduate and Professional Student Assembly, University of Minnesota

Mary Haga Travel Grant **(2009)** – Xi Chapter, Graduate Women in Science

National Science Foundation Graduate Research Fellowship **(2008-2011)** – National Science Foundation

Wayland E. Noland Fellowship **(2007-2008)** – University of Minnesota

American Institute of Chemists Outstanding Senior Award **(2006)** – University of St. Thomas

Barry M. Goldwater Scholarship **(2005)** – Barry M. Goldwater Scholarship Program

ACS Award in Analytical Chemistry **(2005)** – University of St. Thomas

William D. Larson Chemistry Scholarship **(2005)** – University of St. Thomas

Peer-Reviewed Publications

M.A. Maurer-Jones, S.A. Love, S. Meierhofer, B.J. Marquis, Z. Liu, C.L. Haynes. Toxicity of Nanoparticle to Brine Shrimp: An Introduction to Nanotoxicity and Interdisciplinary Science. *Journal of Chemical Education.* **2012**, (accepted).

M.A. Maurer-Jones, J.R. Christenson, C.L. Haynes. TiO_2 Nanoparticle-Induced ROS Correlates with Immune Cell Dysfunction. *Journal of Nanoparticle Research*. **2012**, (in press).

M.A. Maurer-Jones, C.L. Haynes. Toward Correlation in *In Vivo* and *In Vitro* Nanotoxicology Studies. *Journal of Law, Medicine, and Ethics.* **2012**, (in press).

S.A. Love, **M.A. Maurer-Jones**, Y.-S. Lin, J.W. Thompson, C.L. Haynes. Assessment of Nanoparticle Toxicity. *Annual Review of Analytical Chemistry*. **2012**, 5, 181-205.

M.A. Maurer-Jones, B.J. Marquis, Ö.H. Ersin, Y-.S. Lin, C.L. Haynes. The Bench Scientist's Perspective on the Unique Considerations in Nanoparticle Regulation. *Journal of Nanoparticle Research.* **2011**,13, 1389-1400.

M.A. Maurer-Jones, Y-.S. Lin, C.L. Haynes. Functional Assessment of Metal Oxide Nanoparticles in Immune Cells. *ACS Nano*. **2010**, 4, 3363-3373.

B.J. Marquis, **M.A. Maurer-Jones**, K.A. Braun, C.L. Haynes. Amperometric Assessment of Functional Changes in Nanoparticle-Exposed Immune Cells: Varying Au Nanoparticle Exposure Time and Concentration. *Analyst*. **2009**, 134, 2293-2300.

M.A. Maurer-Jones, K.C. Bantz, S.A. Love, B.J. Marquis, C.L. Haynes. Toxicity of Therapeutic Nanoparticles. *Nanomedicine*. **2009**, 4, 219-241.

M.A. Jones, A. Kramer, M. Humbert, T. Vanadurongvan, J. Maurer, M.T. Bowser, A.J. Borgerding. Analysis and Monitoring of Volatile Analytes from Aqueous Solutions by Extractions into the Gas Phase Using Microdialysis Membranes and Coupling to Fast GC. *Analytical Chemistry* **2008**, 80, 123-128.

Presentations

Contributed Interactive Poster. "Monitor of Ag^+ Dissolution from Ag Nanoparticles for the Understanding of Toxicity to *Shewanella oneidensis*." Society of Environmental Toxicology and Chemistry 33rd Annual North American Meeting, Long Beach, CA. **November 2012.**

Contributed Poster. "Impact of TiO_2 Nanoparticles on Bacterial Biofilm Formation." Gordon Research Conference – Environmental Sciences: Water, Holderness, NH. **June 2012.**

Contributed Poster. "Assessment of Ion Dissolution from Ag Nanoparticles using Ion Selective Electrodes and Subsequent Toxicity in *Shewanella oneidensis.*" Gordon Research Seminar – Environmental Sciences: Water, Holderness, NH. **June 2012.**

Contributed Lecture. "Impact of TiO_2 Nanoparticles on Bacterial Biofilm Formation." 243rd American Chemical Society National Meeting, San Diego, CA. **March 2012.**

Contributed Lecture. "Assessment of Ion Dissolution from Silver Nanoparticles using Ion Selective Electrodes and Subsequent Toxicity Studies in *Shewanella oneidensis*." 243rd American Chemical Society National Meeting, San Diego, CA. **March 2012.**

Invited Lecture. "Fundamental Study of Cellular Response after Exposure to Nanoparticles." Doctoral Dissertation Fellows Seminar, Minneapolis, MN. **November 2011.**

Contributed Poster. "Fundamental Assessment of the Impacts of TiO_2 Nanoparticles on *Shewanella oneidensis*." Gordon Research Conference – Environmental Nanotechnology, Waterville Valley, NH, **June 2011**.

Contributed Lecture. "Fundamental Study of the Cellular Response after Exposure to TiO_2 Nanoparticles." 62nd Pittsburgh Conference on Analytical Chemistry and Applied Spectroscopy, Atlanta, GA. **March 2011**.

Invited Lecture. "Fundamental Assessment of TiO_2 Nanoparticle Toxicity Using Carbon-Fiber Microelectrode Amperometry." Society of Toxicology Northland Chapter Meeting, St. Paul, MN. **October 2010**.

Contributed Lecture. "Functional Assessment of Metal Oxide Nanoparticle Effects on Cell Function." Chemistry Graduate Student Research Symposium, Minneapolis, MN. **May 2010**.

Contributed Poster. "Toxicity of Metal Oxide Nanoparticles: A Study on the Impact of Porosity on Cell Function." 4th International Conference on Nanotechnology: Occupational and Environmental Health, Helsinki, Finland. **August 2009**.

Contributed Poster. "Exploring the Effects of TiO_2 Nanoparticles on Mast Cell Function." Society of Applied Spectroscopy Regional Meeting, St. Paul, MN. **May 2009**.

Contributed Poster. "Exploring the Effects of TiO_2 Nanoparticles on Mast Cell Function." NIH Chemical Biology Interface Training Grant Symposium, St. Paul, MN. **May 2009**.

Contributed Poster. "Exploring the Effects of TiO_2 Nanoparticles on Cell Function with Carbon-Fiber Microelectrode Amperometry." 60th Pittsburgh Conference on Analytical Chemistry and Applied Spectroscopy, Chicago, IL. **March 2009**.

Contributed Poster. "Extraction of Gas Phase Analytes from Aqueous Solutions Using Microdialysis Membranes." 231st National Meeting of the American Chemical Society, Atlanta, GA. **March 2006**.

Contributed Poster. "Extraction of Gas-Phase Analytes from Aqueous Solutions." 28th International Symposium on Capillary Chromatography and Electrophoresis, Las Vegas, NV. **May 2005**.

Contributed Poster. "A Cryofocusing Sampling Technique to Determine Selenium-Containing VOCs in Selenium Enriched Broccoli." 18th National Conference on Undergraduate Research, Indianapolis, IN. **April 2004**.

Contributed Poster. "Exploration of Chromatographic Resolution Due to the Effect of Injection Pulse Duration." Minnesota Academy of Sciences meeting, St. Paul, MN. **April 2003**.

Grants Co-Authored

"Evaluating Beneficial Bacteria Function following Engineered Nanoparticle Exposure," National Science Foundation, **July 2011 - funded**.

"Evaluating Beneficial Bacteria Function following Engineered Nanoparticle Exposure," National Science Foundation, **February 2011**.

Teaching Experience

Guest Lecturer **(Spring/Fall 2011)** - Department of Chemistry, University of Minnesota

- CHEM 8152: Analytical Spectroscopy – Acted as substitute lecturer for Dr. Christy Haynes for two lectures and helped write an exam question
- CHEM 2121: Process Analytical – Acted as substitute lecturer for Dr. Christy Haynes for two lectures and helped write exam questions

Research Mentor **(2009 – present)** – Haynes Research Group, Department of Chemistry, University of Minnesota

- Directed Sarah Connolly's research on reactive oxygen species (ROS) assay development to assess toxicity of TiO_2 nanoparticles
- Directed Jenna Christenson's research on ROS assay development to assess toxicity of TiO_2 nanoparticles, which resulted in her authorship on an article in *Journal of Nanoparticle Research*
- Directed Gregory Gibson's research on the development of *Shewanella oneidensis* as a nanotoxicity model organism
- Directed Cole Christensen's research on the toxicity of TiO_2 nanoparticles to *S. oneidensis*, which has resulted in his authorship on an article that is in preparation

Mentorship Program for Aspiring Chemistry Teachers (MPACT) Participant **(Spring 2011)** – Department of Chemistry, University of Minnesota

- Observed class lectures, led two lectures, helped write and grade exams, and aided the implementation of POGIL activities within classroom lectures

Preparing Future Faculty – Teaching in Higher Education **(Fall 2010)** – Graduate School (GRAD 8101), University of Minnesota

- Completed coursework dealing with a wide range of higher education teaching-focused topics including pedagogical theory and curriculum development

Teaching Assistant **(2008 – 1 semester)** – Process Analytical Chemistry (CHEM 4121) laboratory TA, University of Minnesota

- Led pre-lab discussion, assisted students in learning laboratory techniques, designed and implemented grading rubric, held tutor and office hours

Teaching Assistant **(2007 – 1 semester)** – General Chemistry (CHEM 1011) laboratory TA, University of Minnesota

- Led pre-lab discussion, graded lab reports, held tutor and office hours

Chemistry Tutor **(2003-2006)** – Focus on General Chemistry concepts, University of St. Thomas

- Aided students in learning General Chemistry material

Service and Leadership Activities

Women In Science and Engineering **(2008-present)** – University of Minnesota

Student Workshop Committee **(2008-present)** – Department of Chemistry, University of Minnesota

Poster judge for undergraduate research proposals **(2011)** – Department of Chemistry, University of Minnesota

Chemistry Day Outreach Event**(2009-present)** – West 7^{th} Community Center, St. Paul, Minnesota

Cool Chemistry Outreach **(2008-2009, 2011)** – Women in Science and Engineering, University of Minnesota

Dragon Fly TV participant **(2008)** – Public Broadcasting Service

ACS Student Affiliate Chapter President/Vice President **(2004-2006)** – University of St. Thomas

Professional Affiliations

American Chemical Society

Society of Environmental Toxicology and Chemistry

Iota Sigma Pi – Honor Society of Women in Chemistry